Carboxyl and Ethynyl-Substituted Dithiafulvenes and Tetrathiafulvalene Vinylogues: Synthesis, Properties, and Applications

by

© Yunfei Wang

A thesis submitted to the School of Graduate Studies in partial fulfilment of

the requirements for the degree of

Master of Science

Department of Chemistry

Memorial University of Newfoundland

November 2015

St. John's Newfoundland

Abstract

This thesis describes a systematic study of new dithiafulvene (DTF) and tetrathiafulvalene vinylogue (TTFV) derivatives as redox-active π-conjugated molecular materials. The content of this thesis work is divided into two major parts. In the first part, a series of carboxylate ester and carboxyl-substituted DTFs and TTFVs were synthesized and their electronic and electrochemical redox properties were characterized by UV-Vis spectroscopic and cyclic voltammetric analyses. The carboxyl-TTFV was applied as a redox-active ligand to complex with zinc ions, forming a stable Zn-TTFV coordination product. The structural, electrochemical, and thermal properties of the coordination product were investigated by infrared spectroscopy, powder X-ray diffraction, cyclic voltammetry, and differential scanning calorimetric analyses. Furthermore, the microscopic morphological and porosity properties of the Zn-TTFV coordination product were measured by scanning electron microscopy and nitrogen gas adsorption experiments. In the second part, a series of ethynyl-substituted DTF regioisomers was synthesized and then used as starting materials to construct further π-extended derivatives through oxidative dithiafulvenyl coupling and Cu-catalyzed alkynyl homocoupling reactions. The resulting π-conjugated systems were subjected to UV-Vis absorption and cyclic voltammetric analyses to examine their electronic properties and redox reactivity. Based on the characterization studies, a understanding of the structure-property-reactivity relationships for these compounds has been established.

Acknowledgements

First of all, I would like to thank my supervisor Dr. Yuming Zhao for giving me the opportunity to study in his group. He helped me a lot throughout my program and made me familiar with how to carry out scientific research. I would also like to thank Dr. Sunil Pansare and Dr. Francesca Kerton who have been serving as my committee members during my M.Sc. program. Dr. Micheal Katz is particularly acknowledged here for his kind assistance in solving the XRD structures.

I would also like to thank my group as well as students from other research groups at the Chemistry Department, who have offered me very generous help. Especially, I want to acknowledge two of my former group members, Dr. Guang Chen and Ms. Kathleen Woolridge, for their valuable time and patience in teaching me new techniques and knowledge during the period when I first just joined the group. I would like to thank Dr. Celine Schneider, Ms. Linda Winsor and other C-Cart staff for their kind assistance in all the instrumental analyses described in this dissertation.

Last but not least, I would like to extend my thanks to all the faculty and staff of the Chemistry Department who have endeavored to create such a great educational and training environment for students like me. Memorial University and NSERC are sincerely acknowledged for their generous funding support of my study and research at Memorial University. Finally, I want to thank my family members and friends who have been always supportive to me throughout my M.Sc. program.

Contents

List of Figures

List of Schemes

List of Tables

List of Abbreviations and Symbols

APPI	atmospheric pressure photo ionization
aq	aqueous
BET	Brunauer-Emmett-Teller
ca.	circa
calcd	calculated
cm	centimeter(s)
CV	cyclic voltammetry
d	doublet
DSC	differential scanning calorimetry
DTF	dithiafulvene or dithiafulvenyl
Et	ethyl
exTTF	π-extended tetrathiafulvalene
FTIR	Fourier transform infrared

g	gram(s)
h	hour(s)
HRMS	high resolution mass spectrometry
Hz	hertz
IR	infrared
ITO	indium tin oxide
J	coupling constant
m	multiplet
m/z	mass to charge ratio
MALDI-TOF	matrix assisted laser desorption/ionization-time of flight
Me	methyl
mg	milligram(s)
MHz	megahertz
min	minute(s)
mL	milliliter(s)
mmol	millimole(s)
mol	mole(s)

m.p.	melting point
MS	mass spectrometry
mV	millivolt(s)
mW	milliwatt(s)
nm	nanometer(s)
NMR	nuclear magnetic resonance
ppm	parts per million
PXRD	powder X-ray diffraction
s	singlet
satd	saturated
SWNT	single-walled nanotubes
t	triplet
TFA	trifluoroacetic acid
THF	tetrahydrofuran
TLC	thin-layer chromotography
TMEDA	*N,N,N',N'*-tetramethylethylenediamine
TMS	trimethylsilyl

TMSA	trimethylsilylacetylene
TTF	tetrathiafulvalene
TTFAQ	anthraquinone-type π-extended tetrathiafulvalene
TTFV	tetrathiafulvalene vinylogue
UV-Vis	ultraviolet-visible
V	volt(s)
XRD	X-ray diffraction
δ	chemical shift
ϵ	molar attenuation coefficient
λ_{max}	maximum absorption wavelength

Chapter 1

Introduction to Tetrathiafulvalene and Tetrathiafulvalene Vinylogues

1.1 Tetrathiafulvalene and π-Extended Tetrathiafulvalenes

The discovery of tetrathiafulvalene (TTF) as the first organic conductor can be dated back to the seminal paper published by Fred Wudl and co-workers in 1970,[1] although Hünig[2] and Coffen[3] should also be given the credit for their independent work on TTF in the early 1970s. Following this early work, TTF and its derivatives have quickly emerged as the most famous class of organic electron donors, which is testified by over ten thousand scientific papers published in the current literature dealing with their synthesis, properties and applications.[4] In materials chemistry, TTF has been widely applied as a redox-active building block for the preparation of organic electronic materials and supramolecular assemblies because TTF, when interacting with a suitable

electron acceptor(s), can give rise to charge-transfer complexes with excellent metallic conductivity.[5–9] The remarkable electron-donating properties of TTF arise from its unique aromaticity-stabilized cationic states after releasing one and/or two electrons (see Scheme 1.1).[5–12]

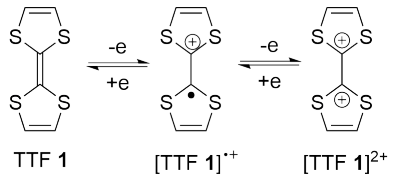

Scheme 1.1: Sequential single-electron transfers of TTF **1** showing the stepwise conversion of its two nonaromatic dithiole rings into aromatic ditholium units upon oxidation.

In the dication of TTF, the two dithiolium moieties are known to be perpendicular to one another so as to minimize the disfavored charge repulsion. Attachment or annulation of π-conjugated groups to the two dithiole rings has turned out to be a very popular modification strategy for generating TTF derivatives which not only retain the redox-activity of pristine TTF, but also achieve significantly reduced charge repulsion and hence lowered oxidation potentials as well as enhanced microscopic ordering (*e.g.*, π-stacking). These properties are particularly beneficial to the development of functional organic electronic materials and molecular devices. In modern TTF chemistry, a vast array of π-extended TTF analogues (henceforth referred to as exTTFs) has been designed and synthesized. Synthetically, π-extension of TTF can be attained by either appending π-conjugated moieties to the dithiole units (*e.g.*, dibenzo-TTF **2** shown in Figure 1.1) or having a π-spacer(s) inserted in between the two dithiole rings, such as the anthraquinoidal and vinylogous exTTFs **3** and

4 in Figure 1.1. Many of the known exTTFs have been found to show excellent redox, optoelectronic, and supramolecular properties, which in turn led to wide-ranging applications in advanced π-conjugated materials.[7,9,12,13]

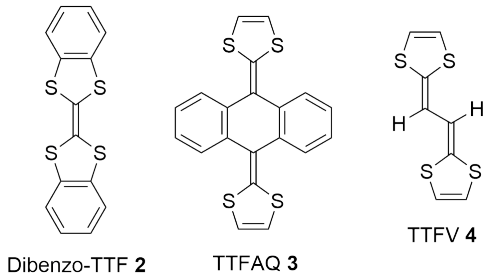

Figure 1.1: Structures of exTTFs **2**-**4**.

1.2 Tetrathiafulvalene Vinylogues

1.2.1 Properties and Application of Tetrathiafulvalene Vinylogues

Tetrathiafulvalene vinylogues (TTFVs) are π-extended analogues of TTF bearing extended vinyl bridges between the two dithiole rings of TTF (*e.g.*, compound **4** in Figure 1.1).[11,12,14] Similar to the pristine TTF, TTFVs are also excellent electron donors and can undergo reversible electron transfers under mild redox conditions.[14–18] Of particular interest is the class of aryl-substituted TTFVs which show interesting conformational switching properties governed by redox processes.[15,17–19] For instance, the structure of diphenylated TTFV **5** can be transformed from a pseudo *cis* to a complete *trans* conformation upon oxidation (Scheme 1.2). In the neutral state, TTFV **5** favors a *cis*-like conformation because it has the least steric interactions

between the phenyl and dithiole rings. After being oxidized into a dication, the electrostatic repulsion between the two dithiolium rings becomes a dominant force dictating the conformational preference. Obviously, the fully *trans* geometry satisfies the need for minimal charge repulsion within the TTFV dication.

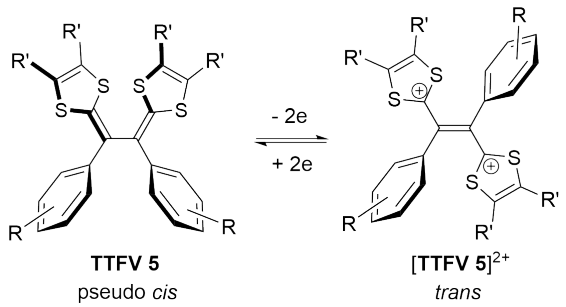

Scheme 1.2: Redox-induced conformational switching of diphenyl-TTFV **5**.

There has been a surge in the study of TTFV-based π-conjugated molecular and macromolecular materials over the past few years, although the very first use of TTFVs in materials development started several decades ago. The following section provides a brief review of the most recent advancement in the field of TTFV-based functional materials. Herein, various examples are selected to highlight the versatility of TTFV as both a structural and functional component in novel nanomaterials and molecular devices. In most of these studies, the remarkable redox activity and controllable conformational switching behavior of TTFVs were taken advantage of to generate enhanced structural and electronic properties as well as to introduce certain "intelligent functions", such as switchable selectivity in molecular recognition and supramolecular interactions.

In 2014, a stimuli-responsive TTFV-fluorene co-polymer **29** was collaboratively developed by Zhao and Adronov (Figure 1.2).[20] The co-polymer was synthesized

through a Sonogashira cross-coupling polymerization between a phenylacetylene-substituted TTFV and 2,7-diiodofluorene. This co-polymer was found to wrap around single-walled carbon nanotubes (SWNTs), especially small-diameter SWNTs, via strong π–π interactions to form stable polymer/SWNT suspension in toluene. Addition of trifluroacetic acid (TFA) to the suspension resulted in a facile protonation of the TTFV moieties in the co-polymer, accompanied by a dramatic conformational change of the polymer backbone. As such, the polymer-SWNT interactions were disrupted, leading to efficient release of pristine SWNTs from the polymer-SWNT supramolecular complexes. The controlled stimuli-responsiveness of TTFV-fluorene co-polymer **29** along with other similar TTFV-based polymers[21,22] previously developed by the Zhao group can find application in the fabrication of SWNT-based semiconducting devices, where polymer dispersants or additives are used in the early stage of solution-phase processing, but need to be removed completely later on to avoid unwanted contamination or doping effects.

A TTFV-anthracene molecular tweezer **30** (Figure 1.3) was synthesized by Zhao and co-workers in 2013 by using a Cu-catalyzed alkyne-azide coupling reaction.[23,24] The combination of TTFV and anthracene facilitated the binding to fullerenes via π-stacking and/or charge-transfer interactions. Of great interest is that this molecular tweezer can selectively bind to C_{70} in the presence of a large excess of C_{60}, because the π-cavity created by the TTFV moiety of the tweezer has a shape that fits better for ellipsoidal C_{70} than spherical C_{60}. This study has demonstrated a new molecular design approach to making more efficient and highly selective receptors for various fullerenes.

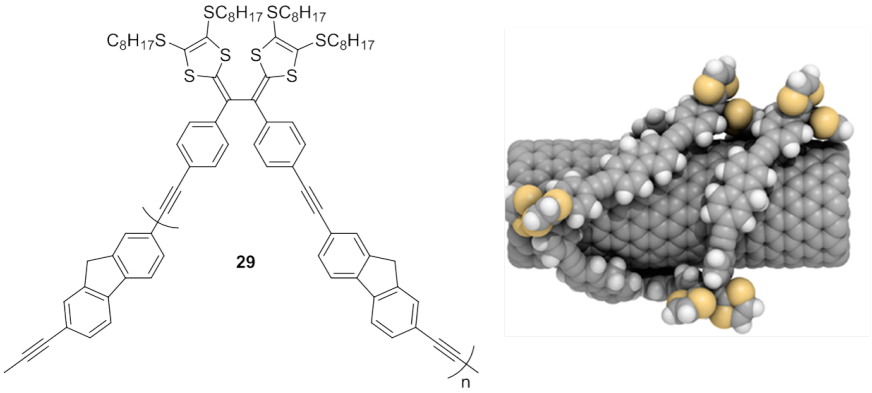

Figure 1.2: A stimuli-responsive TTFV-fluorene co-polymer **29** (left) and the molecular model showing it wrapping around a SWNT (right). Reprinted (adapted) with permission from (Liang, S.; Zhao, Y.; Adronov, A. *J. Am. Chem. Soc.* **2014**, *136*, 970-977.). Copyright (2014) American Chemical Society.

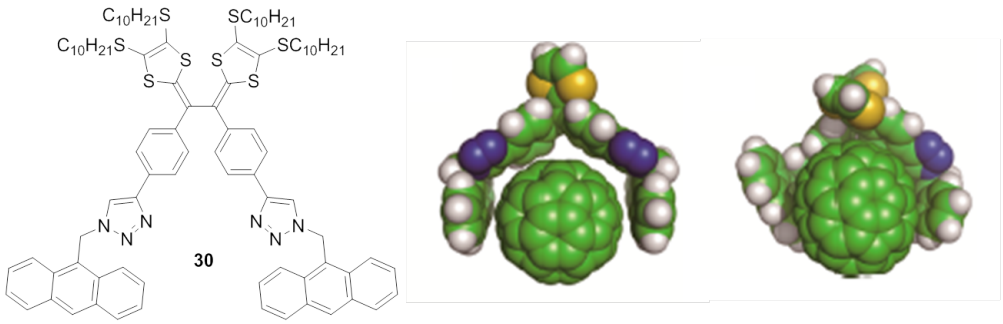

Figure 1.3: A tweezer-like TTFV-anthracene molecule **30** (left), and the optimized molecular structure for the 1 : 1 complexes of **30** with C_{60} (middle) and **30** with C_{70} fullerene (right). Reprinted (adapted) with permission from (Mulla, K.; Shaik, H.; Thompson, D. W.; Zhao, Y. *Org. Lett.* **2013**, *15*, 4532-4535.). Copyright (2013) American Chemical Society.

The TTFV unit can also be utilized to create redox-active organic-inorganic hybrid compounds. An example of these can be found from a recent paper by Lorcy and co-workers (see Figure 1.4),[25] in which a pyridyl-TTFV compound **31** was devised as a redox-active ligand since the pyridyl group can readily form coordination bonds with various metal ions. The reaction between **31** and $Mo(CO)_6$ resulted in a coordination-driven self-assembled complex. The complex containing two TTFV ligands and two $Mo(CO)_4$ fragments was found to have a square-shaped macrocyclic structure due to the complementarity of angle, size, and orientation of the TTFV ligand **31** and the *cis*-$Mo(CO)_4$ fragment. Furthermore, cyclic voltammetric analysis was performed to show that the redox activity of the TTFV moieties within the complex was still retained.

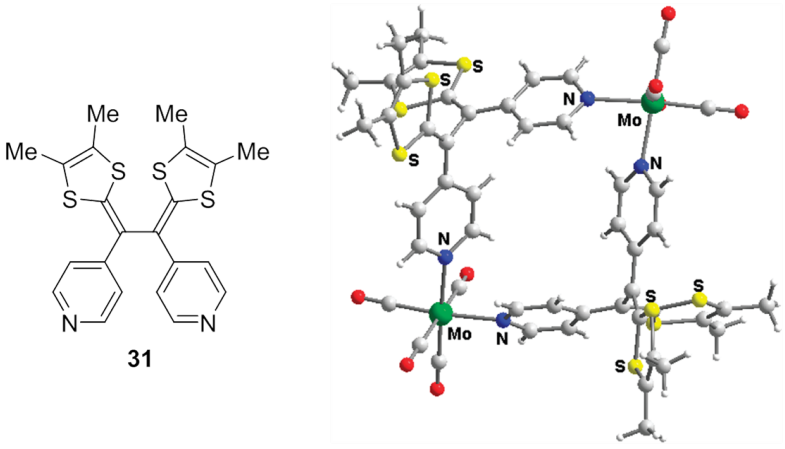

Figure 1.4: Structure of pyridyl-TTFV ligand **31** (left), and the crystal structure of its complex with $Mo(CO)_4$ (right). Reprinted (adapted) with permission from (Gontier, E.; Bellec, N.; Brignou, P.; Gohier, A.; Guerro, M.; Roisnel, T.; Lorcy, D. *Org. Lett.* **2010**, *12*, 2386-2389.). Copyright (2010) American Chemical Society.

A TTFV-alkyne shape-persistent macrocycle **32** was prepared by the Zhao group in 2010 (Figure 1.5).[26,27] It was synthesized from a phenylacetylenic TTFV precursor through a threefold Hay coupling approach in the presence of Cu and Pd catalysts under highly dilute conditions. Herein the preorganized *cis*-like conformation of the TTFV moiety in the precursor was believed to be a key contributor to the successful macrocyclization. This TTFV-alkyne macrocycle was found to show a reversible redox behavior, but the oxidation and reduction potentials were found to be much higher than those of the phenylacetylenic TTFV precusor. This result was attributed to the geometric constraint of the *cis*-TTFV moiety embedded in the macrocyclic structure.

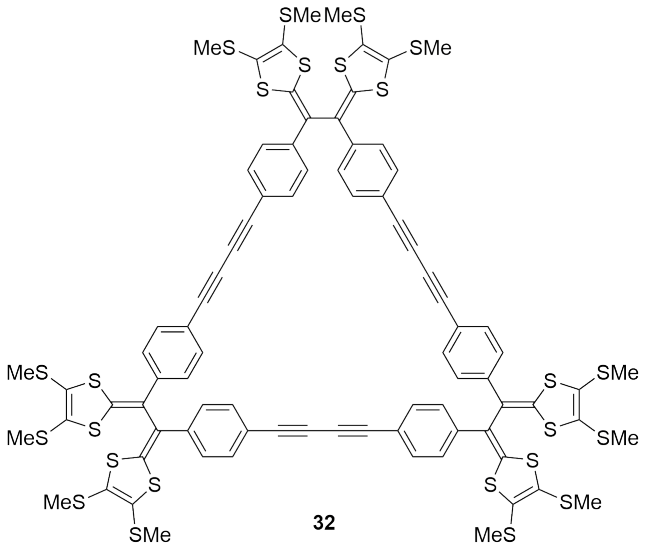

Figure 1.5: Structure of the shape-persistent TTFV-alkyne macrocycle **32**.

Very recently, a redox-regulated TTFV molecular rotor (Scheme 1.3) was prepared by Chen and Zhao,[28] which extended the application of TTFVs to molecular machines. Based on the rationalization that the two phenyl groups of phenyl-substituted TTFVs favor disrotation in the neutral state and conrotation in the oxidized state, a molecular gearset was designed and synthesized by linking two benzyltriptycene molecular rotors to a TTFV central unit. Dynamic NMR studies have shown that the two triptycyl rotors of this redox-active gearset can rotate at a faster rate in the oxidized state than in the neutral state, which means that the redox states of the TTFV moiety exert a significant control over the rotational properties of the two triptycyl rotors covalently bonded to it.

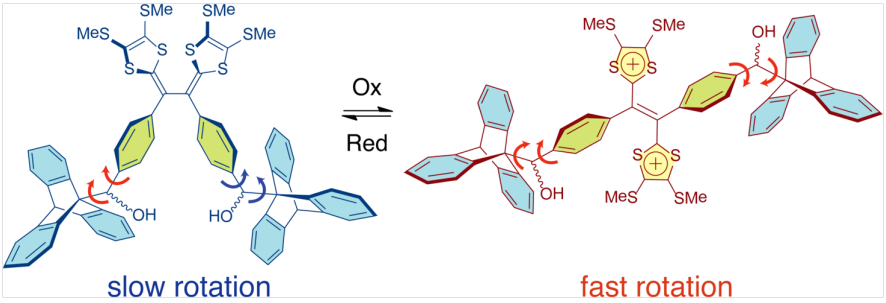

Scheme 1.3: Redox-regulated rotary motion of a bis(9-triptycyl)-TTFV system. Reprinted (adapted) with permission from (Chen, G.; Zhao, Y. *Org. Lett.* **2014**, *16*, 668-671.). Copyright (2014) American Chemical Society.

1.2.2 Synthetic Methods for Tetrathiafulvalene Vinylogues

A straightforward synthetic strategy for making various TTFV-containing structures is illustrated by the retrosynthesis in Scheme 1.4, in which two sequential bond disconnection steps eventually lead to two precursors, thione **6** and aldehyde **7**. Typically,

the R group of aldehyde **7** is desired to be an aryl group so as to facilitate the radical dimerization reaction. So far, this synthetic route has been dominantly employed in TTFV synthesis mainly for two reasons: (i) both the thione and aldehyde precursors have easy synthetic accessibility, and (ii) both the olefination and dimerization reactions are generally high-yielding.

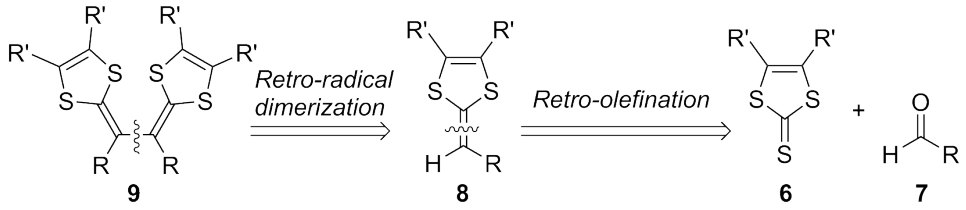

Scheme 1.4: Retrosynthetic analysis of TTFVs.

The olefination reaction between an aldehyde precursor and its thione counterpart can be performed in several different ways. So far, the most efficient one developed is the phosphite-promoted approach illustrated in Scheme 1.5.[29,30] Since this direct olefination reaction requires a relatively high reaction temperature, it is only applicable to the cases where the starting materials and products are thermally stable. After the olefination, a dithiafulvene (DTF) intermediate **8** is obtained. Dimerization reaction of **8** can be induced by addition of an oxidizing reagent such as iodine to afford TTFVs **9** (Scheme 1.5).[31]

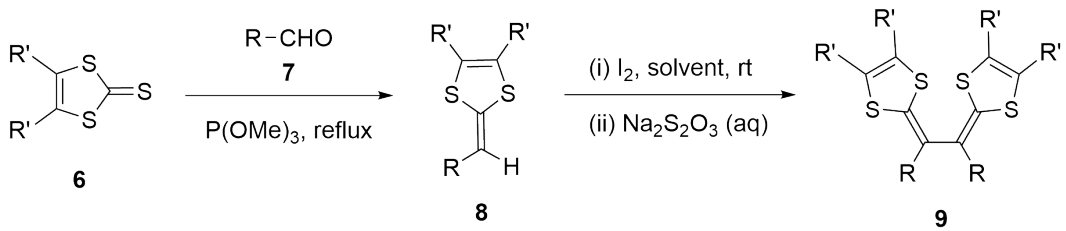

Scheme 1.5: General reactions conditions for making TTFVs.

The mechanism of the DTF oxidative dimerization reaction begins with a single-electron transfer from DTF to the oxidant, forming the corresponding DTF radical cation. The DTF radical cation will then undergo dimerization to form a new carbon-carbon bond, and the acidic protons in the resulting dimer intermediate will be eliminated (deprotonation) to give the TTFV product. The TTFV product will be oxidized again under the oxidative conditions to form a stable TTFV dication. When the oxidative dimerization is complete, a reducing agent is then added to quench the excess oxidant and to regenerate the neutral TTFV as the major product (Scheme 1.6).

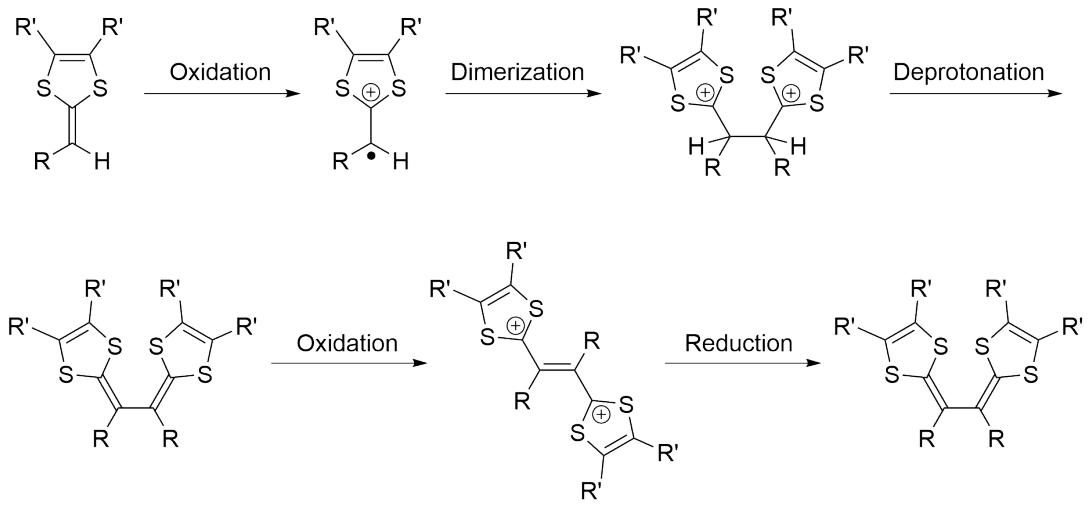

Scheme 1.6: Mechanism of the DTF oxidative dimerization reaction.

The preparation of thione precursor **6** can be readily executed through the approach developed by Hoyer's group in 1979.[32] As shown in Scheme 1.7, the synthesis begins with the reaction between carbon disulfide and sodium metal, resulting in a dithiolate intermediate that can be further stabilized by complexation with Zn(II) ion. The zinc complex **10** then reacts with a certain electrophile (*e.g.*, an alkyl halide) to generate the thione product, while the substituents attached to the dithiole ring in the product can be readily modified by the electrophile chosen for the reaction. (Scheme 1.7).

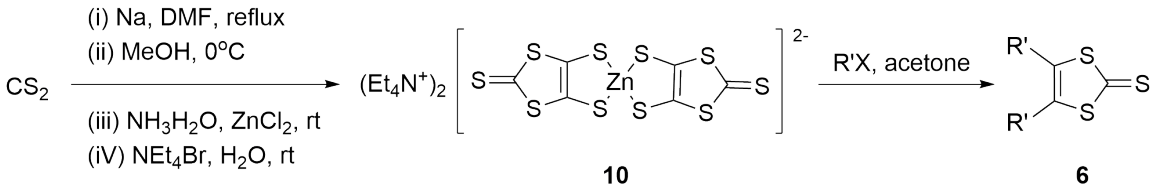

Scheme 1.7: Synthesis of thione **6**.

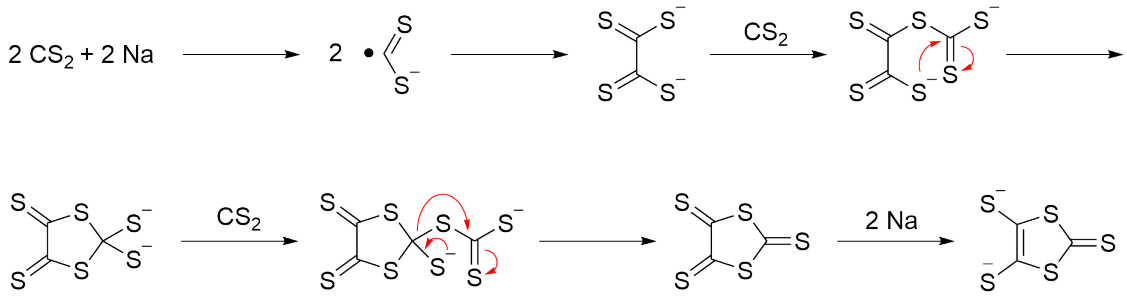

Scheme 1.8: Mechanism of the formation of the dithiolate compound.

Scheme 1.8 shows the detailed mechanism for the formation of the dithiolate intermediate in the first step of thione synthesis.[33] The reduction of carbon disulfide by sodium metal at first leads to a radical species which quickly dimerizes. The dimeric intermediate will continue to react with another two molecules of carbon

disulfide to produce the dithiolate compound after a series of rearrangement as shown in Scheme 1.8. At the last stage, a five-member ring dithiolate anion is formed. Since this anion cannot be isolated as a stable product, coordination with Zn(II) ion is performed to generate a red-colored solid complex that is stable for storage and able to undergo facile substitution reactions to give various thione products.

1.3 Motivations for This Thesis Work

Because of their excellent electron-donating properties, TTFV and derivatives have been increasingly used as functional building blocks in organic/inorganic materials. Research in this area has also been greatly fueled up by the well-established modern synthetic methodologies (*e.g.*, metal-catalyzed coupling, click chemistry) which allow a large variety of functional groups to be readily attached to the TTFV structure. At the outset of this M.Sc. thesis work, some new forefronts in microporous nanomaterials had just emerged to capture growing attention from both academia and industry; especially, the so-called metal-organic frameworks (MOFs) and covalent organic frameworks (COFs) are two types of actively investigated new nanomaterials, owing to their salient properties such as enormous surface area, defined pore size, and robust mechanical strength. It is therefore predictable that chemical modifications on MOFs and COFs with various existing functional molecular building blocks will become a major research trend in this area. Through this approach, novel microporous materials will be continuously developed to exhibit unprecedented "smart functions" applicable to a wide range of electronic, photonic, and biological applications.

Redox-activity is a useful means to exert precise control over the structural and

electronic properties of nanomaterials and molecular devices. The application of TTF derivatives as redox-active building blocks in materials science and nanotechnology has been studied for decades. As briefly summarized before, the application of TTFV is still a relatively underdeveloped research topic compared with other types of TTF derivatives. Although some significant progresses have been made in TTFV-containing polymers, oligomers, macrocycles, and molecular machines over the past few years, there have been no reports on using TTFV as structural components in making microporous polymers and frameworks. Synthetically, it is a highly feasible task to do so, if certain linker groups (*e.g.*, carboxyl group) are to be anchored to the TTFV moiety. Carboxylated TTFV derivatives had not been known in the literature prior to this thesis work; however, they can offer many possibilities for new material design and development, in view of the synthetic versatility of the carboxyl group towards various commonly used linkage groups (*e.g.*, amides, esters). The carboxyl group also presents an effective ligand to coordinate with transition metal ions, which in turn provides synthetic access to novel organic-inorganic hybrid materials, such as MOFs. Along this line, Chapter 2 of this thesis describes the study of carboxylated TTFVs in terms of synthesis, electronic properties, and interactions with Zn(II) ion to form organic-inorganic hybrid materials.

Aside from materials/application-oriented studies, the fundamental structural and reactivity properties of TTFV derivatives still need more research efforts to be well understood. So far, most of the TTFV compounds reported in the literature are phenyl-derived, wherein the phenyl groups are substituted by different groups at *ortho*, *meta*, and/or *para* positions. Therefore, the effect of regioisomeric substitution is a topic of significant fundamental interest, because the substitution motif plays

an important role in controlling the structure and properties of a TTFV compound. To shed more light on this aspect, a systematic investigation of various alkynyl-substituted phenyl TTFV regioisomers has been carried out. with the main objective targeted at elucidating the substitution effect on the structural, electronic properties, and related redox reactivity. The detailed results of this study are outlined in Chapter 3.

Chapter 2

Carboxyl-Substituted Tetrathiafulvalene Vinylogues and Related Metal-Organic Hybrids

2.1 A Brief Introduction to Metal-Organic Frameworks

A metal-organic framework, abbreviated as MOF, is a coordination polymer with an open framework containing potential voids. The coordination polymer refers to a coordination compound continuously extending in one, two or three dimensions through coordination bonds.[34] MOFs were first invented by Yaghi's group in the late 1990s. The emergence of MOFs as a new class of functional porous materials immediately attracted a broad attention and quickly became a very hot research area in modern materials science and engineering.[35–42] Currently, MOFs have found extensive uses

in gas storage, separation, catalysis and chemical sensing, while new applications in pharmaceuticals, drug delivery, and medicinal imaging are being actively pursued. MOFs are built up with organic ligands and metal ions. The organic ligands are usually carboxylate or pyridine derivatives, while the metal ions can be zinc, copper, nickel, manganese, ruthenium, and other transition metals. Since the formation of coordination bonds between ligands and metal ions is spontaneous, the synthesis of MOFs can be done under mild conditions, which is another advantage of MOFs.[36,43–48]

MOF-5, which is a classic example of MOFs,[49] is made of 1,4-benzene- dicarboxylate and zinc ions (Figure 2.1). The benzenedicarboxylate acts as a linkage between two zinc centers, and each zinc center coordinates with six benzenedicarboxylate ligands. In this way, the structure of MOF-5 is extend three-dimensionally to form a highly ordered polymeric network made up of numerous cubic units. The cavity in each cubic unit constitutes the micropore in MOF-5. As such, MOF-5 was found to feature an outstanding surface area of 3000 m^3 g^{-1} and rich porosity suitable for adsorption of methane (*i.e.*, gas storage).[50]

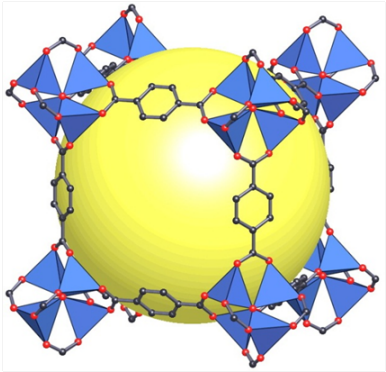

Figure 2.1: Single crystal structure of MOF-5. Color scheme is as follows: Zn (blue polyhedra), O (red spheres), C (black spheres). From [Eddaoudi, M.; Kim, J.; Rosi, N.; Vodak, D.; Wachter, J.; O'Keeffe, M.; Yaghi, O. M. *Science* **2002**, *295*, 469-472.]. Reprinted with permission from AAAS.

Very recently, some TTF-based ligands have been employed to make organic-inorganic hybrid materials with redox activity; for example, the two MOFs **33** and **34** illustrated in Figures 2.2 and 2.3.[51–54] Typical MOFs are insulators and therefore not quite suitable for applications where high charge mobility is needed for porous materials based devices (*e.g.*, fuel cells, supercapacitors, and batteries). The introduction of redox-active TTF units into the MOF backbones allows the charge mobility to be significantly improved and thus opens the door to more useful applications in electronic and optoelectronic devices. Similar to TTF, TTFVs can also serve as excellent electron donors to give rise to high electrical conductivity upon doping. Moreover, the redox-controlled conformational switching behavior of TTFVs make them intriguing stimuli-responsive building blocks to form framework systems with interesting structural dynamic equilibrium. Since the use of TTFVs as ligands for MOFs has never been reported in the literature previously, the main objective of the work described in

this chapter is focused on investigating the potential of carboxylated TTFVs as functional structural components in the preparation of MOFs and/or related microporous materials.

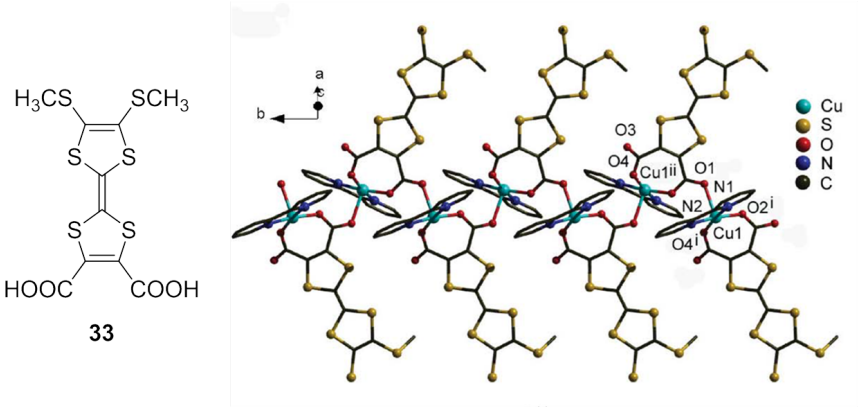

Figure 2.2: Structure of the TTF-dicarboxylate ligand **33** (left), and the coordination polymer of **33** with copper(II) (right). Reproduced from Ref. 51 with permission from The Royal Society of Chemistry.

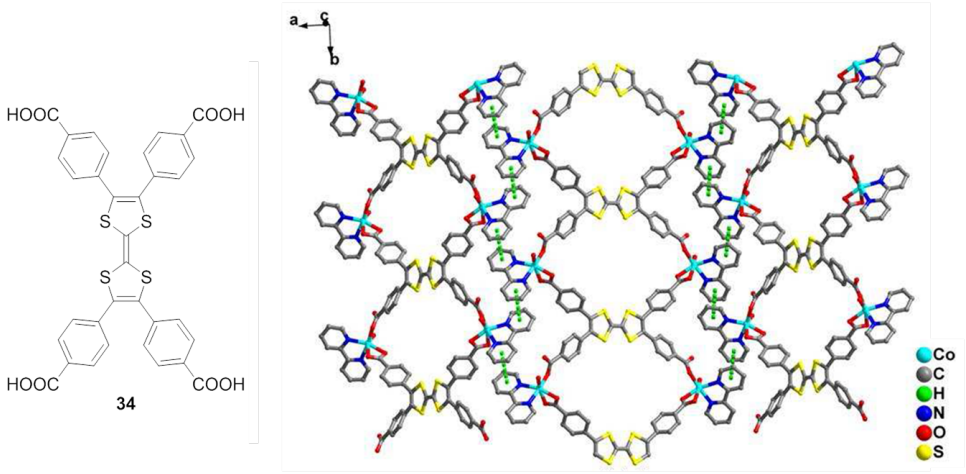

Figure 2.3: Structure of the TTF-tetrabenzoate ligand **34** (left), and the coordination polymer of **34** with cobalt(II) (right). Reprinted (adapted) with permission from (Chen, B.; Lv, Z.-P.; Leong, C. F.; Zhao, Y.; D'Alessandro, D. M.; Zuo, J. -L. *Cryst. Growth Des.* **2015**, *15*, 1861-1870.). Copyright (2015) American Chemical Society.

2.2 Results and Discussion

2.2.1 Synthesis of Carboxylated DTFs and TTFVs

In this work, a carboxyl-substituted TTFV compound **16** (Figure 2.4) was synthesized as a redox-active organic ligand for coordination with zinc ions to pursue microporous coordination polymers. The carboxylate can act as a monodentate, chelating bidentate or bridging bidentate ligand, through which three-dimensional coordination polymers might be generated.[55] The zinc ion can form a strong coordination bond with the carboxylate, yielding a tetrahedral or octahedral coordination geometry at the metal center.[56] If the coordination polymer forms a three-dimensional crystalline

structure, it is more likely to give rise to a very high degree of porosity and extremely large surface area.

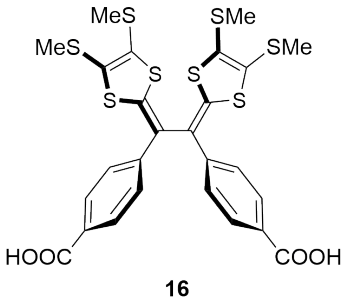

16

Figure 2.4: Carboxyl-substituted TTFV ligand **16**.

The synthesis of carboxyl-TTFV **16** and its DTF precursor **15** was conducted via a route well established for similar aryl-substituted TTFV derivatives.[26,27] As shown in Scheme 2.1, thione **11** was first reacted with benzaldehyde **12** in the presence of trimethylphosphite at 105 °C.[30] This olefination reaction went completion within 3 hours to give DTF **13** in 77% yield after column chromatographic separation. Compound **13** was then subjected to an oxidative dimerization in CH_2Cl_2 at room temperature using iodine as oxidant. The dimerization reaction afforded TTFV **14** as a stable yellow solid in 80% yield. Saponification was then performed on compound **14** in a solution of NaOH in water and methanol to finally yield carboxyl-TTFV **16** in 84% yield. Compound **16** showed relatively poor solubility in non-polar organic solvents, but could be readily dissolved in polar organic solvents such as MeOH, EtOH, THF, and DMSO.[57] For comparison purposes, carboxyl-DTF **15** was also prepared through hydrolysis of DTF **13** under similar reaction conditions to the synthesis of **16**.

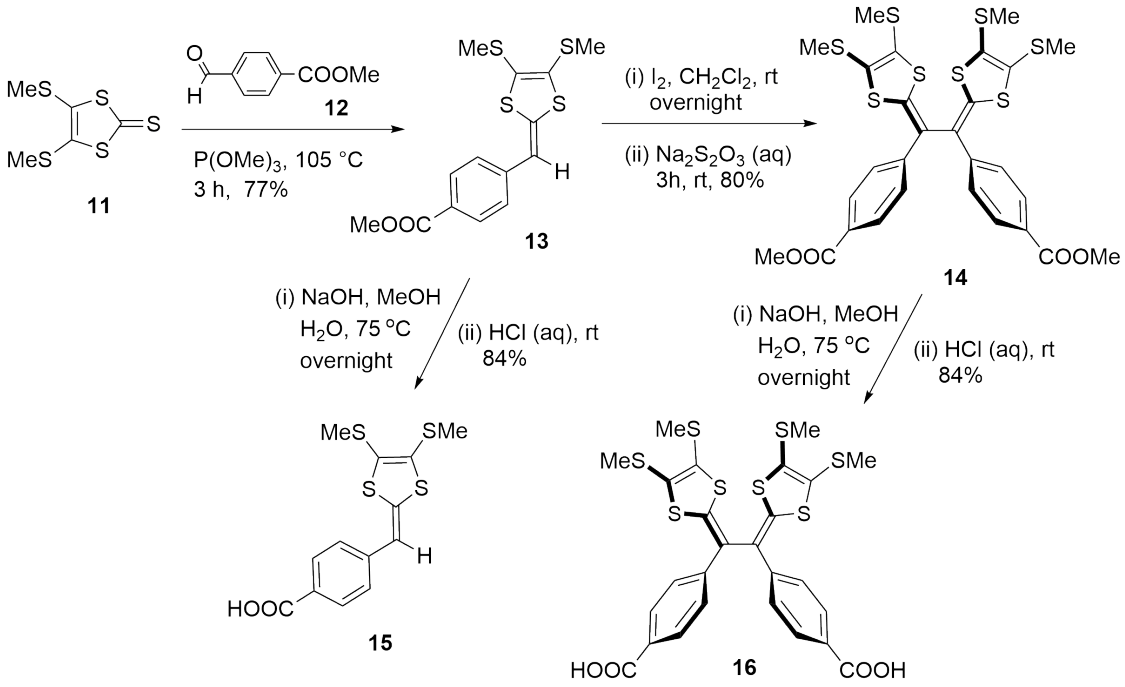

Scheme 2.1: Synthesis of carboxyl-substituted TTFV **16** and DTF **15**.

2.2.2 Characterizations of Carboxylated DTFs and TTFVs

The electronic properties of TTFVs **14** and **16** as well as their DTF precursors **13** and **15** were investigated by UV-Vis absorption spectroscopy. Figure 2.5 shows the UV-Vis absorption spectra of these compounds, in which the maximum absorption wavelengths (λ_{max}) of all the compounds appear to be nearly identical at *ca.* 385 nm. There are, however, slight variations in the cut-off energies of long-wavelength absorption bands. To further understand the origins of these long-wavelength absorption bands, time-dependent density functional theory (TD-DFT) calculations were conducted using the *Gaussian 09* software package (see Table 2.1 for details).

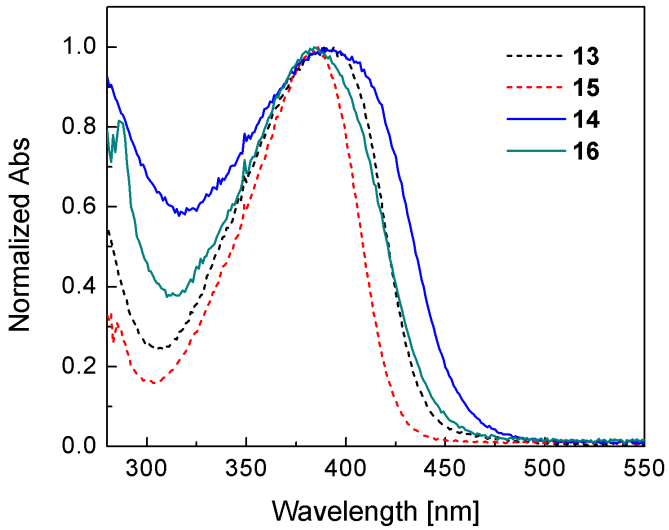

Figure 2.5: UV-Vis spectra of TTFVs **14** and **16** (solid lines) and DTF **13** and **15** (dashed lines). Compounds **13** and **14** were measured in CH_2Cl_2, while compounds **15** and **16** were in THF.

In the DFT calculations, the molecular geometries of **16** and **15** were first optimized at the B3LYP/6-31G(d) level of theory and were validated to be the global energy minima by frequency check (*i.e.*, zero imaginary frequency). Figures 2.6 and 2.7 show the calculated structures of compounds **15** and **16**. As can be seen, the structure of TTFV **16** is highly twisted, suggesting poor π-electron delocalization across the entire molecular structure. The structure of **15**, however, is less sterically crowded and thus more planar in structure. The optimized structures were then subjected to TD-DFT calculations at the same level of theory, taking only singlet transitions into consideration (nstate = 20). Table 2.1 summarizes the significant electronic transitions as well as the energies and assignments of MO characters related to them.

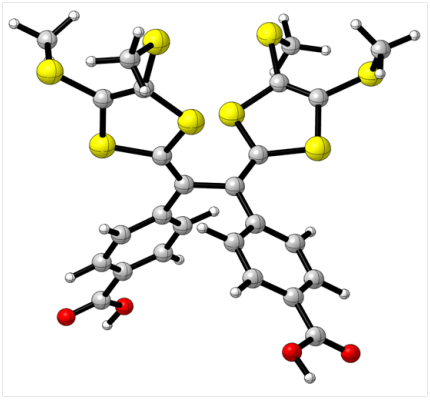

Figure 2.6: Optimized geometry of compound **16** at the B3LYP/6-31G(d) level.

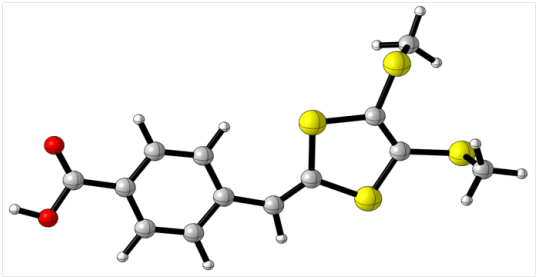

Figure 2.7: Optimized geometry of compound **15** at the B3LYP/6-31G(d) level.

The UV-Vis data and DFT calculation results point to that the degrees of π-delocalization for the TTFVs and DTF compounds are quite similar. This outcome is congruous with the fact that diphenyl-TTFVs generally prefer a twisted *cisoid* conformation in the ground state, which in theory significantly disrupts the π-delocalization within the molecules.[15,18,19] Therefore, even though the molecular sizes of TTFVs **14** and **16** are doubled in comparison with their DTF precursors **13** and **15**, the degrees of π-electron delocalization in these molecules are still retained at a similar level in the ground state.

Entry	λ_{cacld} (nm)	f	MO Character	λ_{obs} (nm)
16	412.24	0.1565	H-1 → L+1 (0.15720), H → L (0.68251)	386
	357.08	0.1277	H-1 → L+1 (-0.36323), H → L+3 (0.59044)	
	355.07	0.3012	H-1 → L+1 (0.64406), H → L (-0.14195), H → L+2 (0.20536), H → L+5 (-0.11757)	
	291.54	0.1378	H-1 → L+5 (0.56611), H → L+4 (0.26197), H → L+6 (0.24790), H → L+8 (0.16802)	289
15	363.05	0.1793	H → L (0.32141), H → L+1 (0.59046), H → L+2 (0.20277)	385
	359.62	0.5263	H → L (0.59860), H → L+1 (-0.35664)	256
	243.74	0.2305	H-4 → L (0.52610), H → L+4 (0.41511), H → L+5 (0.12900)	

Table 2.1: Summary of TD-DFT calculation results for compounds **16** and **15**. (Only transitions with oscillator strength (f) greater than 0.1 are listed.)

2.2.3 Preparation of Zn-TTFV Coordination Products

With carboxyl-TTFV **16** in hand, the preparation of coordination products with Zn(II) ions was undertaken. As outlined in Scheme 2.2, compound **16** was first mixed with two molar equivalents of $Zn(NO_3)_2{\cdot}6H_2O$ in EtOH, and to this solution triethylamine was allowed to slowly diffuse in.[43,58] In a period of 4 days, coordination

product **18** was gradually formed as a yellow colored solid, which was insoluble in common solvents. By the same approach, the complex of carboxyl-DTF **15** with Zn(II) ions was also produced as a yellow powder. When the coordination product **18** was oxidized or acidified, it changed color dramatically (Figure 2.8), which can be attributed to the redox characteristics of TTFV (see Scheme 2.3).

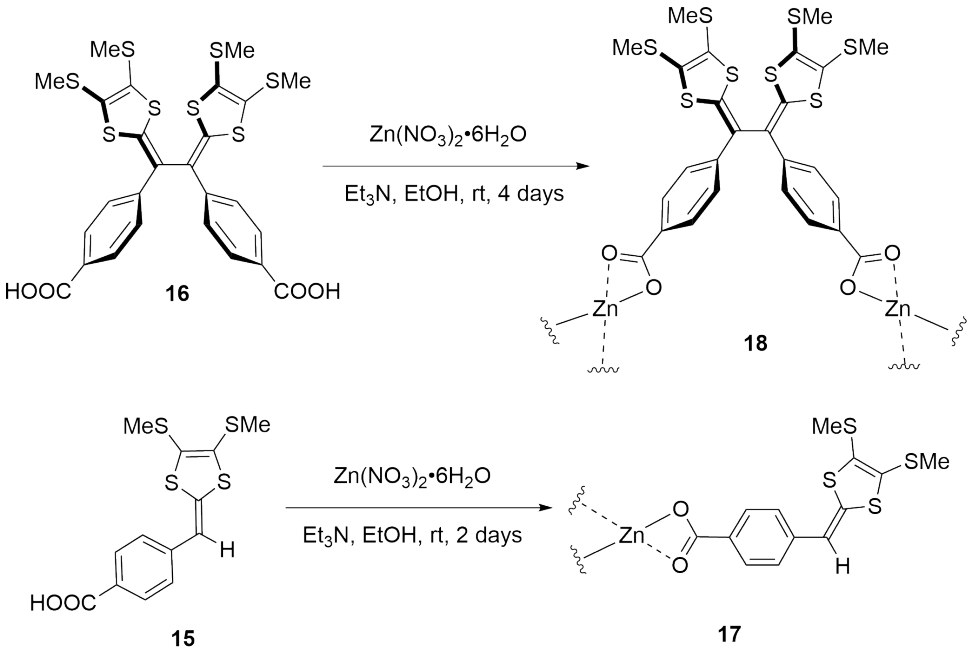

Scheme 2.2: Preparation of coordination products **17** and **18**.

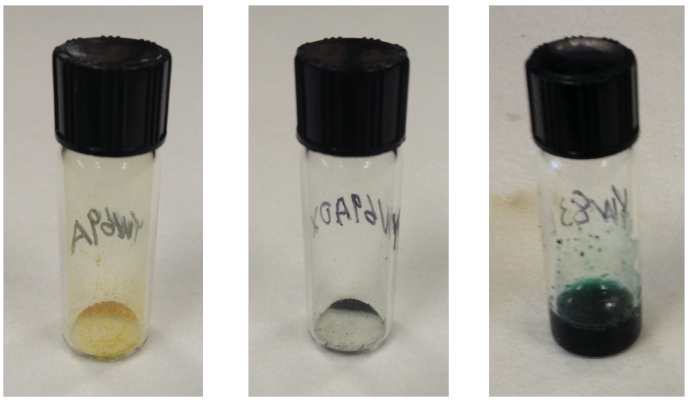

Figure 2.8: Photographs of compound **18** in different states: neutral (left), oxidized by I_2 vapor (middle), acidified by H_2SO_4 (right).

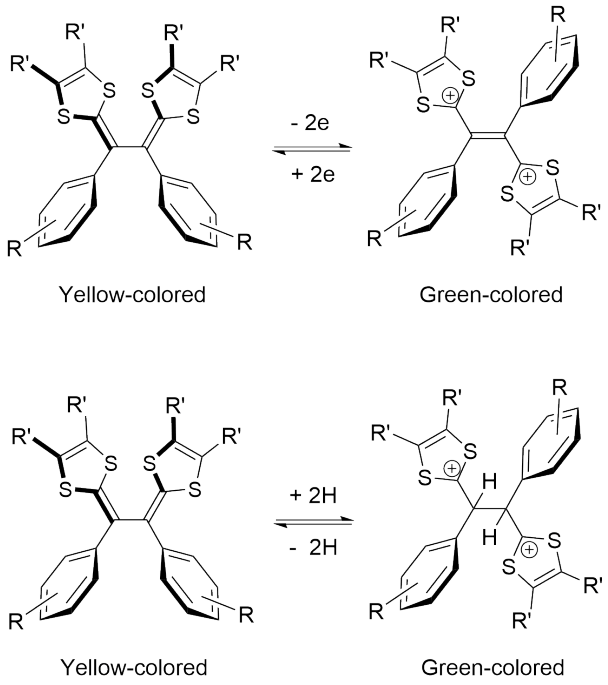

Scheme 2.3: Mechanism of the color change of aryl-substituted TTFVs.

2.2.4 Characterization of Zn-TTFV Coordination Products

The structural properties of Zn-TTFV coordination product **18** and Zn-DTF complex **17** were examined by IR spectroscopy (Figure 2.9). Compared with the IR spectra of carboxyl-TTFV **16** and carboxyl-DTF **15**, the vibrational bands of free carboxyl groups were evidently absent in the spectra of **18** and **17**, confirming that the carboxyl groups were completely coordinated with Zn(II) ions.

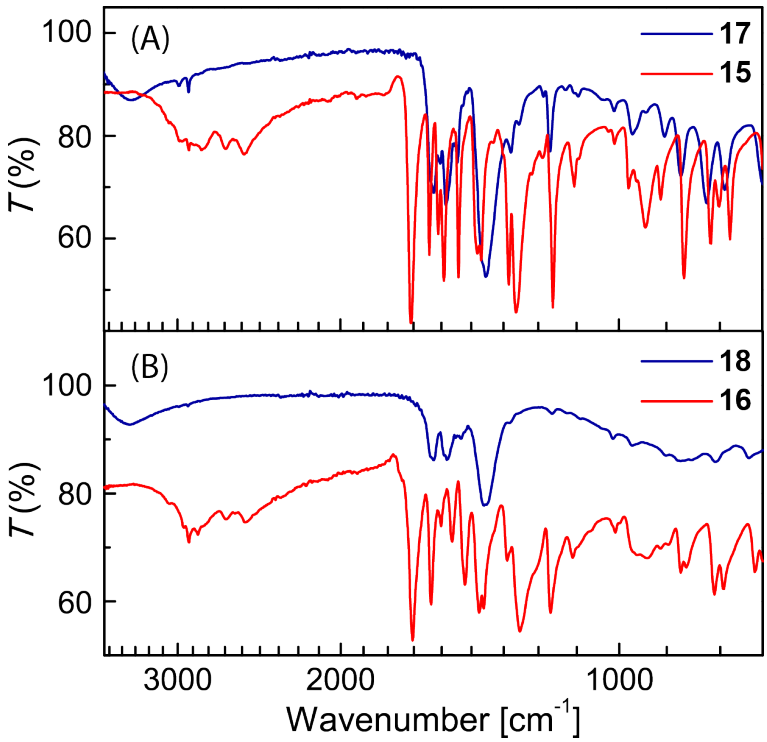

Figure 2.9: FTIR spectra of compounds **15**-**18**.

The crystalline properties of the coordination product **18** were examined by powder X-ray diffraction (PXRD) analysis. The diffraction patterns were found to be those of zincite, which is a mineral form of ZnO (Figure 2.10). The PXRD results suggest that the synthesis of coordination product **18** also generated ZnO as

a byproduct. As all the diffraction peaks in the XRD spectrum belong to ZnO, it is believed that ZnO is the only crystalline component the product mixture. Two possible scenarios can then be conceived to account for the composition of the coordination product **18**: (i) It is a mixture of amorphous Zn-TTFV coordination polymers contaminated with some crystalline ZnO byproduct; (ii) There was no complexation happened between Zn(II) ions and the carboxyl-TTFV ligand; instead, the TTFV ligand was only bonded to the ZnO surface after ZnO was generated. To clarify this issue, a control experiment in which carboxyl-TTFV **16** was mixed with ZnO directly under the same conditions of the preparation of compound **18** was conducted. The resulting solid product of this exeperiment was analyzed by IR spectroscopy (Figure 2.11), and the data clearly rules out the second scenario, since no IR bands due to organic compounds can be observed in the IR spectrum. Clearly, the carboxyl-TTFV **16** ligand does not complex with ZnO. This therefore corroborates first scenario proposed above. The coordination product **18** was formed as expected, but it was not the only product of the synthesis. Some ZnO was also formed possibly by the reaction of Zn(II) ion with residual H_2O in the solvent under basic conditions. The $Zn(OH)_2$ was then slowly converted into ZnO, but not as a major component in the complexation product. In the future work, more carefully controlled experimental conditions, such as the use of an air-tight hydrothermal reactor with inert gas protection, should be adopted to avoid the formation ZnO.

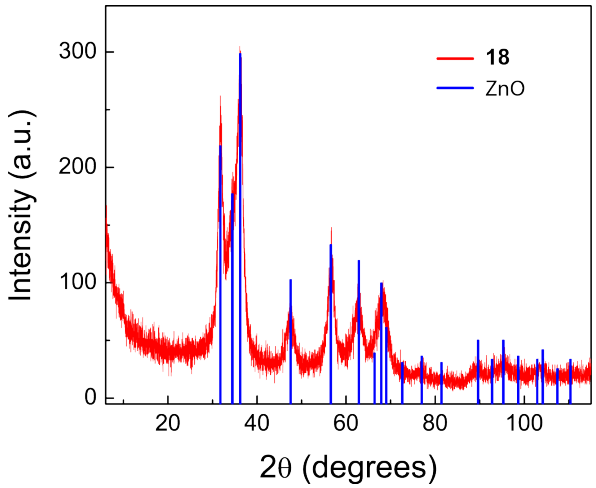

Figure 2.10: PXRD patterns of the coordination product **18** (red line) in comparison with the diffraction data of zincite ZnO (blue bars).

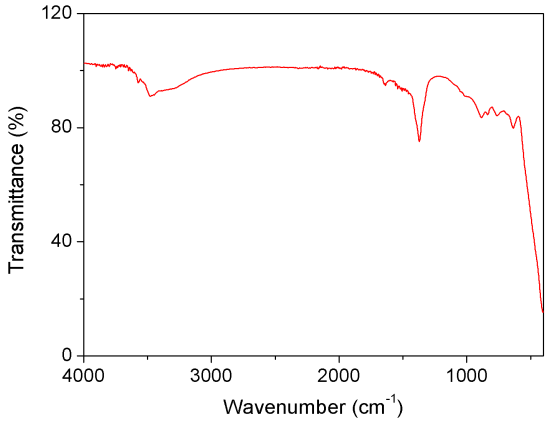

Figure 2.11: FTIR spectrum of the coordination product of **16** with ZnO.

The coordination product **18** after oxidation with iodine vapour showed the same diffraction patterns to its neurtral state; that is, only the signals of ZnO are present (Figure 2.12). This result indicates that the oxidized Zn-TTFV coordination product is still non-crystalline. The crystalline properties of Zn-DTF complex **17** were also examined by powder X-ray diffraction (PXRD) analysis. Neither crystalline Zn-DTF structures nor ZnO could be seen from the diffraction data (Figure 2.13). One possible explanation is that the reaction between carboxyl-DTF **15** and Zn(II) ions was much faster than that of carboxyl-TTFV **16**, leading to the formation of only amorphous coordination product. In the meantime, most the Zn(II) ions were consumed by complexation with **15**, leaving little chance for the ZnO byproduct to form

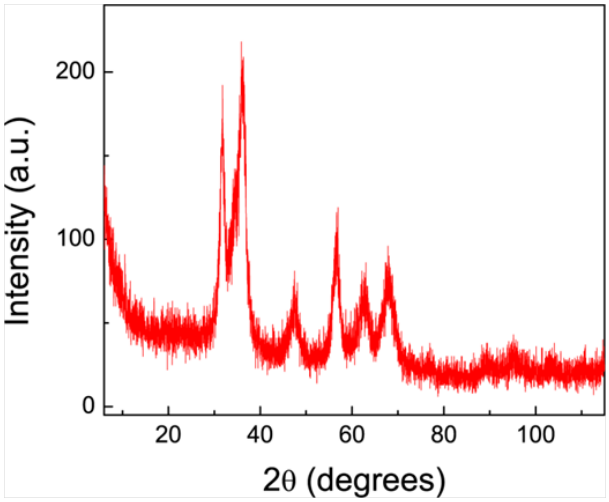

Figure 2.12: PXRD patterns of the coordination product **18** after oxidation with iodine vapour.

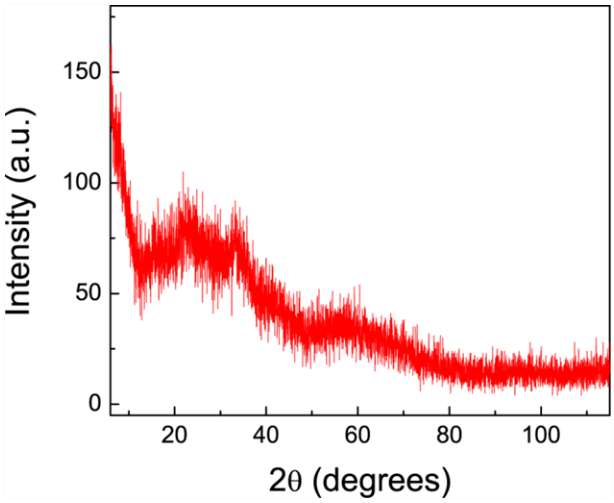

Figure 2.13: PXRD patterns of Zn-DTF complex **17**.

To assess the porous properties of the coordination product **18**, nitrogen gas adsorption analysis was conducted at 77 K. The adsorption isotherm shown in Figure 2.14 indicates a Type-II adsorption behavior. Application of the Brunauer-Emmett-Teller (BET) model gave a BET surface area of 148.2 m^2 g^{-1} and an adsorption average pore diameter of 10.2 nm. This surface area is smaller than that of pure ZnO particles and the average pore diameter is larger.[59–61] The result indicates that the Zn-TTFV coordination product within the mixture **18** does not give a significant degree of microporosity, thus decreasing the surface area of the mixture compared with pure ZnO particles. Nitrogen gas adsorption experiments were also performed on Zn-DTF complex **17**. The experimental results did not lead to any meaningful measurements of BET surface area and microporosity, indicating a lack of porous structures in the solid of **17**.

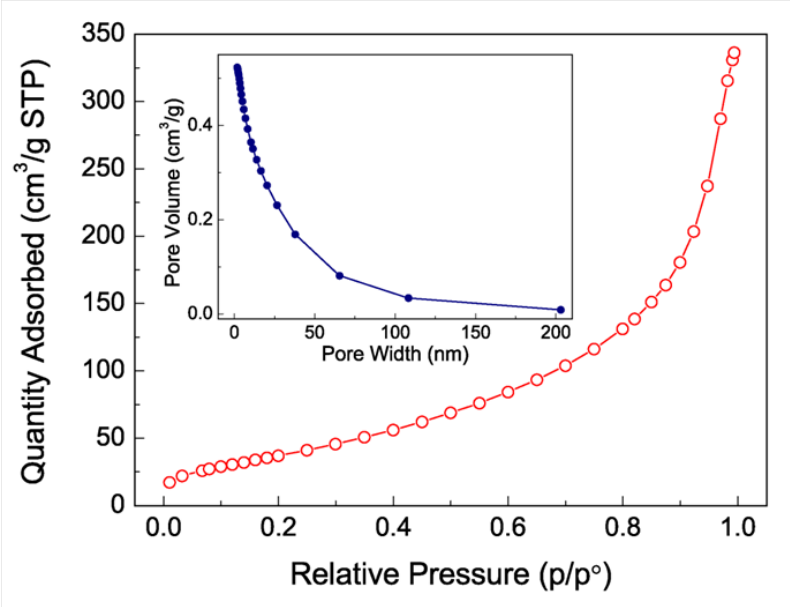

Figure 2.14: Nitrogen adsorption isotherm of coordination product **18** measured at 77 K. Inset: pore size distributions.

The electrochemical redox properties of compounds **13**-**18** were characterized by cyclic voltammetry, and the detailed cyclic voltammograms are shown in Figure 2.15. For methyl ester-appended DTF **13** (Figure 2.15A), an anodic peak was observed at +0.82 V in the first cycle of scan, which is due to the single-electron oxidation of the dithiole moiety into the dithiolium radical cation. In the reverse scan, a cathodic peak emerged at +0.54 V which is assigned to the bielectronic reduction of the TTFV product electrochemically generated on the electrode surface via the DTF dimerization reaction.[18,19] In the following scan cycles, the redox wave pair characteristic of TTFV at Epa = +0.62 V and Epc = +0.54 V was found to gradually increase in intensity as a result of increasing electrochemical dimerization. The same electrochemical redox patterns can be seen in the cyclic voltammograms of carboxyl-DTF **15** and Zn-DTF complex **17** (Figure 2.15C and 2.15E); however, their redox poten-

tials showed a slight degree of variation. Experimentally, the cyclic voltammogram of **17** was determined from its solid thin film compressed on the working electrode surface. It is interesting to note that Zn-DTF complex **17** retained the redox activity and electrochemical reactivity of DTF even in the solid state.

The cyclic voltammograms of compounds **14** and **16** both featured a reversible redox wave pair due to the simultaneous bielectronic transfers occurring at the TTFV moieties (Figure 2.15B and 2.15D). In the cyclic voltammogram of Zn-TTFV coordination product **18** (measured from a solid film prepared in the same way as **17**), the redox wave pair of TTFV is discernible but much weaker than that of Zn-DTF complex **17** (Figure 2.15F), suggesting that the electrochemical activity of Zn-TTFV coordination product is considerably reduced in comparison with the smaller-sized Zn-DTF complex.

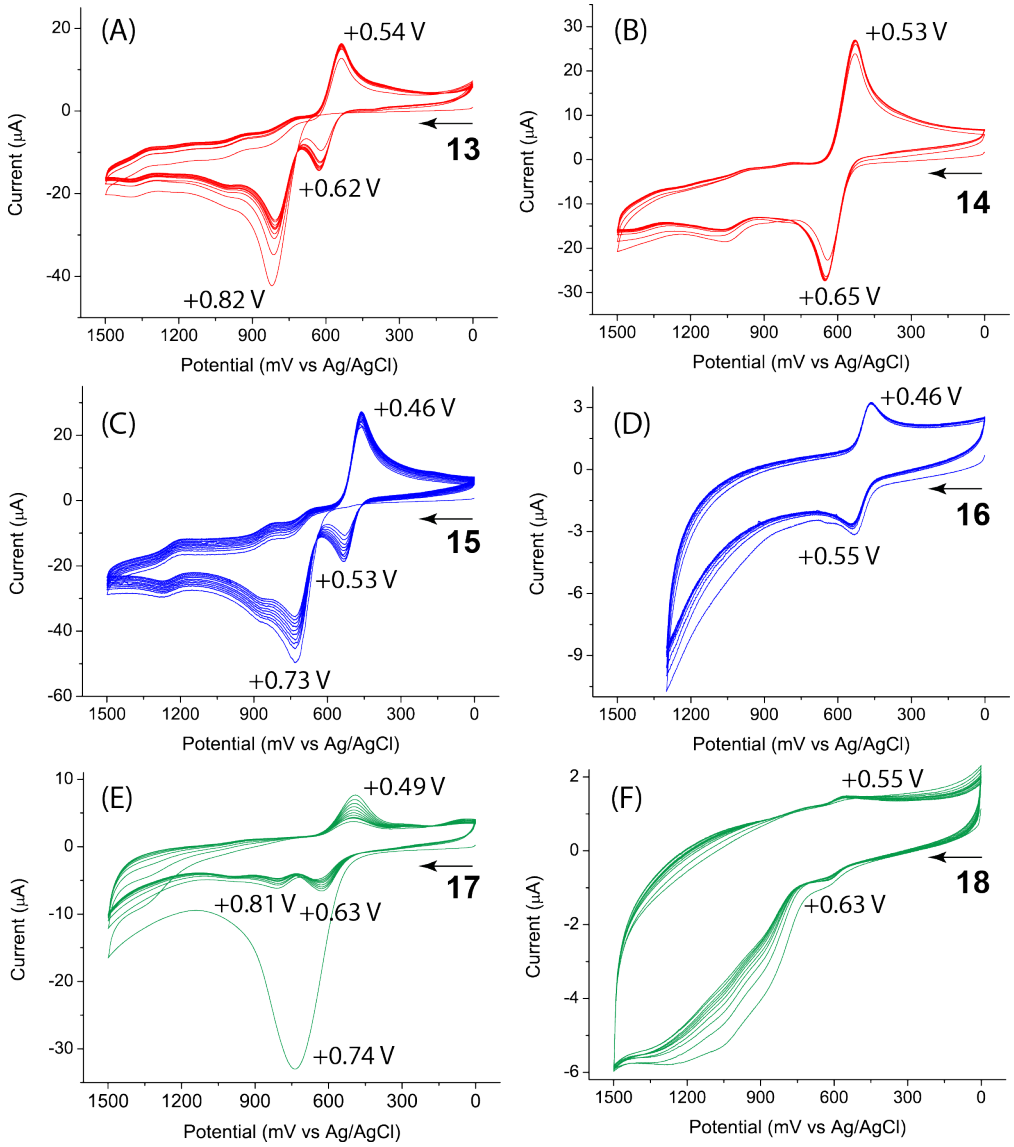

Figure 2.15: Cyclic voltammograms of compounds **13**-**18**. Experimental conditions: supporting electrolyte: Bu_4NBF_4 (0.1 M), working electrode: glassy carbon, counter electrode: Pt wire, reference electrode: Ag/AgCl (3 M NaCl), scan rate: 200 mV s^{-1}. Compounds **13** (1.5 mM), **14** (0.73 mM), **17** (solid film), and **18** (solid film) were measured in CH_2Cl_2. Compounds **16** (0.76 mM) and **15** (1.5 mM) were measured in CH_3CN.

The thermal stability of coordination product **18** and Zn-DTF complex **17** were evaluated by differential scanning calorimetric (DSC) analysis, and the measured DSC traces are illustrated in Figure 2.16. The DSC data of Zn-TTFV **18** (Figure 2.16A) manifested very good thermal stability up to 400 °C, without any significant melting or decomposition except a slight phase transition at 272 °C. Comparatively, the DSC trace of carboxyl-TTFV ligand **16** showed a distinctive melting process at 317 °C, which was immediately followed by a prominent sharp exothermic peak at 326 °C (Figure 2.16B). The exothermic process is possibly due to a chemical reaction(s); however, the exact reaction awaits further investigation to clearly elucidate. Zn-DTF **17** gave a moderate endothermic peak at 152 °C and a significant exothermic peak at 358 °C (Figure 2.16C). For carboxyl-DTF **15**, a notable melting point was observed at 199 °C, and the melting was followed by certain exothermic processes in the range of 200 to 285 °C. The DSC results indicated that the formation of Zn-TTFV coordination product could give rise to considerably improved thermal stability, a property particularly beneficial for practical device and material applications.

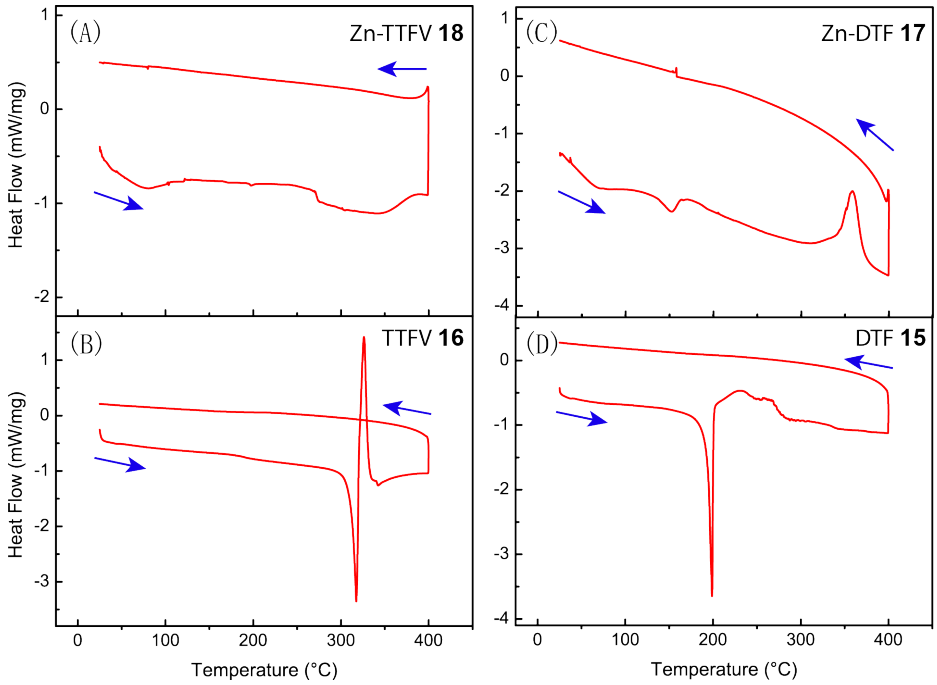

Figure 2.16: DSC traces of compounds **15-18** measured under a nitrogen atmosphere. Scan range: 25-400 °C, scan rate: 10 °C min^{-1}.

2.3 Conclusions

In summary, carboxyl-TTFV **16** and carboxyl-DTF **15** have been synthesized as redox-active ligands to coordinate with zinc ions. The electronic and electrochemical properties of the TTFV and DTF compounds were found to be in line with other related TTFV and DTF derivatives. Of great interest is that the coordination products with Zn(II) ions retain the redox activity and electrochemical reactivity of their TTFV and DTF ligands in the solid state. Another significant added value is the thermal robustness of the Zn-TTFV coordination product. Collectively, the good electrochemical and thermal properties point to a promising prospect for them to be

further developed into practically useful organicinorganic hybrid materials through the coordination approach. The Zn-TTFV coordination product unfortunately did not give desirable crystallinity and microporosity. At this stage, meaningful single-crystal diffraction data has not yet been successfully determined. Without such data clear understanding of the detailed solid-state structural properties cannot be established. The observation of ZnO byproduct in the synthesis of Zn-TTFV complex suggests that the amine diffusion method is not ideal for the coordination polymer formation. One major effort in the the future work should thus be concentrated on searching for the optimal conditions to allow crystalline coordination polymer to be formed in high purity. In this aspect, the commonly used hydrothermal conditions for MOF synthesis deserve a favorable consideration. Another effort should be made is to tune the side groups of the TTFV ligand to produce zinc coordination products with better crystallinity. Overall, the current work has cast a light on the fundamental redox and solid-state properties of the class of TTFV-based organic-inorganic hybrid materials, and the findings disclosed should offer useful guidance to further material design and development.

2.4 Experimental Procedures

Chemicals were purchased from commercial suppliers and used directly without purification. All reactions were conducted in standard, dry glassware and under an inert atmosphere of nitrogen unless otherwise noted. Evaporation and concentration were carried out with a water-aspirator. Flash column chromatography was performed with silica gel 60 (240-400 mesh). Thin-layer chromatography (TLC) was carried out

with silica gel F254 covered on plastic sheets and visualized by UV light. Melting points were measured on an SRS OptiMelt melting point apparatus. ^{1}H and ^{13}C NMR spectra were measured on a Bruker Avance III 300 MHz multinuclear spectrometer. Chemical shifts (δ) are reported in ppm downfield relative to the signal of the internal reference $SiMe_4$. Coupling constants (J) are given in Hz. Infrared spectra (IR) were recorded on a Bruker Alfa spectrometer. HRMS analyses were performed on an Agilent 6230 TOF LC/MS instrument using an APPI ionizer. UV-Vis absorption spectra were measured on a Cary 6000i spectrophotometer. Cyclic voltammetric analyses were carried out in a standard three-electrode setup controlled by a BASi epsilon workstation. Differential scanning calorimetric (DSC) analyses were performed on a Mettler-Toledo DSC1 calorimeter. Powder X-ray diffraction (PXRD) data was collected on a Rigaku Ultima IV diffractometer equipped with a copper X-ray source at the wavelength of 1.54 nm. Scanning electron microscopy (SEM) was performed on an FEI MLA 650 FEG microscope. BET surface area and pore size analyses were performed on a Micromeritics TriStar II Plus instrument. The degassing was done on a Flow Prep 060 instrument. The calculations were carried out with the MicroActive for TriStar II Plus software (Version 2.02). Thione **11** was prepared according to literature procedures.[32,62]

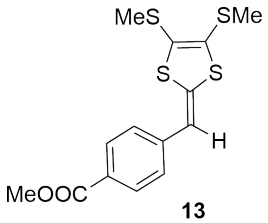

13

DTF 13: A mixture of methyl 4-formylbenzoate **12** (1.83 g, 11.1 mmol) and

thione **11** (3.03 g, 13.4 mmol) in $P(OMe)_3$ (100 mL) was stirred and heated at 105 °C for 3 h. The excess $P(OMe)_3$ was removed by vacuum distillation. The residue was purified by silica column chromatography (EtOAc/hexanes, 1:9) to afford compound DTF **13** (2.93 g, 8.55 mmol, 77%) as a yellow crystalline solid. mp 88.6–90.9 °C; ^{1}H NMR (300 MHz, $CDCl_3$) δ 8.01 (d, J = 8.4 Hz, 2H), 7.25 (d, J = 8.3 Hz, 2H), 6.51 (s, 1H), 3.91 (s, 3H), 2.45 (s, 3H), 2.44 (s, 3H); ppm; ^{13}C NMR (75 MHz, $CDCl_3$) δ 166.8, 140.5, 136.2, 129.9, 127.9, 126.7, 126.3, 124.5, 113.3, 52.0, 19.0, 18.9 ppm; FTIR (neat): 2914, 1704, 1599, 1567, 1545, 1492, 1422, 1265, 1175, 1096, 851, 798, 693, 470 cm^{-1}; APPI-HRMS (m/z, positive mode): [M^+] calcd for $C_{14}H_{14}O_2S_4$, 341.9877; found, 341.9878.

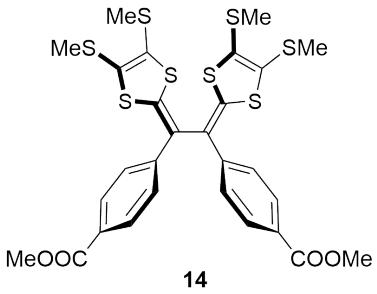

14

TTFV 14: A mixture of DTF **13** (0.25 g, 0.73 mmol) and I_2 (0.55 g, 2.2 mmol) in CH_2Cl_2 (100 mL) was stirred at rt overnight. Then a satd $Na_2S_2O_3$ solution (aq, 90 mL) was added. The mixture was stirred for another 3 h at rt. The organic layer was separated, washed with H_2O, dried over $MgSO_4$, and concentrated under vacuum. The residue was purified by silica column chromatography (EtOAc/hexanes, 1:4) to afford compound **14** (0.20 g, 0.29 mmol, 80%) as a yellow solid. mp 183.9–185.4 °C; ^{1}H NMR (300 MHz, $CDCl_3$) δ 7.97 (d, J = 8.7 Hz, 4H), 7.46 (d, J = 8.7 Hz, 4H), 3.89 (s, 6H), 2.44 (s, 6H), 2.38 (s, 6H) ppm; ^{13}C NMR (75 MHz, $CDCl_3$)

δ 166.6, 141.1, 140.3, 130.1, 129.1, 127.9, 126.1, 125.5, 122.9, 52.0, 18.9, 18.8 ppm; FTIR (neat): 2942, 2918, 1709, 1600, 1519, 1473, 1430, 1273, 1182, 1107, 766, 713, 465 cm^{-1}; APPI-HRMS (*m/z*, positive mode): [M^+] calcd for $C_{28}H_{26}O_4S_8$, 681.9597; found, 681.9584.

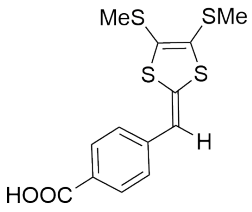

15

Carboxyl-DTF 15: A mixture of DTF **13** (0.30 g, 0.88 mmol) and NaOH (0.56 g, 14 mmol) in MeOH/H_2O (240 mL, 3:1) was stirred at 75 °C overnight. The solvent MeOH was removed under vacuum, and the residue was diluted to 100 mL with H_2O and acidified to pH 4 with HCl (aq). The precipitate formed was subjected to suction filtration to afford compound **15** (0.24 g, 0.73 mmol, 84%) as a yellow solid. mp 191.0–193.2 °C; ^{1}H NMR (300 MHz, DMSO-d_6) δ 12.86 (s, 1H), 7.94 (d, J = 8.4 Hz, 2H), 7.32 (d, J = 8.3 Hz, 2H), 6.82 (s, 1H), 2.47 (s, 3H), 2.45 (s, 3H) ppm; ^{13}C NMR (75 MHz, DMSO-d_6) δ 166.9, 139.7, 134.6, 129.7, 127.4, 127.3, 126.3, 122.7, 113.7, 18.3, 18.1 ppm; FTIR (neat): 2914-2540 (br), 1677, 1602, 1567, 1545, 1490, 1408, 1291, 1178, 850, 796, 505, 470 cm^{-1}; APPI-HRMS (*m/z*, negative mode) [M^-] calcd for $C_{13}H_{12}O_2S_4$, 327.9720; found, 327.9727.

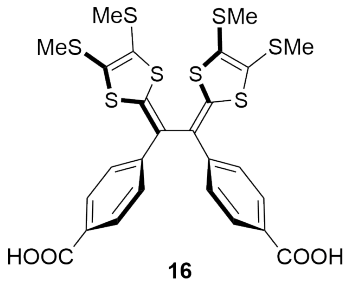

16

Carboxyl-TTFV 16: A mixture of TTFV **14** (50.0 mg, 0.0732 mmol) and NaOH (46.9 mg, 1.17 mmol) in MeOH/H_2O (40 mL, 3:1) was stirred at 75 °C overnight. The solvent MeOH was removed under vacuum, and the residue was diluted to 50 mL with H_2O and acidified to pH 4 with HCl (aq). The precipitate formed was extracted with EtOAc, washed with H_2O, dried over $MgSO_4$, and concentrated under vacuum to afford compound **16** (40.3 mg, 0.0615 mmol, 84%) as a yellow solid. mp 292.9–295.7 °C; ^{1}H NMR (300 MHz, DMSO-d_6) δ 7.94 (d, J = 8.5 Hz, 4H), 7.48 (d, J = 8.4 Hz, 4H), 2.48 (s, 6H), 2.40 (s, 6H) ppm; ^{13}C NMR (75 MHz, DMSO-d_6) δ 166.7, 140.0, 139.1, 130.0, 128.8, 126.8, 125.9, 125.1, 122.7, 18.22, 18.20 ppm; FTIR (neat): 2916-2536 (br), 1672, 1596, 1515, 1467, 1416, 1280, 1186, 789, 541, 469 cm^{-1}; APPI-HRMS (m/z, negative mode) [M$^-$] calcd for $C_{26}H_{22}O_4S_8$, 653.9284; found, 653.9293.

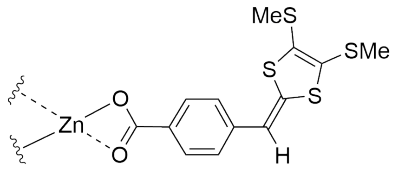

17

Zn-DTF 17: A solution of DTF **15** (20.0 mg, 0.0610 mmol) and $Zn(NO_3)_2{\cdot}6H_2O$ (21.8 mg, 0.0733 mmol) in EtOH (40 mL) was added into a vial, which was placed

in a jar containing Et_3N/EtOH (6 mL, 1:2). The jar was sealed and left standing for 2 days. The precipitate formed in the vial was collected by centrifugation and rinsed with EtOH to afford Zn-DTF **17** (15.1 mg) as a yellow solid. FTIR (neat): 3360, 2990, 2916, 1585, 1559, 1538, 1494, 1392, 1187, 803, 768, 472 cm^{-1}.

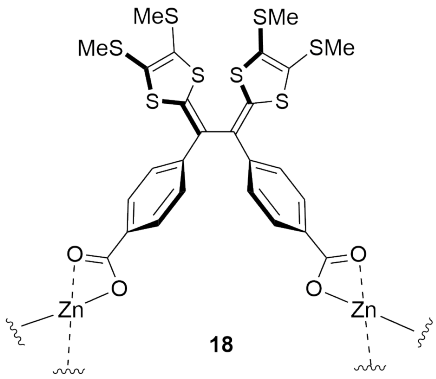

18

Zn-TTFV 18: A solution of TTFV **16** (0.12 g, 0.18 mmol) and $Zn(NO_3)_2{\cdot}6H_2O$ (0.11 g, 0.37 mmol) in EtOH (350 mL) was added into a beaker, which was placed in a larger beaker containing Et_3N/EtOH (40 mL, 1:1). The larger beaker was sealed and left standing for 4 days. The precipitate formed within the smaller beaker was collected by centrifugation and rinsed with EtOH to afford Zn-TTFV **18** (50.8 mg) as a yellow solid. FTIR (neat): 3381, 1586, 1535, 1400, 857, 787 cm^{-1}.

Chapter 3

Ethynyl-Substituted Tetrathiafulvalene Vinylogues

3.1 Introduction

The application of π-conjugated materials has achieved tremendous advancement in the cutting-edge fields such as molecular electronics, chemo-/bio-sensors, light-emitting devices, and organic photovoltaics.[63–69] From the chemistry perspective, continued efforts to explore π-molecular building blocks with novel properties and functions are still imperative and highly needed. Over the past few years, TTFVs have been used to prepare various π-conjugated systems.[20,22–24,26,27] Of note is the previous study by a former group member, Dr. Guang Chen, on certain alkynylated TTFV polymers **20** synthesized from the oxidative polymerization of oligoyne-centered dithiafulvene analogues **19** (Scheme 3.1).[26,27] The synthetic design in Chen's work utilized a linear-shaped oligoyne group in combination with two DTF end moi-

eties. The alkynyl and DTF groups were at *para* positions of a phenyl ring, as such the shape of the molecule was kept in a nearly linear structure. The oxidative coupling reactivity of the two DTF endgroups in compounds **19** make them prone to polymerization to form π-extended polymeric frameworks.[23,24,26,27,70] It has been found that the oligoyne-centered dithiafulvene analogues **19** could be efficiently polymerized through oxidative coupling reactions under chemical or electrochemical conditions. In particular, polymer thin films could be readily generated on conductive electrode surfaces (*e.g.*, glassy carbon and ITO) when compounds **19** were subjected to positive applied potentials under various electrochemical conditions. The resulting polymer films not only showed good conductivity but also retained the reversible redox activities of the TTFV units; for example, the CV profiles of polymers **20** in Figure 3.1 clearly show a reversible redox behavior typical of TTFV.

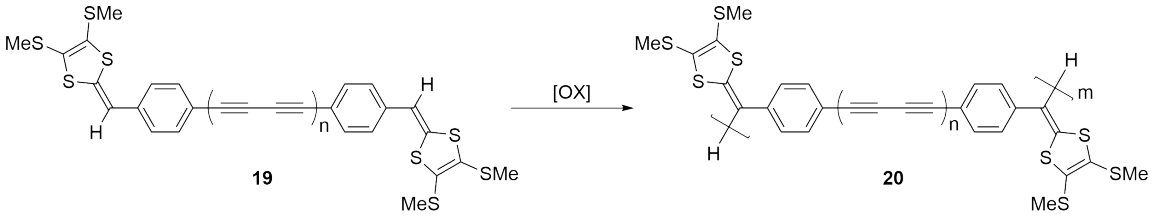

Scheme 3.1: Polymerization of oligoyne-centered DTF analogs.

While the *para*-substitution pattern in **19** allowed linear-shaped conjugated polymers to be constructed by simple chemical oxidation or electrodeposition method, the idea of using other types of alkynyl-substituted phenyl-DTFs as building blocks for various conjugated molecules or macrocycles has also intrigued Zhao's research group for years. Along this line, another former group member, Stephen Bouzan, had synthesized and investigated a class of ethynylated phenyl-DTFs **22** (Scheme

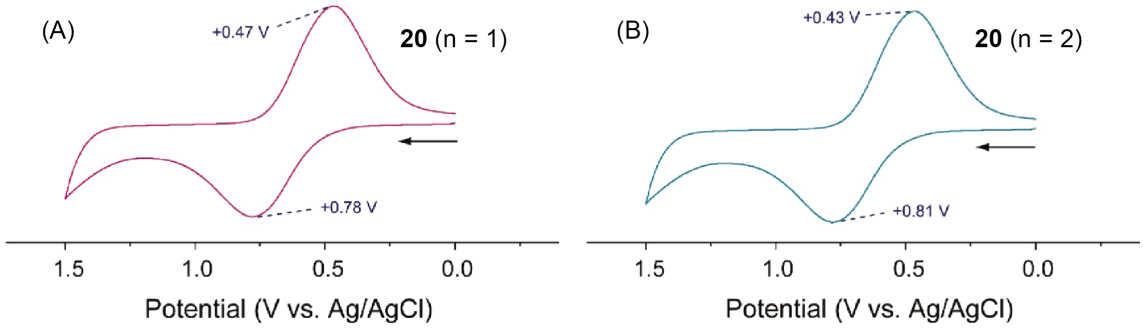

Figure 3.1: Cyclic voltammograms of polymer **20** thin films. Experimental conditions: supporting electrolyte: Bu_4NBF_4 (0.1 M), solvent: CH_2Cl_2, working electrode: ITO glass, counter electrode: Pt wire, reference electrode: Ag/AgCl, scan rate: 50 mV s^{-1}. Reprinted (adapted) with permission from (Chen, G.; Mahmud, I.; Dawe, L. N.; Daniels, L. M.; Zhao, Y. *J. Org. Chem.* **2011**, *76*, 2701-2715.). Copyright (2011) American Chemical Society.

3.2) in his MSc thesis work. However, Stephen's work was not complete and there are still many interesting issues awaiting further investigations and clarification. In this chapter, a systematic study of the alkynylated phenyl-DTFs **22** and their various π-extended derivatives has been carried out. Scheme 3.2 illustrates the two synthetic routes, namely, oxidative DTF coupling and alkynyl homocoupling, employed in this work.

3.2 Results and Discussion

3.2.1 Synthesis

This work began with the synthesis of the three regioisomers of diyne-centered dithiafulvene analogues, **24a-c** (Figure 3.2). As building blocks, the three isomers would

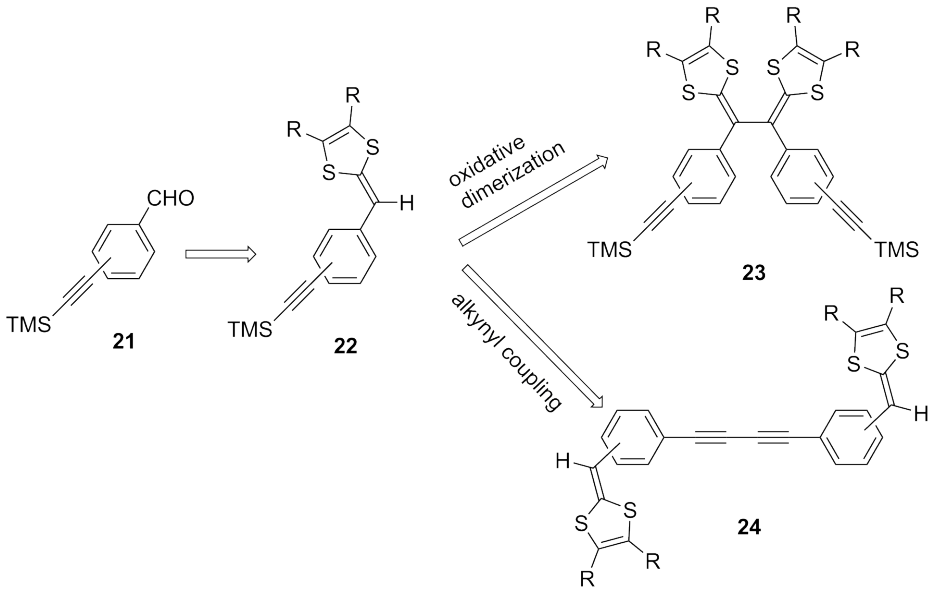

Scheme 3.2: Synthetic routes to make π-extended systems from various alkynylated phenyl-DTFs.

give rise to π-conjugated materials with different structures and properties as a result of their different molecular shapes and π-conjugation patterns. In this context, it is of fundamental importance to conduct comparative studies on the properties and reactivities of **24a-c** as well as on the π-extended systems derived from them.

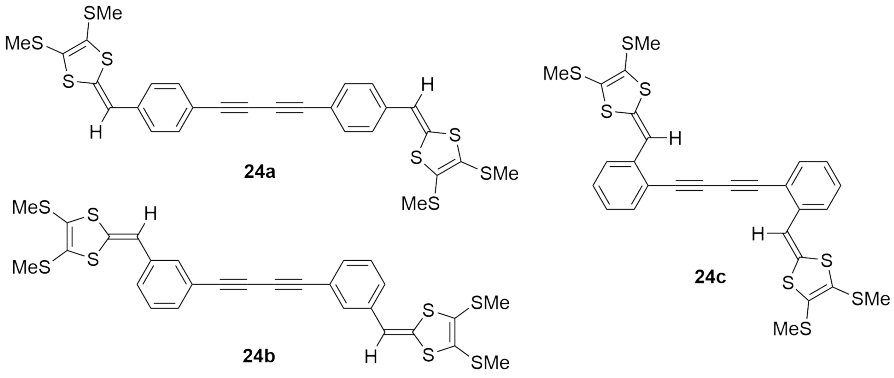

Figure 3.2: Regioisomers of diyne-centered dithiafulvene analogues.

The synthesis started from the preparation of ethynyl-DTFs **22a-c**, which was exe-

cuted through a phosphite-promoted olefination method using trimethylsilylethynyl-substituted benzaldehydes **21a-c** and thione **11** as the starting materials (Scheme 3.3).[29,30] Experimentally, the three olefination reactions were completed in 3 hours at 105 °C, giving the desired products **22a-c** with similar yields. Compounds **22a-c** were then subjected to an oxidative coupling in CH_2Cl_2 at room temperature using iodine as an oxidant (Scheme 3.3).[31] The reactions yielded ethynyl-TTFVs **23a-c** in very good yields. The yield of the *ortho*-isomer was lower than the other two isomers likely due to the steric effect from its *ortho*-substituent. Note that in some of our previous works, certain *ortho*-substituents (Br and Me) were found to retard the deprotonation step in the oxidative dimerization mechanism, leading to the formation of an unique bis-spiro structure other than the typical TTFV product (Scheme 3.4).[71,72] This scenario however did not happen in the oxidative dimerization of *ortho*-ethynyl DTF **22c**, because the ethynyl group is linear-shaped and much less bulky.

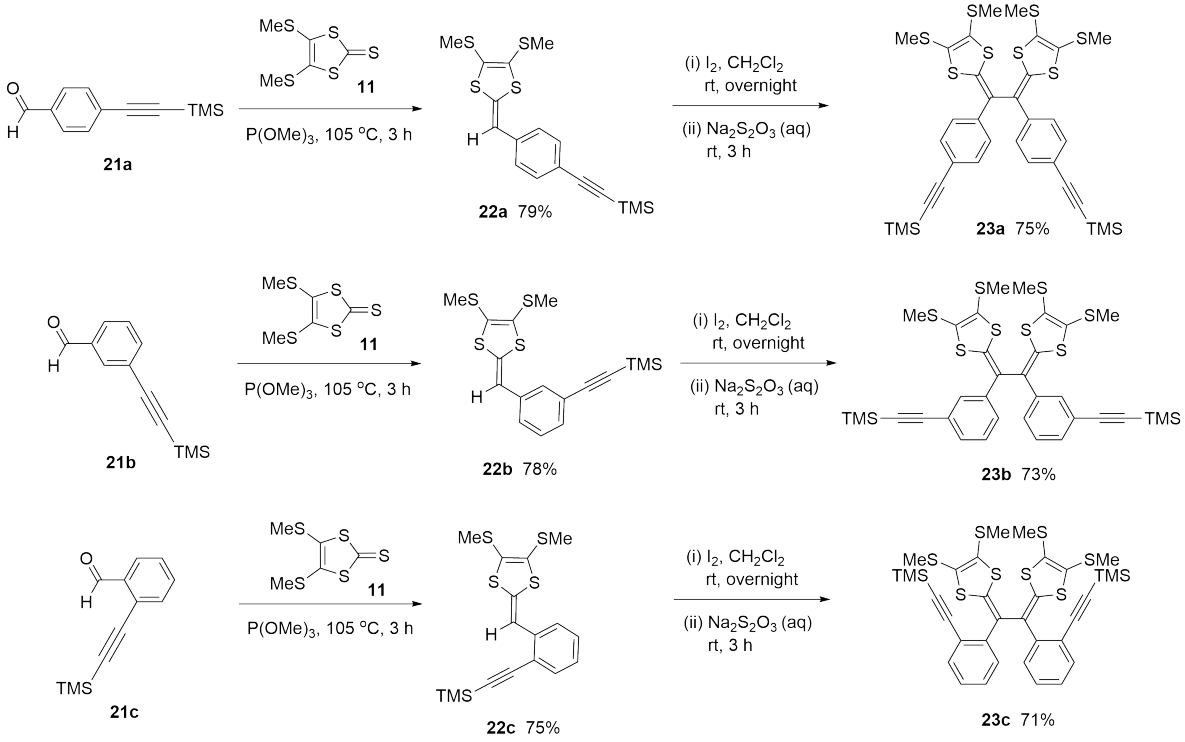

Scheme 3.3: Synthesis of ethynyl-DTFs **22a-c** and TTFVs **23a-c**.

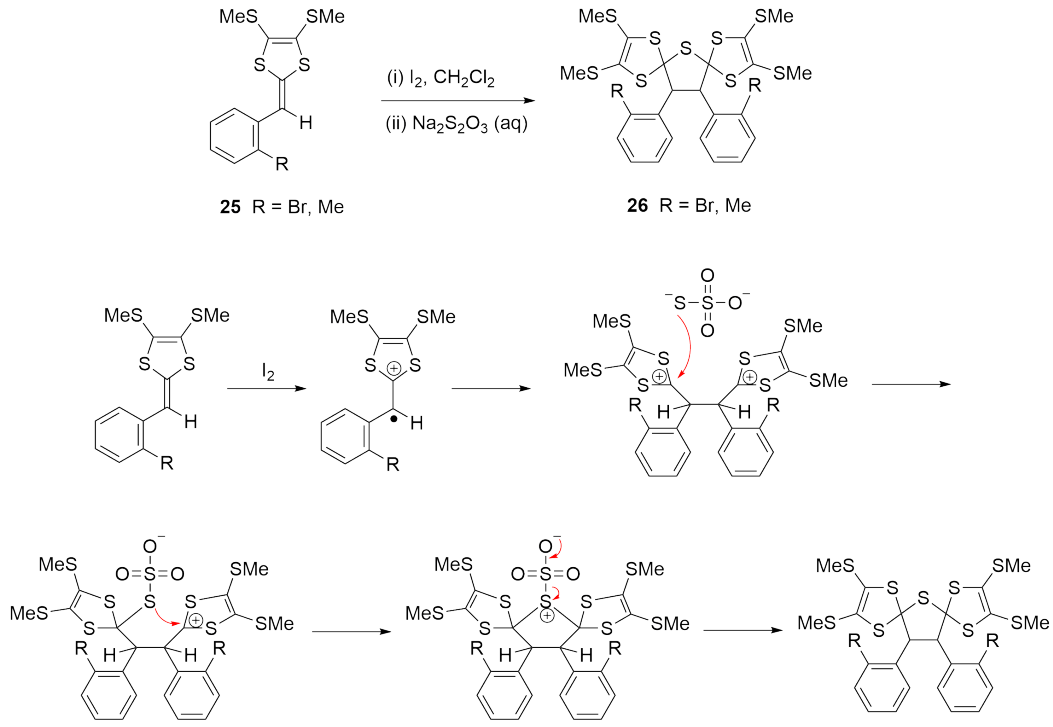

Scheme 3.4: Proposed mechanism for the formation of the bis-spiro product **26**.

Besides the oxidative dimerization reactions, the ethynyl-DTFs could also be synthetically elaborated to attain π-extension through alkynyl coupling reactions. Scheme 3.5 outlines the Hay coupling reactions of desilylated **22a-c**.[73] The synthesis began with protiodesilylation with K_2CO_3 to first generate free terminal alkyne intermediates, which after a brief workup were immediately subjected to alkynyl homocoupling catalyzed by CuI/TMEDA, affording diyne-centered DTFs **24a-c** in satisfactory yields. Products **24a** and **24b** are yellow colored solids, whereas **24c** shows an intense orange color, suggesting that it has very different electronic absorption properties than the other two isomers.[74]

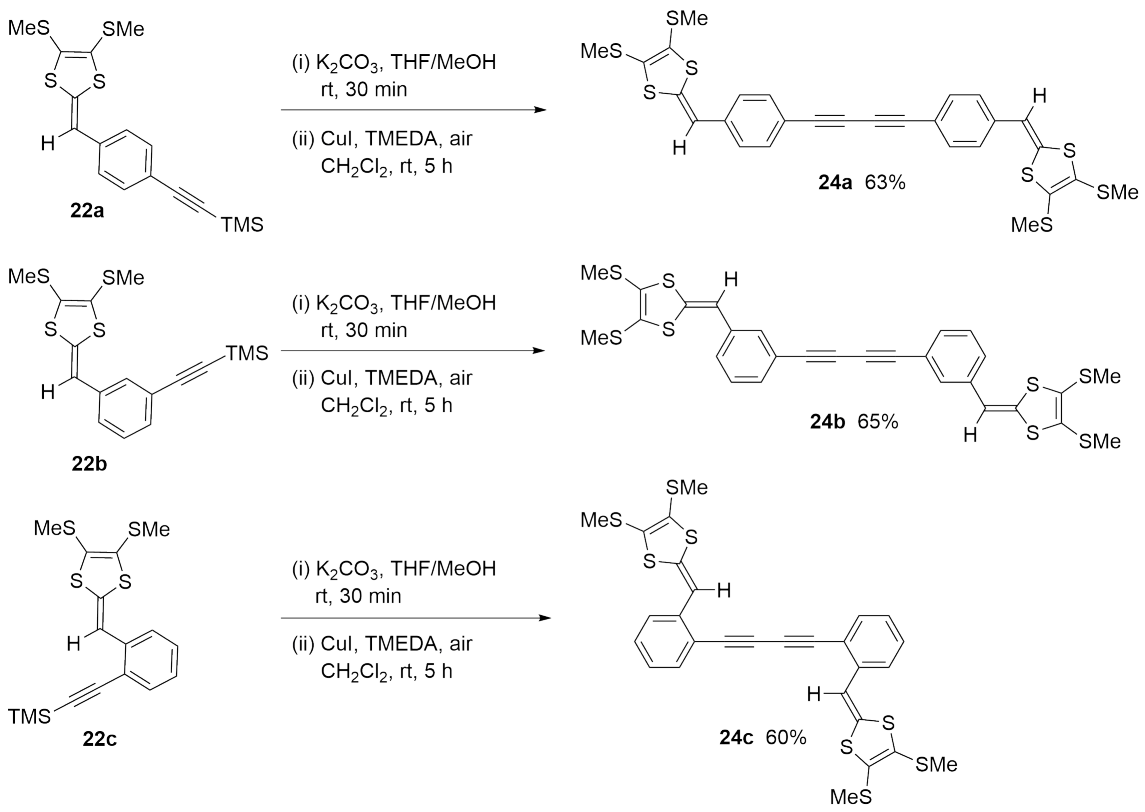

Scheme 3.5: Synthesis of diyne-centered DTFs **24a-c**.

3.2.2 Characterization

The electronic absorption properties of ethynyl-DTFs and their related π-derivatives were studied by UV-Vis spectroscopy. As can be seen from Figure 3.3, the three DTF isomers **22a-c** show $\pi \rightarrow \pi^*$ transition bands with similar molar absorptivities. The maximum absorption wavelengths (λ_{max}) shift in the order of **22a** (384 nm) > **22b** (376 nm) > **22c** (357 nm), giving a qualitative comparison of the degree of π-delocalization among the three isomers. The observation of **22c** showing the lowest λ_{max} value in the three isomers can be reasonably correlated with its *ortho*-substitution structure which engenders the most significant steric interactions between the ethynyl group and the DTF moiety to attenuate the π-conjugation.

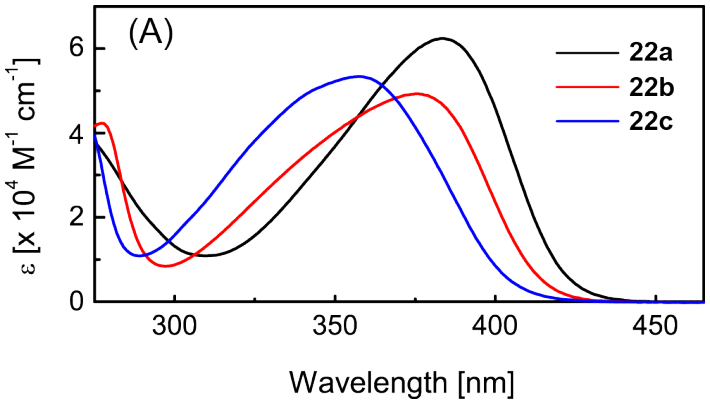

Figure 3.3: UV-Vis absorption spectra of compounds **22a-c**, measured in CH_2Cl_2 at room temperature.

The $\pi \rightarrow \pi^*$ transition bands of TTFV isomers **23a-c** show the same trend of λ_{max} shift (*i.e.*, *para* > *meta* > *ortho*) as that in **22a-c**, but the extent of variation is much greater (Figure 3.4). For *para*-isomer **23a** the λ_{max} value is observed at 380 nm, which is nearly identical to that of its DTF precursor **22a** and indicates that

the central TTFV moiety in **23a** does not contribute to increasing π-delocalization due to its twisted *cis*-like conformation.[15,19,75] Compared with **23a**, the absorption peak of *meta*-isomer **23b** shows a significant blueshift to 350 nm, which is suggestive that the π-electron delocalization in **23b** is more disrupted than **23a**. The absorption spectrum of *ortho*-isomer **23c** differs pronouncedly from its other two isomers, wherein the λ_{max} value at 329 nm is considerably blueshifted. In addition, the spectrum of **23c** features a broad absorption slope in the range of *ca.* 350 to 500 nm. Worth noting is that such a spectral profile bears great resemblance to that of a bis(1-naphthyl)-TTFV compound previously reported by Stephen Bouzan (see Figure 3.5).[76] Given that the central TTFV moiety of the bis(1-naphthyl)-TTFV has been confirmed to assume a completely planar *trans* conformation by X-ray analysis, the molecular shape of **23c** is thus deemed as adopting a similar *trans* motif. Further evidence of this conformational argument can be drawn from cyclic voltammetric analysis (*vide infra*).

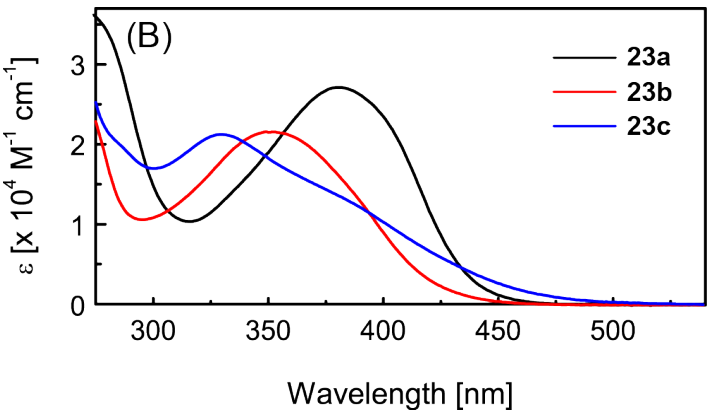

Figure 3.4: UV-Vis absorption spectra of compounds **23a-c**, measured in CH_2Cl_2 at room temperature.

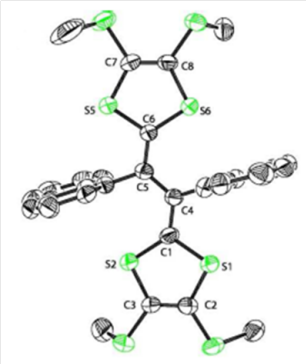

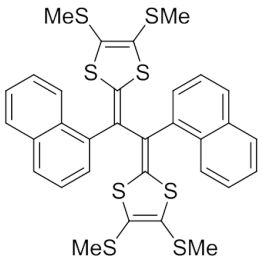

27

Figure 3.5: Single crystal structure of bis(1-naphthyl)-TTFV **27**. Reproduced from Ref. 76 with permission from The Royal Society of Chemistry.

The UV-Vis spectral profiles of diyne-centered DTFs **24a-c** varied significantly from one to another (Figure 3.6). The spectrum of diyne **24a** shows an absorption peak centred at 423 nm, with absorptivity in the range of 270-350 nm being very low. The spectral envelope of **24b** is substantially blueshifted relative to **24a**, showing three well-resolved bands at 339, 316, and 295 nm and a shoulder peak at 361 nm, respectively. The spectrum of **24c** gives two intense $\pi \rightarrow \pi^*$ bands at 398 and 332 nm. Overall, the λ_{max} values of the diyne-centered DTFs **24a-c** follow an order of *para* >*ortho* > *meta*, which is different from those of DTFs **22a-c** and TTFVs **23a-c**. An empirical rationalization for such spectroscopic behavior can be made based on the π-delocalization degree argument; that is, the DTF-phenylene-diyne skeletons of compounds **24a** and **24c** are in linear π-conjugation, whereas that of compound **24b** is cross-conjugated due to its *meta*-substitution pattern.

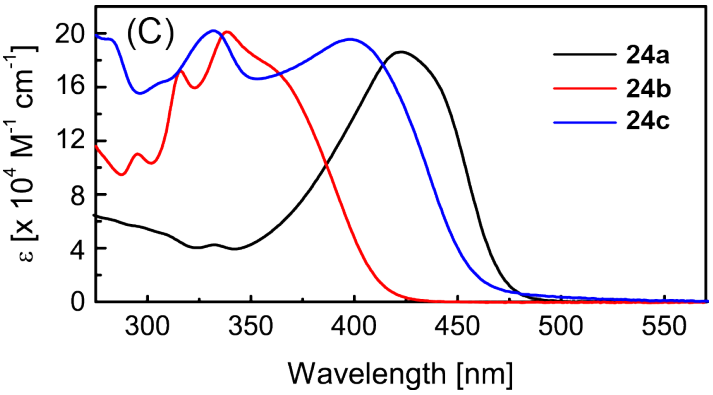

Figure 3.6: UV-Vis absorption spectra of compounds **24a-c**, measured in CH_2Cl_2 at room temperature.

The redox properties of compounds **22a-c** and **23a-c** were characterized by cyclic voltammetry (CV), and the detailed voltammograms are shown in Figure 3.7. When scanned in the positive direction, DTFs **22a-c** all show a similar anodic peak at *ca.* +0.8 V which can be assigned to the formation of a [$DTF^{\cdot+}$] radical cation via a single-electron oxidation step. In the reverse scan, a cathodic peak at +0.48 V is seen in the voltammograms of *para*- and *meta*-isomers **22a** and **22b**. Compared with the voltammograms of TTFVs **23a** and **23b**, the origin of this current peak can be assigned to the two-electron reduction of the [$TTFV^{2+}$] dication formed on the working electrode surface through electrochemical oxidative dimerization.[19,77] For *ortho*-isomer **22c**, the reverse CV scan reveals two cathodic peaks at +0.59 and +0.33 V respectively in the positive potential window. These two peaks are ascribed to the stepwise single-electron transfers occurring on the [$TTFV^{2+}$] product, which is evidenced by the nearly identical reduction features observed in the voltammogram of *ortho*-ethynyl TTFV **23c**. In the negative potential window, all the voltammograms of **22a-c** show a noticeable cathodic peak around -0.47 V. The intensity of this

peak shows dependence on scan rate; that is, at relatively slow rate this peak just diminishes. It is therefore reasoned that this particular cathodic peak is associated with some intermediary species formed electrochemically which would readily diffuse away from the working electrode surface.

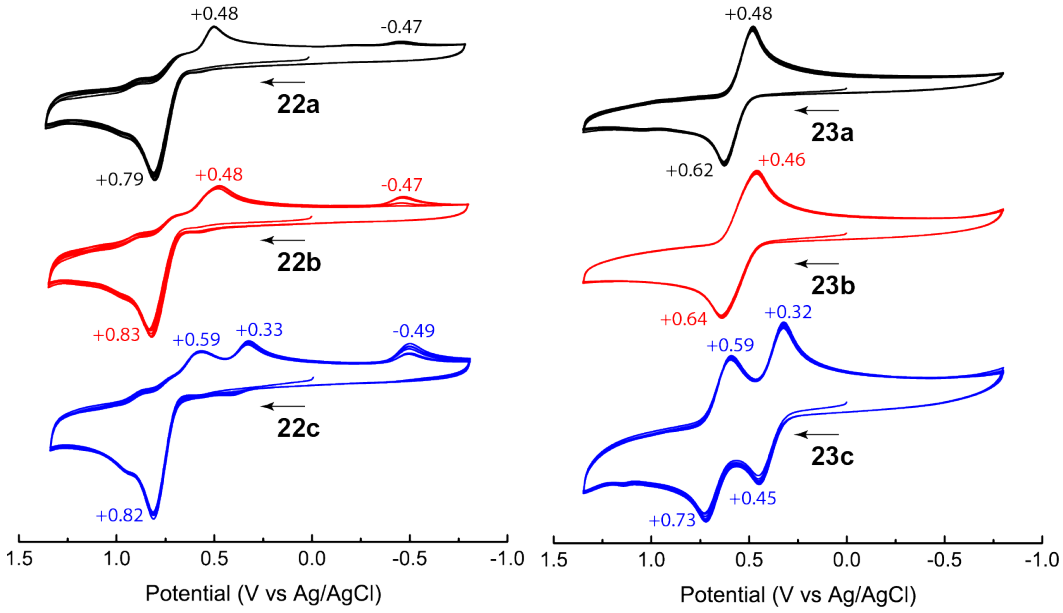

Figure 3.7: Cyclic voltammograms of compounds **22a**–**c** and **23a**–**c** measured in CH_2Cl_2 at room temperature. Experimental conditions: supporting electrolyte: Bu_4NBF_4 (0.1 M), working electrode: glassy carbon, counter electrode: Pt wire, reference electrode: Ag/AgCl (3 M NaCl), scan rate: 200 mV s^{-1}.

The voltammograms of TTFVs **23a** and **23b** both show a similar reversible redox wave pair, which can be unambiguously assigned to the simultaneous two-electron redox processes on the diphenyl-substituted TTFV moiety which normally would take a twisted *cis*-like conformation. Significantly different are the patterns in the voltammogram of *ortho*-isomer **23c**, in which the redox processes of TTFV undergo

two distinct single-electron steps. Such CV behavior, according to the previous studies by Yamashita and Zhao, alludes to a scenario that the TTFV moiety in **23c** prefers a planar *trans* conformation which can stabilize the first [$TTFV^{\cdot+}$] radical cation intermediate during oxidation.[75,76] The *ortho*-alkynyl groups in **23c** are believed to play a key role in directing the central TTFV conformation.

Likewise, the CV analysis of diyne-centered DTFs **24a-c** also discloses notable substitution effects on their redox properties (Figure 3.8). The voltammograms of *para*- and *meta*-isomers **24a** and **24b** show the typical DTF oxidation peak at *ca.* +0.8 V along with a steadily growing redox wave pair due to the formation of TTFV during multicycle CV scans. The TTFV product is not quite soluble in the solvent, so it can accumulate on the surface of the electrode to give a thin film after multicycle scans. The CV results confirm that **24a** and **24b** can readily undergo electrochemical polymerization through the oxidative DTF coupling.[19,26,78,79] Interestingly, such reactivity appears to be disfavoured in the case of *ortho*-isomer **24c**, for there is no observation of the characteristic TTFV redox wave pair in its voltammogram. Worth noting is that the CV profile of **24c** exhibits an irreversible pattern with a few weak cathodic current peaks discernible in the reverse scans (see the inset in Figure 3.8), suggesting that the oxidation of **24c** is followed by some swift chemical transformations to form redox-inactive species.

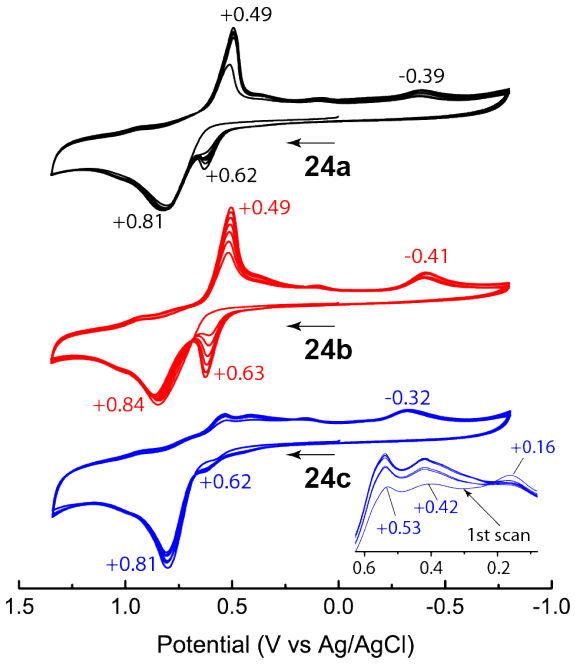

Figure 3.8: Cyclic voltammograms of compounds **24a-c** measured in CH_2Cl_2 at room temperature. Experimental conditions: supporting electrolyte: Bu_4NBF_4 (0.1 M), working electrode: glassy carbon, counter electrode: Pt wire, reference electrode: Ag/AgCl (3 M NaCl), scan rate: 200 mV s^{-1}.

To gain a deeper insight into the redox reactivity, diyne-centered DTFs **24a-c** were subjected to chemical oxidation using iodine as an oxidant. In line with the electrochemical analysis, diynes **24a** and **24b** under oxidative conditions were efficiently converted into corresponding TTFV-diyne oligomers (Scheme 3.6), which were validated by MALDI-TOF MS analysis (Figure 3.9). The mass spectra of the polymerization products poly-[**24a**] and poly-[**24b**] both show the formation of oligomers ranging from dimer to pentamer.

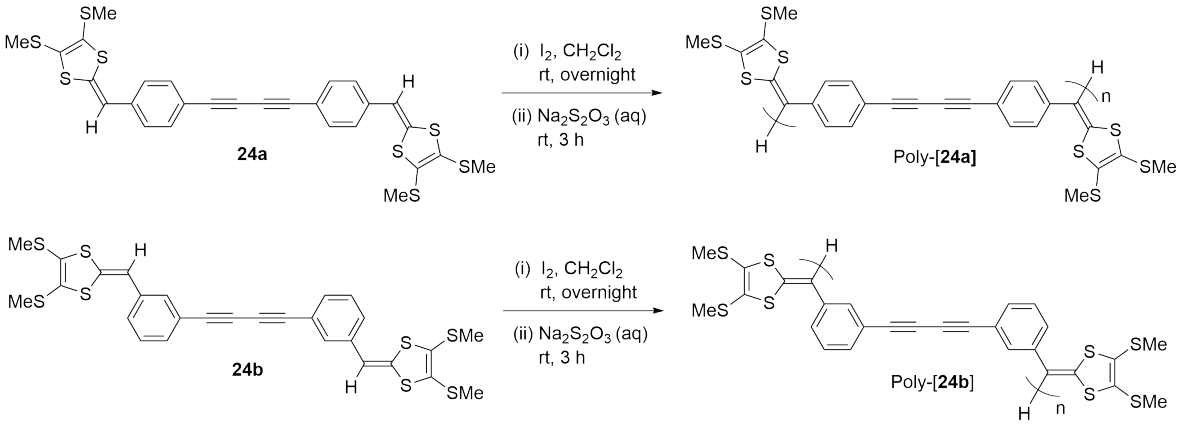

Scheme 3.6: Oxidative polymerization of diyne-centered DTFs **24a** and **24b**.

The same oxidative treatment of *ortho*-isomer **24c**, to our great surprise, ended up with the formation of a major product **28** in 30% yield (Scheme 3.7), along with a number of intractable byproducts. MALDI-TOF MS analysis confirmed that the byproducts were not TTFV-diyne oligomeric products (Figure 3.10). The mechanism for the formation of **28** is a rather complex one and awaits further investigations to be fully disclosed. At this juncture, a two-fold intramolecular cycloaddition pathway is tentatively proposed (Scheme 3.8) to account for the formation of the fused aromatic moieties in compound **28**.[80,81]

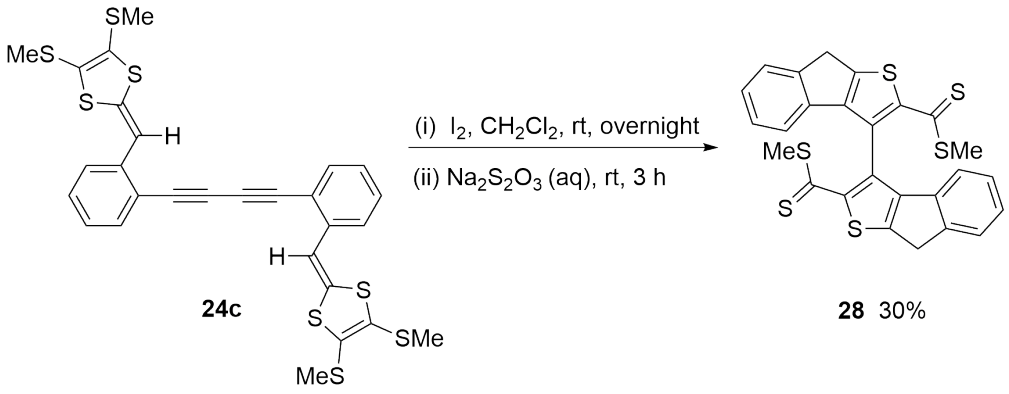

Scheme 3.7: Oxidation reaction of *ortho*-isomer **24c**.

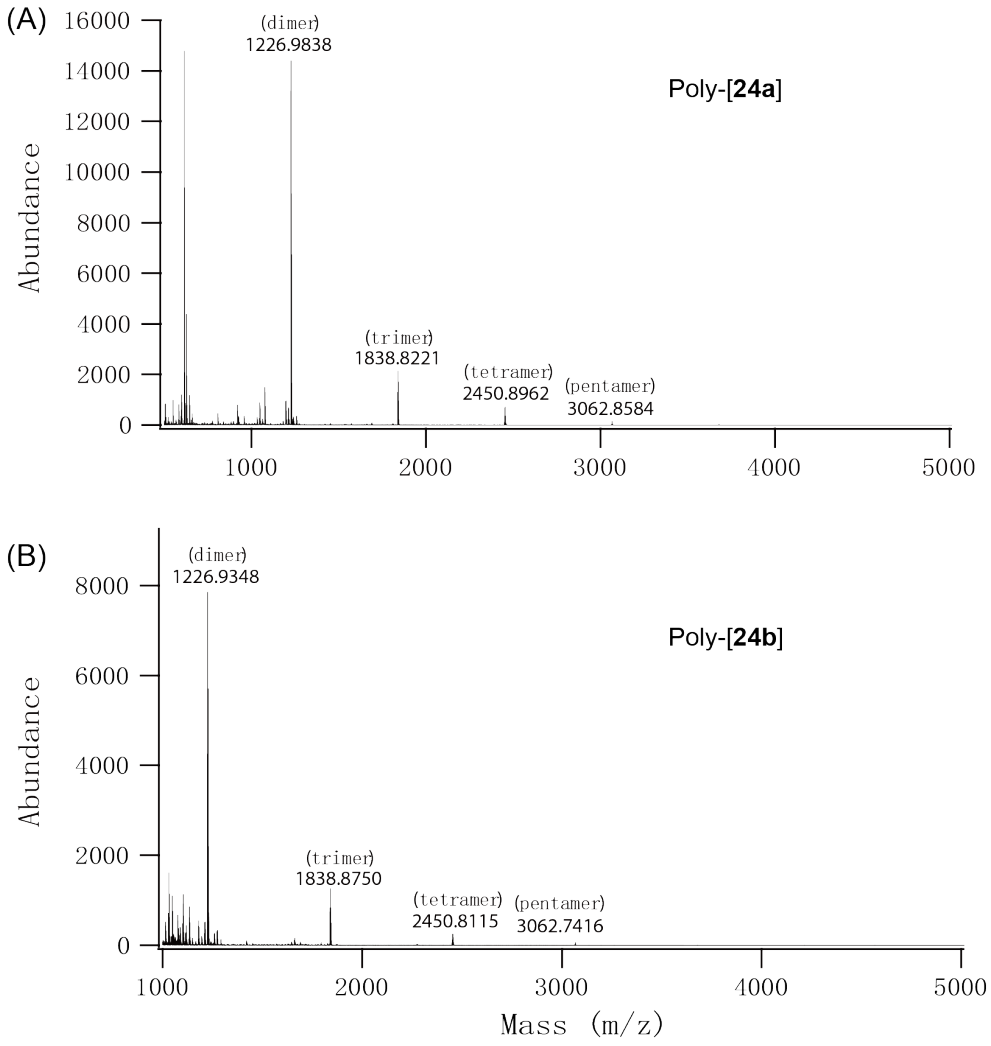

Figure 3.9: MALDI-TOF mass spectra of poly-[**24a**] and poly-[**24b**].

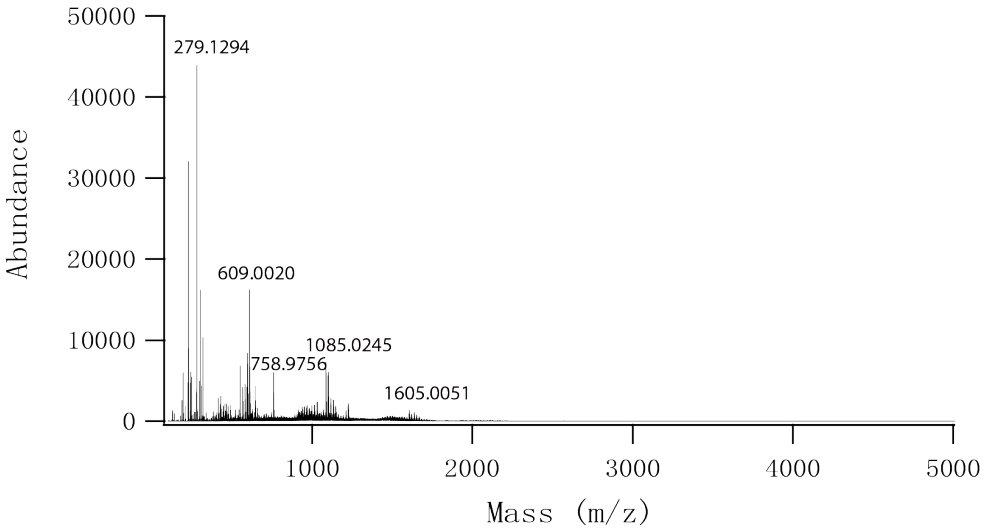

Figure 3.10: MALDI-TOF mass spectra of byproducts of **28**.

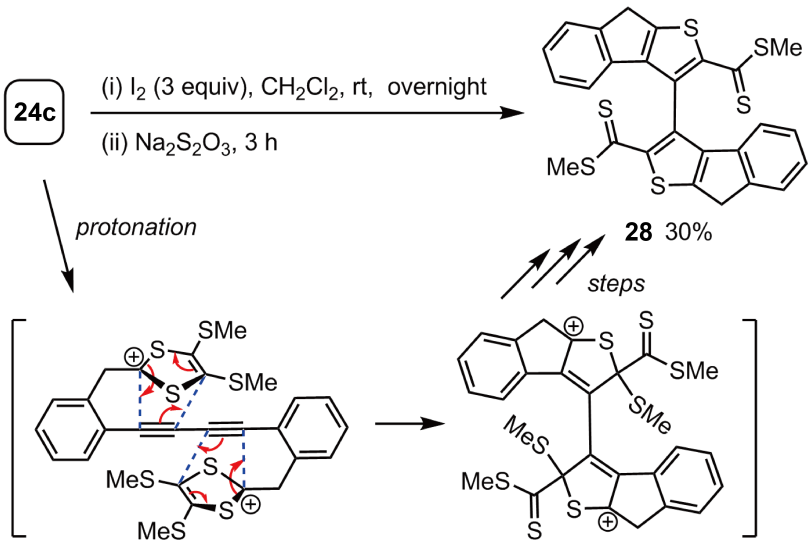

Scheme 3.8: Proposed mechanism for the formation of **28**.

The electronic absorption properties of compound **28** were studied by UV-Vis spectroscopy. It shows two absorption wavelengths at 343 nm and 415 nm (Figure 3.11), indicating a good degree of π-delocalization in the molecule. Density functional theory (DFT) calculations suggest that the two fused aromatic units in **28** are nearly perpendicular to one another (see Figure 3.12) in orientation. The axially chiral biaryl-type structure and the presence of two dithioester groups in the scaffold of **28** point to a potential in ligand design and stereoselective catalysis.[82–87] The cyclic voltammogram of compound **28** clearly shows a reversible redox wave pair in the negative potential region (E_{pa} = -1.08 V, E_{pc} = -1.25 V), without any obvious redox peaks in the positive window (Figure 3.13), which means that compound **28** is an electron acceptor.

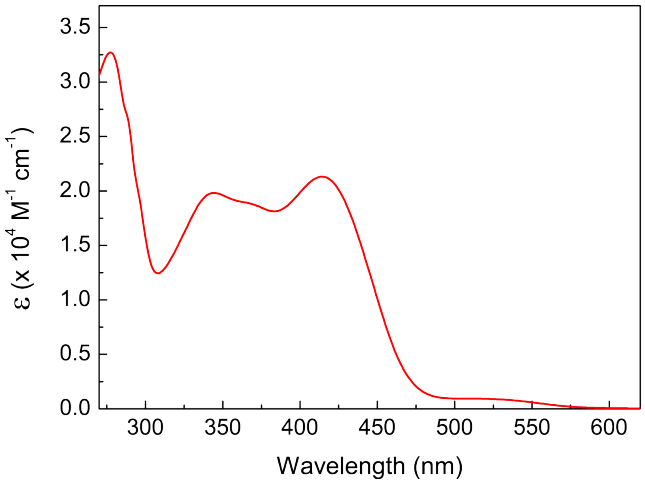

Figure 3.11: UV-Vis absorption spectrum of compound **28** measured in CH_2Cl_2 at room temperature.

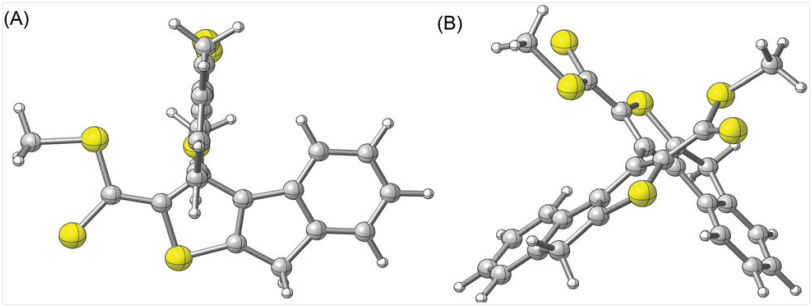

Figure 3.12: Optimized structure of compound **28** at the B3LYP/6-31G(d) level. (A) Front view, (B) Side view.

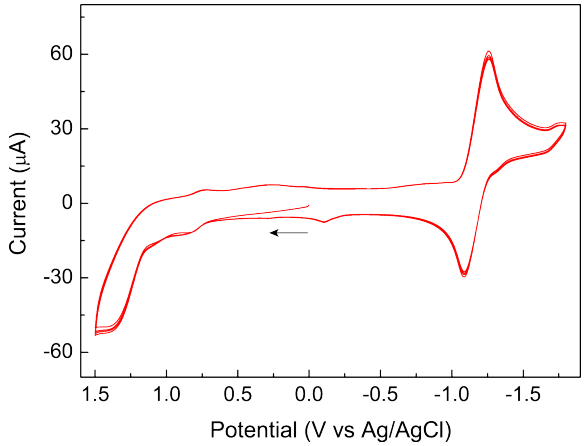

Figure 3.13: Cyclic voltammogram of compound **28** measured in CH_2Cl_2 at room temperature. Experimental conditions: supporting electrolyte: Bu_4NBF_4 (0.1 M), working electrode: glassy carbon, counter electrode: Pt wire, reference electrode: Ag/AgCl (3 M NaCl), scan rate: 200 mV s^{-1}.

To test the possibility of using compound **28** as a ligand for metal ion binding or sensing, UV-Vis titration experiments were conducted. Herein Pb(II) and Fe(III) ions were chosen for testing in view of their good affinity for sulfur-containing ligands.[88–91] The UV-Vis absorption of **28** shows no change with different concentration of Pb(II) ions, only with a small shift due to the concentration vibration (Figure 3.14). In the spectra of UV-Vis titration with Fe(III) ions, the increasing peak at 340 nm was confirmed to be the UV-Vis absorption of Fe(III) ions, so there is no change for the absorption of **28** (Figure 3.15). The result suggests that compound **28** is not an ideal ligand for metal ions, and it needs further structural modification to improve its binding properties for metal ions. One feasible approach is to convert the dithioester groups of compound **28** to dithiocarboxyl groups, which in theory should serve as much better binding sites for various transition metal ions.

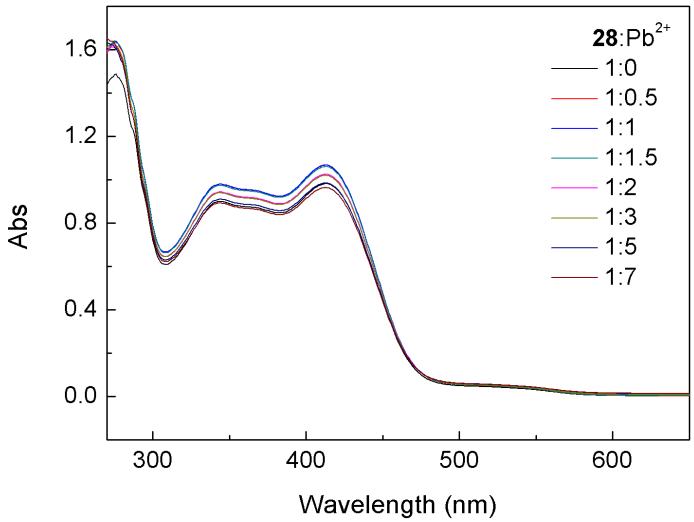

Figure 3.14: UV-Vis absorption spectra monitoring the titration of compounds **28** with Pb(II) ion in THF at room temperature. Molar ratios of **28** to Pd^{2+} are indicated.

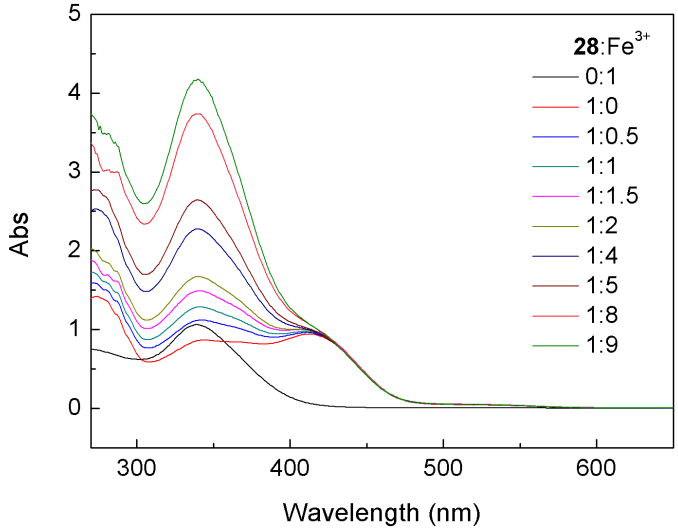

Figure 3.15: UV-Vis absorption spectra monitoring the titration of compounds **28** with Fe(III) ion in THF at room temperature. Molar ratios of **28** to Fe^{3+} are indicated.

3.3 Conclusions

In summary, a series of structurally isomeric ethynyl-DTFs and their π-extended derivatives have been systematically synthesized and characterized. The studies show that the different substitution patterns in these compounds exert important effects on their electronic and redox properties. Worth highlighting is that *ortho*-ethynyl substituted TTFV derivatives and conjugated diyne systems behave in a dramatically different way in terms of electronic absorption and redox reactivity compared with their *para*- and *meta*-isomers. The structure-property-reactivity relationships established herein offer a useful guidance to the ongoing research of DTF and alkyne based conjugated materials. The biaryl compound generated by the oxidation of *ortho*-diyne-centered DTF awaits further investigations in synthesis, mechanisms, and properties.

3.4 Experimental Procedures

Chemicals were purchased from commercial suppliers and used directly without purification. All reactions were conducted in standard, dry glassware and under an inert atmosphere of nitrogen unless otherwise noted. Evaporation and concentration were carried out with a water aspirator. Flash column chromatography was performed with silica gel 60 (240-400 mesh). Thin-layer chromatography (TLC) was carried out with silica gel F254 covered on plastic sheets and visualized by UV light. Melting points were measured on a SRS OptiMelt melting point apparatus. ^{1}H and ^{13}C NMR spectra were measured on a Bruker Avance III 300 MHz multinuclear spectrometer.

Chemical shifts (δ) are reported in ppm downfield relative to the signal of the internal reference $SiMe_4$. Coupling constants (J) are given in Hz. Infrared spectra (IR) were recorded on a Bruker Alfa spectrometer. HRMS analyses were performed on an Agilent 6230 TOF LC/MS instrument using an APPI ionizer and a QSTAR XL hybrid quadrupole/TOF mass spectrometer equipped with an o-MALDI ion source. UV-Vis absorption spectra were measured on a Cary 6000i spectrophotometer. Cyclic voltammetric analyses were carried out in a standard three-electrode setup controlled by a BASi epsilon workstation. Thione **11** was prepared according to literature procedures.[32,62]

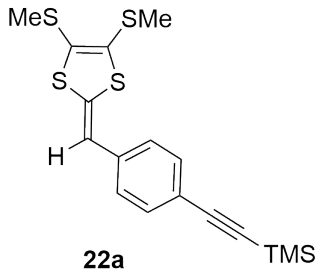

22a

***para*-Ethynyl-DTF 22a**: A mixture of 4-(trimethylsilylethynyl)benzaldehyde **21a** (0.20 g, 0.99 mmol) and thione **11** (0.27 g, 1.2 mmol) in $P(OMe)_3$ (15 mL) was stirred and heated at 105 °C for 3 h. The excess $P(OMe)_3$ was removed by vacuum distillation. The residue was purified by silica gel column chromatography (CH_2Cl_2/hexanes, 1:9) to afford compound DTF **22a** (0.30 g, 0.79 mmol, 79%) as a yellow solid. m.p. 90–91 °C; ^{1}H NMR (300 MHz, $CDCl_3$) δ 7.43 (d, J = 8.4 Hz, 2H), 7.12 (d, J = 8.2 Hz, 2H), 6.44 (s, 1H), 2.44 (s, 3H), 2.43 (s, 3H), 0.25 (s, 9H) ppm. The data is consistent with literature report.[26,27]

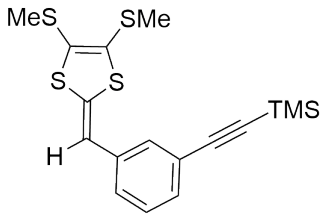

22b

***meta*-Ethynyl-DTF 22b**: A mixture of 3-(trimethylsilylethynyl)benzaldehyde **21b** (0.20 g, 0.99 mmol) and thione **11** (0.27 g, 1.2 mmol) in $P(OMe)_3$ (15 mL) was stirred and heated at 105 °C for 3 h. The excess $P(OMe)_3$ was removed by vacuum distillation. The residue was purified by silica gel column chromatography (CH_2Cl_2/hexanes, 1:9) to afford compound DTF **22b** (0.29 g, 0.77 mmol, 78%) as a yellow liquid. ^{1}H NMR (300 MHz, $CDCl_3$) δ 7.29 (s, 1H), 7.28–7.26 (m, 2H), 7.19–7.14 (m, 1H), 6.41 (s, 1H), 2.44 (s, 3H), 2.42 (s, 3H), 0.26 (s, 9H) ppm; ^{13}C NMR (75 MHz, $CDCl_3$) δ 136.4, 133.5, 130.4, 129.5, 128.6, 127.8, 126.7, 124.2, 123.6, 113.9, 105.1, 94.5, 19.2, 19.0, 0.1 ppm; FTIR (neat) 2956, 2919, 2152, 1560, 1477, 1419, 1247, 840, 759, 685, 485 cm^{-1}; HRMS (APPI, positive) m/z $[M + H]^+$ calcd for $C_{17}H_{20}S_4Si$ 381.0290, found 381.0288.

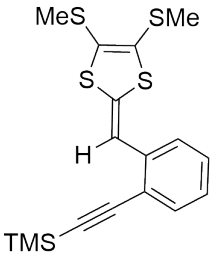

22c

***ortho*-Ethynyl-DTF 22c**: A mixture of 2-(trimethylsilylethynyl)benzaldehyde

21c (0.20 g, 0.99 mmol) and thione **11** (0.27 g, 1.2 mmol) in $P(OMe)_3$ (15 mL) was stirred and heated at 105 °C for 3 h. The excess $P(OMe)_3$ was removed by vacuum distillation. The residue was purified by silica gel column chromatography (CH_2Cl_2/hexanes, 1:9) to afford compound DTF **22c** (0.28 g, 0.74 mmol, 75%) as a yellow liquid. ^{1}H NMR (300 MHz, $CDCl_3$) δ 7.45 (d, J = 7.5 Hz, 1H), 7.35–7.31 (m, 2H), 7.13–7.06 (m, 1H), 6.98 (s, 1H), 2.45 (s, 3H), 2.41 (s, 3H), 0.27 (s, 9H) ppm; ^{13}C NMR (75 MHz, $CDCl_3$) δ 138.1, 134.4, 132.9, 128.7, 127.7, 125.7, 125.1, 124.4, 121.2, 113.2, 103.7, 100.2, 19.2, 19.1, 0.2 ppm; FTIR (neat) 2955, 2919, 2149, 1563, 1497, 1443, 1247, 1095, 838, 751, 644, 502 cm^{-1}; HRMS (APPI, positive) m/z $[M + H]^+$ calcd for $C_{17}H_{20}S_4Si$ 381.0290, found 381.0286.

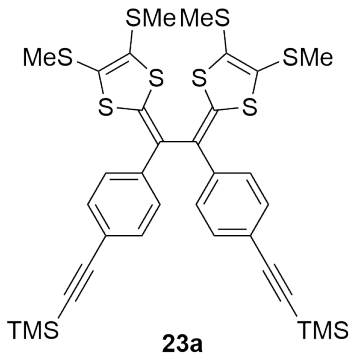

23a

***para*-Ethynyl-TTFV 23a**: A mixture of DTF **22a** (0.10 g, 0.26 mmol) and I_2 (0.20 g, 0.79 mmol) in CH_2Cl_2 (35 mL) was stirred at rt overnight. Then a satd $Na_2S_2O_3$ solution (aq, 30 mL) was added. The mixture was stirred for another 3 h at rt. The organic layer was separated, washed with H_2O, dried over $MgSO_4$, and concentrated under vacuum. The residue was purified by silica column chromatography (CH_2Cl_2/hexanes, 1:3) to afford compound TTFV **23a** (75.4 mg, 0.0995 mmol, 75%) as a yellow solid. m.p. 180–181 °C; ^{1}H NMR (300 MHz, $CDCl_3$) δ 7.38 (d, J = 8.6

Hz, 4H), 7.30 (d, J = 8.7 Hz, 4H), 2.42 (s, 6H), 2.38 (s, 6H), 0.23 (s, 18H) ppm. The data is consistent with literature report.[26,27]

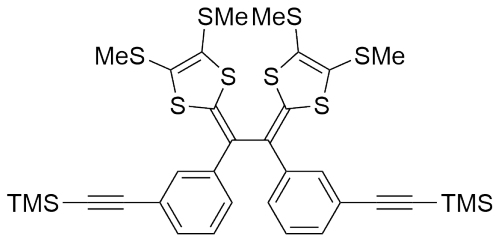

23b

***meta*-Ethynyl-TTFV 23b**: A mixture of DTF **22b** (0.10 g, 0.26 mmol) and I_2 (0.20 g, 0.79 mmol) in CH_2Cl_2 (35 mL) was stirred at rt overnight. Then a satd $Na_2S_2O_3$ solution (aq, 30 mL) was added. The mixture was stirred for another 3 h at rt. The organic layer was separated, washed with H_2O, dried over $MgSO_4$, and concentrated under vacuum. The residue was purified by silica column chromatography (CH_2Cl_2/hexanes, 1:3) to afford compound TTFV **23b** (73.1 mg, 0.0964 mmol, 73%) as a yellow solid. m.p. 51–52 °C; ^{1}H NMR (300 MHz, $CDCl_3$) δ 7.47 (s, 2H), 7.32–7.27 (m, 4H), 7.25–7.21 (m, 2H), 2.42 (s, 6H), 2.40 (s, 6H), 0.25 (s, 18H) ppm; ^{13}C NMR (75 MHz, $CDCl_3$) δ 137.6, 137.4, 130.9, 130.1, 128.8, 128.3, 127.2, 125.3, 123.7, 123.6, 105.2, 94.7, 19.1, 19.0, 0.1 ppm; FTIR (neat) 2953, 2917, 2152, 1523, 1489, 1419, 1246, 838, 757, 693, 468 cm^{-1}; HRMS (APPI, positive) m/z [M + H]$^+$ calcd for $C_{34}H_{38}S_8Si_2$ 759.0350, found 759.0360.

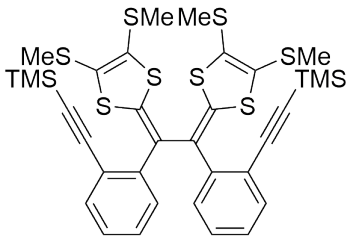

23c

***ortho*-Ethynyl-TTFV 23c**: A mixture of DTF **22c** (0.10 g, 0.26 mmol) and I_2 (0.20 g, 0.79 mmol) in CH_2Cl_2 (35 mL) was stirred at rt overnight. Then a satd $Na_2S_2O_3$ solution (aq, 30 mL) was added. The mixture was stirred for another 3 h at rt. The organic layer was separated, washed with H_2O, dried over $MgSO_4$, and concentrated under vacuum. The residue was purified by silica column chromatography (CH_2Cl_2/hexanes, 1:3) to afford compound TTFV **23c** (71.2 mg, 0.0939 mmol, 71%) as an orange solid. m.p. 99–100 °C; ^{1}H NMR (300 MHz, $CDCl_3$) δ 7.35–7.27 (m, 4H), 7.18-7.06 (m, 4H), 2.46 (s, 6H), 2.35 (s, 6H), 0.25 (s, 18H) ppm; ^{13}C NMR (75 MHz, $CDCl_3$) δ 141.5, 134.7, 133.4, 130.0, 128.7, 127.7, 127.1, 126.2, 123.5, 122.6, 104.7, 97.7, 19.2, 18.9, 0.2 ppm; FTIR (neat) 2953, 2919, 2155, 1538, 1471, 1431, 1246, 835, 752, 669, 459 cm^{-1}; HRMS (APPI, positive) *m/z* [M + H]$^+$ calcd for $C_{34}H_{38}S_8Si_2$ 759.0350, found 759.0355.

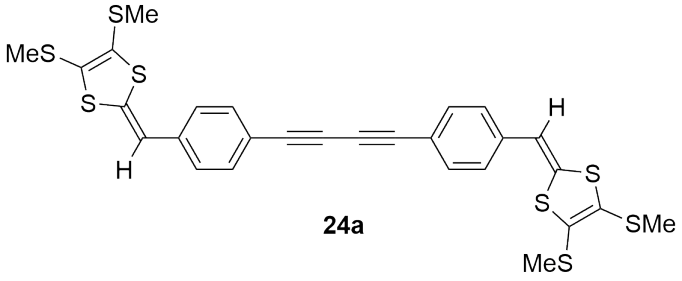

24a

***para*-Diyne-centered DTF 24a**: A mixture of DTF **22a** (0.10 g, 0.26 mmol) and $K_2CO_3 \cdot 1.5\ H_2O$ (0.13 g, 0.79 mmol) in THF/MeOH (30 mL, 1:1) was stirred at rt for 30 min, then concentrated under vacuum. The residue was dissolved in CH_2Cl_2 (30 mL), washed with H_2O, dried over $MgSO_4$ and filtered. Then a CH_2Cl_2 solution (5 mL) of CuI (0.15 g, 0.79 mmol) and TMEDA (0.16 mL, 1.1 mmol) was added. The mixture was stirred under air for 5 h at rt, then washed with H_2O, dried over $MgSO_4$, and concentrated under vacuum. The residue was purified by silica column chromatography (CH_2Cl_2/hexanes, 1:3) to afford compound DTF **24a** (50.4 mg, 0.0821 mmol, 63%) as a yellow solid. m.p. 170–171 °C; ^{1}H NMR (300 MHz, $CDCl_3$) δ 7.49 (d, J = 8.4 Hz, 4H), 7.16 (d, J = 8.3 Hz, 4H), 6.46 (s, 2H), 2.45 (s, 6H), 2.44 (s, 6H) ppm. The data is consistent with literature report.[26,27]

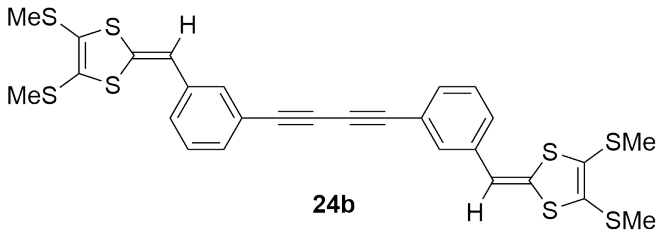

24b

***meta*-Diyne-centered DTF 24b**: A mixture of DTF **22b** (0.10 g, 0.26 mmol) and $K_2CO_3 \cdot 1.5\ H_2O$ (0.13 g, 0.79 mmol) in THF/MeOH (30 mL, 1:1) was stirred at rt for 30 min, then concentrated under vacuum. The residue was dissolved in CH_2Cl_2 (30 mL), washed with H_2O, dried over $MgSO_4$ and filtered. Then a CH_2Cl_2 solution (5 mL) of CuI (0.15 g, 0.79 mmol) and TMEDA (0.16 mL, 1.1 mmol) was added. The mixture was stirred under air for 5 h at rt, then washed with H_2O, dried over $MgSO_4$, and concentrated under vacuum. The residue was purified by silica column chromatography (CH_2Cl_2/hexanes, 1:3) to afford compound DTF **24b** (52.2

mg, 0.0850 mmol, 65%) as a yellow solid. m.p. 109–110 °C; ^{1}H NMR (300 MHz, $CDCl_3$) δ 7.36 (s, 2H), 7.35–7.30 (m, 4H), 7.23–7.18 (m, 2H), 6.42 (s, 2H), 2.45 (s, 6H), 2.44 (s, 6H) ppm; ^{13}C NMR (75 MHz, $CDCl_3$) δ 136.6, 134.1, 130.4, 129.8, 128.7, 127.6, 127.6, 124.3, 122.1, 113.3, 81.7, 74.1, 19.1, 18.9 ppm; FTIR (neat) 3041, 2916, 2851, 2145, 1732, 1569, 1494, 1416, 1312, 960, 887, 807, 680, 463 cm^{-1}; HRMS (APPI, positive) *m/z* $[M + H]^+$ calcd for $C_{28}H_{22}S_8$ 614.9560, found 614.9556.

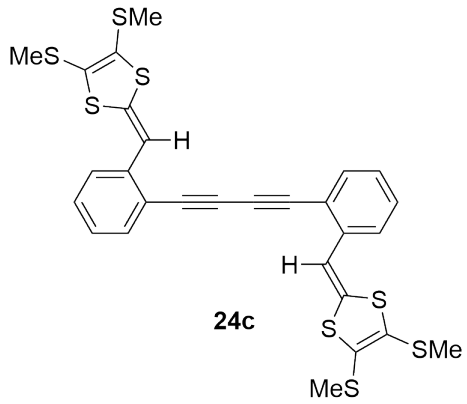

24c

***ortho*-Diyne-centered DTF 24c**: A mixture of DTF **22c** (0.10 g, 0.26 mmol) and $K_2CO_3 \cdot 1.5\ H_2O$ (0.13 g, 0.79 mmol) in THF/MeOH (30 mL, 1:1) was stirred at rt for 30 min, then concentrated under vacuum. The residue was dissolved in CH_2Cl_2 (30 mL), washed with H_2O, dried over $MgSO_4$ and filtered. Then a CH_2Cl_2 solution (5 mL) of CuI (0.15 g, 0.79 mmol) and TMEDA (0.16 mL, 1.1 mmol) was added. The mixture was stirred under air for 5 h at rt, then washed with H_2O, dried over $MgSO_4$, and concentrated under vacuum. The residue was purified by silica column chromatography (CH_2Cl_2/hexanes, 1:3) to afford compound DTF **24c** (48.3 mg, 0.0787 mmol, 60%) as an orange solid. m.p. 124–125 °C; ^{1}H NMR (300 MHz, $CDCl_3$) δ 7.55 (d, J = 7.5 Hz, 2H), 7.42–7.35 (m, 4H), 7.16–7.11 (m, 2H), 6.99 (s,

2H), 2.46 (s, 6H), 2.42 (s, 6H) ppm; ^{13}C NMR (75 MHz, $CDCl_3$) δ 139.1, 135.7, 133.8, 129.3, 128.2, 125.6, 125.3, 123.9, 119.7, 112.4, 81.5, 79.0, 19.1, 19.0 ppm; FTIR (neat) 3053, 2917, 2852, 2133, 1735, 1545, 1496, 1415, 1311, 969, 890, 802, 742, 539, 497 cm^{-1}; HRMS (APPI, positive) *m/z* $[M + H]^+$ calcd for $C_{28}H_{22}S_8$ 614.9560, found 614.9560.

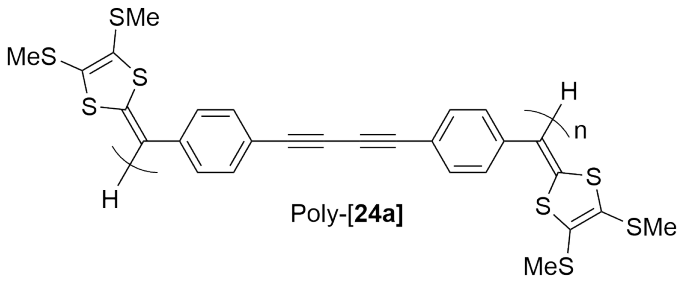

Poly-[24a]: A mixture of DTF **24a** (20.0 mg, 0.0326 mmol) and I_2 (25.0 mg, 0.0984 mmol) in CH_2Cl_2 (25 mL) was stirred at rt overnight. Then a satd $Na_2S_2O_3$ solution (aq, 20 mL) was added. The mixture was stirred for another 3 h at rt. The organic layer was separated, washed with H_2O, dried over $MgSO_4$, and concentrated under vacuum to afford product poly-[**24a**] (19.6 mg, crude yield 98%) as a yellow solid. HRMS (MALDI, positive) *m/z* $[M + H]^+$ calcd for $C_{56}H_{42}S_{16}$ (n = 2) 1226.8891, found 1226.9838, calcd for $C_{84}H_{62}S_{24}$ (n = 3) 1838.8221, found 1838.9366, calcd for $C_{112}H_{82}S_{32}$ (n = 4) 2450.7552, found 2450.8962, calcd for $C_{140}H_{102}S_{40}$ (n = 5) 3062.6883, found 3062.8584.

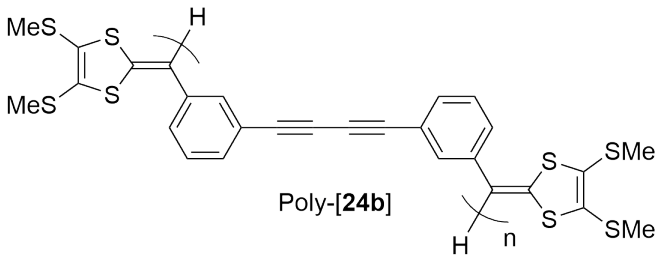

Poly-[**24b**]

Poly-[24b]: A mixture of DTF **24b** (20.0 mg, 0.0326 mmol) and I_2 (25.0 mg, 0.0984 mmol) in CH_2Cl_2 (25 mL) was stirred at rt overnight. Then a satd $Na_2S_2O_3$ solution (aq, 20 mL) was added. The mixture was stirred for another 3 h at rt. The organic layer was separated, washed with H_2O, dried over $MgSO_4$, and concentrated under vacuum to afford product poly-[**24b**] (19.2 mg, crude yield 96%) as a yellow solid. HRMS (MALDI, positive) *m/z* $[M + H]^+$ calcd for $C_{56}H_{42}S_{16}$ (n = 2) 1226.8891, found 1226.9348, calcd for $C_{84}H_{62}S_{24}$ (n = 3) 1838.8221, found 1838.8750, calcd for $C_{112}H_{82}S_{32}$ (n = 4) 2450.7552, found 2450.8115, calcd for $C_{140}H_{102}S_{40}$ (n = 5) 3062.6883, found 3062.7416.

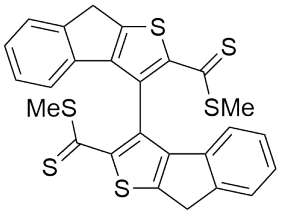

28

3,3'-bi(thieno[2,3-b]-1H-indene) 28: A mixture of DTF **24c** (0.10 g, 0.16 mmol) and I_2 (0.12 g, 0.47 mmol) in CH_2Cl_2 (100 mL) was stirred at rt overnight. Then a satd $Na_2S_2O_3$ solution (aq, 90 mL) was added. The mixture was stirred for another 3 h at rt. The organic layer was separated, washed with H_2O, dried

over $MgSO_4$, and concentrated under vacuum. The residue was purified by silica column chromatography (CH_2Cl_2/hexanes, 1:3) to afford compound **28** (25.1 mg, 0.0481 mmol, 30%) as a red solid. ^{1}H NMR (300 MHz, $CDCl_3$) δ 7.43 (d, J = 7.1 Hz, 2H), 7.15-7.02 (m, 4H), 6.70 (d, J = 7.3 Hz, 2H), 3.97 (s, 4H), 2.54 (s, 6H) ppm; ^{13}C NMR (75 MHz, $CDCl_3$) δ 214.8, 152.9, 151.9, 148.3, 145.4, 138.3, 127.4, 127.3, 125.6, 124.7, 119.3, 35.6, 21.2 ppm; FTIR (neat) 3050, 2923, 2853, 1607, 1526, 1458, 1408, 1367, 1271, 1187, 1042, 732 cm^{-1}; HRMS (APPI, positive) m/z [M + H]$^+$ calcd for $C_{26}H_{18}S_6$ 522.9806, found 522.9808.

Chapter 4

Conclusions and Future Work

This MSc dissertation has accomplished the studies of two classes of TTFV based compounds. In the first project, carboxyl-DTF and carboxyl-TTFV were synthesized and characterized. The electronic and electrochemical properties of the DTF and TTFV compounds were found to be in line with other related DTF and TTFV derivatives. These compounds were used as redox-active ligands to coordinate with zinc ions. The Zn-DTF complex formed was found to retain the redox activity and electrochemical reactivity of its DTF ligand in the solid state. The coordination reaction between carboxyl-TTFV and zinc ions resulted in a mixture of Zn-TTFV coordination product and ZnO. The Zn-TTFV coordination product showed better thermal stability but weaker redox activity than its TTFV ligand. At this stage, the exact structure of the Zn-TTFV coordination product cannot be determined because it showed no crystallinity and lacks of defined microporosity. Therefore, The future work should move towards tuning the side groups of the TTFV ligand to produce zinc coordination products with better crystallinity. Overall, this work has cast a

light on the fundamental redox and solid-state properties of the class of DTF and TTFV-based organic-inorganic hybrid materials, and the findings disclosed offer a useful guidance to further material design and development.

In the second project, a series of structurally isomeric ethynyl-DTFs, ethynyl-TTFVs and diyne-centered DTFs were systematically synthesized and characterized. The *ortho*-substituted isomers were found to behave in a dramatically different way in terms of electronic absorption and redox reactivity compared with their *para*- and *meta*-isomers. Of great interest is that the *para*- and *meta*-diyne-centered DTFs can undergo oxidative polymerization to form π-extended oligomers, while the *ortho*-diyne-centered DTF ended up with a biaryl product through an intramolecular cycloaddition pathway. The biaryl-type structure and the presence of two thioester groups point to a potential in stereoselective catalysis and ligand design, and the synthesis, mechanism and properties of the biaryl compound awaits further investigation. Overall, the structure-property-reactivity relationships established herein is beneficial for the ongoing research of DTF/TTFV and alkyne based conjugated materials.

Bibliography

[1] Wudl, F. M.; Smith, G. M.; Hufnagel, E. J. *J. Chem. Soc., Chem. Commun.* **1970**, 1453–1454.

[2] Hünig, S.; Kiesslich, G.; Sceutzow, D.; Zhrandik, R.; Carsky, P. *Int. J. Sulfur Chem., Part C* **1971**, 109–122.

[3] Coffen, D. L.; Chambers, J. Q.; Williams, D. R.; Garrett, P. E.; Canfield, N. D. *J. Am. Chem. Soc.* **1971**, *93*, 2258–2269.

[4] Martín, N. *Chem. Commun.* **2013**, *49*, 7025–7027.

[5] Yamada, J.-I.; Sugimoto, T., eds. *TTF Chemistry: Fundamentals and Applications of Tetrathiafulvalene*. Springer, Berlin, Germany, 2004.

[6] Segura, J. L.; Martín, N. *Angew. Chem. Int. Ed.* **2001**, *40*, 1372–1409.

[7] Simonsen, K. B.; Becher, J. *Synlett* **1997**, *11*, 1211–1220.

[8] Nielsen, M. B.; Lomholt, C.; Becher, J. *Chem. Soc. Rev.* **2000**, *29*, 153–164.

[9] Canevet, D.; Salle, M.; Zhang, G.; Zhang, D.; Zhu, D. *Chem. Commun.* **2009**, 2245–2269.

[10] VandeVondele, J.; Lynden-Bell, R.; Meijer, E. J.; Sprik, M. *J. Phys. Chem. B* **2006**, *110*, 3614–3623.

[11] Nielsen, M. B.; Sauer, S. P. *Chem. Phys. Lett.* **2008**, *453*, 136–139.

[12] Bendikov, M.; Wudl, F.; Perepichka, D. F. *Chem. Rev.* **2004**, *11*, 4891–4946.

[13] Bryce, M. R. *J. Mater. Chem.* **1995**, *5*, 1481–1496.

[14] Frere, P.; Skabara, P. J. *Chem. Soc. Rev.* **2005**, *34*, 69–98.

[15] Zhao, Y.; Chen, G.; Mulla, K.; Mahmud, I.; Liang, S.; Dongare, P.; Thompson, D. W.; Dawe, L. N.; Bouzan, S. *Pure Appl. Chem.* **2012**, *84*, 1005–1025.

[16] Roncali, J. *J. Mater. Chem.* **1997**, *7*, 2307–2321.

[17] Bryce, M. R.; Coffin, M. A.; Clegg, W. *J. Org. Chem.* **1992**, *57*, 1696–1699.

[18] Carlier, R.; Hapiot, P.; Lorcy, D.; Robert, A.; Tallec, A. *Electrochim. Acta* **2001**, *46*, 3269–3277.

[19] Bellec, N.; Boubekeur, K.; Carlier, R.; Hapiot, P.; Lorcy, D.; Tallec, A. *J. Phys. Chem. A* **2000**, *104*, 9750–9759.

[20] Liang, S.; Zhao, Y.; Adronov, A. *J. Am. Chem. Soc.* **2014**, *136*, 970–977.

[21] Liang, S.; Chen, G.; Zhao, Y. *J. Mater. Chem. C* **2013**, *1*, 5477–5490.

[22] Liang, S.; Chen, G.; Peddle, J.; Zhao, Y. *Chem. Commun.* **2012**, *48*, 3100–3102.

[23] Mulla, K.; Shaik, H.; Thompson, D. W.; Zhao, Y. *Org. Lett.* **2013**, *15* 4532–4535.

[24] Mulla, K.; Dongare, P.; Thompson, D. W.; Zhao, Y. *Org. Biomol. Chem.* **2012**, *10*, 2542–2544.

[25] Gontier, E.; Bellec, N.; Brignou, P.; Gohier, A.; Guerro, M.; Roisnel, T.; Lorcy, D. *Org. Lett.* **2010**, *12*, 2386–2389.

[26] Chen, G.; Mahmud, I.; Dawe, L. N.; Daniels, L. M.; Zhao, Y. *J. Org. Chem.* **2011**, *76*, 2701–2715.

[27] Chen, G.; Mahmud, I.; Dawe, L. N.; Zhao, Y. *Org. Lett.* **2010**, *12*, 704–707.

[28] Chen, G.; Zhao, Y. *Org. Lett.* **2014**, *16*, 668–671.

[29] Schou, S. S.; Parker, C. R.; Lincke, K.; Jennum, K.; Vibenholt, J.; Kadziola, A.; Nielsen, M. B. *Synlett* **2013**, *24*, 231–235.

[30] Christensen, C. A.; Batsanov, A. S.; Bryce, M. R. *J. Org. Chem.* **2007**, *72*, 1301–1308.

[31] Hapiot, P.; Lorcy, D.; Tallec, A.; Carlier, R.; Robert, A. *J. Phys. Chem.* **1996**, *100*, 14823–14827.

[32] Steimecke, G.; Sieler, H.-J.; Kirmse, R.; Hoyer, E. *Phosphorus Sulfur Silicon Relat. Elem.* **1979**, *7*, 49–55.

[33] Parg, R. P.; Kilburn, J. D.; Ryan, T. G. *Synthesis* **1994**, 195–198.

[34] Batten, S. R.; Champness, N. R.; Chen, X.-M.; Garcia-Martinez, J.; Kitagawa, S.; Ohrstrom, L.; O'Keeffe, M.; Suh, M. P.; Reedijk, J. *Pure Appl. Chem.* **2013**, *85*, 1715–1724.

[35] Li, H.; Eddaoudi, M.; Groy, T. L.; Yaghi, O. M. *J. Am. Chem. Soc.* **1998**, *120*, 8571–8572.

[36] Cook, T. R.; Zheng, Y.-R.; Stang, P. J. *Chem. Rev.* **2013**, *113*, 734–777.

[37] Suh, M. P.; Park, H. J.; Prasad, T. K.; Lim, D.-W. *Chem. Rev.* **2012**, *122*, 782–835.

[38] Li, J.-R.; Sculley, J.; Zhou, H.-C. *Chem. Rev.* **2012**, *112*, 869–932.

[39] Kreno, L. E.; Leong, K.; Farha, O. K.; Allendorf, M.; Duyne, R. P. V.; Hupp, J. T. *Chem. Rev.* **2012**, *112*, 1105–1125.

[40] Horcajada, P.; Gref, R.; Baati, T.; Allan, P. K.; Maurin, G.; Couvreur, P.; Ferey, G.; Morris, R. E.; Serre, C. *Chem. Rev.* **2012**, *112*, 1232–1268.

[41] Wang, C.; Zhang, T.; Lin, W. *Chem. Rev.* **2012**, *112*, 1084–1104.

[42] Corma, A.; Garcia, H.; Llabres i Xamena, F. X. *Chem. Rev.* **2010**, *110*, 4606–4655.

[43] Yaghi, O. M.; Davis, C. E.; Li, G.; Li, H. *J. Am. Chem. Soc.* **1997**, *119*, 2861–2868.

[44] Stock, N.; Biswas, S. *Chem. Rev.* **2012**, *112*, 933–969.

[45] Yaghi, O. M.; Li, G.; Li, H. *Nature* **1995**, *378*, 703–706.

[46] Huang, L.; Wang, H., Chen, J.; Wang, Z.; Sun, J.; Zhao, D.; Yan, Y. *Microporous Mesoporous Mater.* **2003**, *58*, 105–114.

[47] Tranchemontagne, D. J.; Hunt, J. R.; Yaghi, O. M. *Tetrahedron* **2008**, *64*, 8553–8557.

[48] Cravillon, J.; Munzer, S.; Lohmeier, S.-J.; Feldhoff, A.; Huber, K.; Wiebcke, M. *Chem. Mater.* **2009**, *21*, 1410–1412.

[49] Li, H.; Eddaoudi, M.; O'Keeffe, M.; Yaghi, O. M. *Nature* **1999**, *402*, 276–279.

[50] Eddaoudi, M.; Kim, J.; Rosi, N.; Vodak, D.; Wachter, J.; O'Keeffe, M.; Yaghi, O. M. *Science* **2002**, *295*, 469–472.

[51] Chen, B.; Lv, Z.-P.; Leong, C. F.; Zhao, Y.; D'Alessandro, D. M.; Zuo, J.-L. *Cryst. Growth Des.* **2015**, *15*, 1861–1870.

[52] Zhu, Q.-Y.; Wang, J.-P.; Qin, Y.-R.; Shi, Z.; Han, Q.-H.; Bian, G.-Q.; Dai, J. *Dalton Trans.* **2011**, *40*, 1977–1983.

[53] Ding, Y.; Chen, Q.; Zhong, J.-C.; Munakata, M.; Konaka, H.; Ning, G.-L.; Wang, H.-Z. *Polyhedron* **2008**, *27*, 1393–1400.

[54] Martinez, V.; Gaspar, A. B.; Munoz, M. C.; Ballesteros, R.; Ortega-Villar, N.; Ugalde-Saldivar, V. M.; Moreno-Esparza, R.; Real, J. A. *Eur. J. Inorg. Chem.* **2009**, 303–310.

[55] Schneller, T.; Waser, R.; Kosec, M.; Payne, D., eds. *Chemical Solution Deposition of Functional Oxide Thin Films.* Springer, Berlin, Germany, 2013.

[56] MacGillivray, L. R., ed. *Metal-Organic Frameworks: Design and Application.* John Wiley & Sons, Inc., Hoboken, New Jersey, 2010.

[57] Wang, Y.; Zhao, Y. *Beilstein J. Org. Chem.* **2015**, *11*, 957–965.

[58] Kim, J.; Chen, B.; Reineke, T. M.; Li, H.; Eddaoudi, M.; Moler, D. B.; O'Keeffe, M.; Yaghi, O. M. *J. Am. Chem. Soc.* **2001**, *123*, 8239–8247.

[59] Lee, S.-K.; Kim, A. Y.; Lee, J. Y.; Ko, S. H.; Kim, S. W. *Bull. Korean Chem. Soc.* **2014**, *35*, 2004–2008.

[60] Polarz, S.; Orlov, A. V.; Schuth, F.; Lu, A.-H. *Chem. Eur. J.* **2007**, *13*, 592–597.

[61] Hu, X.; Shen, X.; Huang, R.; Masuda, Y.; Ohji, T.; Kato, K. *J. Alloys Compd.* **2013**, *580*, 373–376.

[62] Moore, A. J.; Bryce, M. R. *Synthesis* **1991**, 26–28.

[63] Muller, T. J. J.; Bunz, U. H. F., eds. *Functional Organic Materials: Syntheses, Strategies and Applications*. Wiley-VCH, Weinheim, Germany, 2006.

[64] Inzelt, G. *Conducting Polymers: A New Era in Electrochemistry*. Springer, Berlin, 2nd edition, 2012.

[65] Facchetti, A. *Chem. Mater.* **2011**, *23*, 733–758.

[66] Beaujuge, P. M.; Fréchet, J. M. J. *J. Am. Chem. Soc.* **2011**, *133*, 20009–20029.

[67] Kim, F. S.; Ren, G.; Jenekhe, S. A. *Chem. Mater.* **2011**, *23*, 682–732.

[68] Rao, M. R.; Sun, S.-S. *Langmuir* **2013**, *29*, 15146–15158.

[69] Takimiya, K.; Osaka, I.; Nakano, M. *Chem. Mater.* **2014**, *26*, 587–593.

[70] Mulla, K.; Zhao, Y. *Tetrahedron Lett.* **2014**, *55*, 382–386.

[71] Bouzan, S.; Dawe, L. N.; Zhao, Y. *Tetrahedron Lett.* **2013**, *54*, 4666–4669.

[72] Woolridge, K.; Goncalves, L. C.; Bouzan, S.; Chen, G.; Zhao, Y. *Tetrahedron Lett.* **2014**, *55*, 6362–6366.

[73] Hay, A. S. *J. Org. Chem.* **1962**, *27*, 3320–3321.

[74] Wang, Y.; Zhao, Y. *Org. Biomol. Chem.* **2015**, *13*, 9575–9579.

[75] Yamashita, Y.; Tomura, M.; Zaman, M. B.; Imaeda, K. *Chem. Commun.* **1998**, 1657–1658.

[76] Bouzan, S.; Chen, G.; Mulla, K.; Dawe, L. N.; Zhao, Y. *Org. Biomol. Chem.* **2012**, *38*, 7673–7676.

[77] Massue, J.; Ghilane, J.; Bellec, N.; Lorcy, D.; Hapiot, P. *Electrochem. Commun.* **2007**, *9*, 677–682.

[78] Inagi, S.; Naka, K.; Iida, D.; Chujo, Y. *Polym. J.* **2006**, *38*, 1146–1151.

[79] Naka, K.; Inagi, S.; Chujo, Y. *J. Polym. Sci. Part A: Polym. Chem.* **2005**, *43*, 4600–4608.

[80] Meazza, G.; Zanardi, G.; Guglielmetti, G.; Piccardi, P. *J. Fluor. Chem.* **1997**, *82*, 175–180.

[81] Mancuso, R.; Gabriele, B. *Molecules* **2014**, *19*, 15687–15719.

[82] Shockravi, A.; Javadi, A.; Abouzari-Lotf, E. *RSC Adv.* **2013**, *3*, 6717–6746.

[83] Viñas, C.; Cirera, M. R.; Teixidor, F.; Sillanpää, R.; Kivekäs, R. *J. Organomet. Chem.* **1997**, *530*, 89–94.

[84] Yusuff, K. K. M.; Karthikeyan, A. R. *Transition Met. Chem.* **1993**, *18*, 435–438.

[85] Nag, K.; Joardar, D. *Inorg. Chim. Acta* **1976**, 111–115.

[86] Cros, G.; Tahar, H. B.; de Montauzon, D.; Gleizes, A.; Coulais, Y.; Guiraud, R.; Bellande, E.; Pasqualini, R. *Inorg. Chim. Acta* **1994**, *227*, 25–31.

[87] Kaub, C.; Augenstein, T.; Bauer, T. O.; Rothe, E.; Esmezjan, L.; Schunemann, V.; Roesky, P. W. *Inorg. Chem.* **2014**, *53*, 4491–4499.

[88] Vahrenkamp, H. *Angew. Chem. Int. Ed.* **1975**, *14*, 322–329.

[89] Vera, M.; Schippers, A.; Sand, W. *Appl. Microbiol. Biotechnol.* **2013**, *97*, 7529–7541.

[90] Davidovich, R. L.; Stavila, V.; Whitmire, K. H. *Coord. Chem. Rev.* **2010**, *254*, 2193–2226.

[91] Lewis, J. A.; Cohen, S. M. *Inorg. Chem.* **2004**, *43*, 6534–6536.

Appendix: NMR Spectra of New Compounds

8.02
7.99
7.36
7.36
7.23
6.51
3.91
2.45
2.44
1.57
0.00
2.00
1.97
1.00
3.02
6.01
f1 (ppm)
SMe
MeS
S
S
H
MeOOC
13

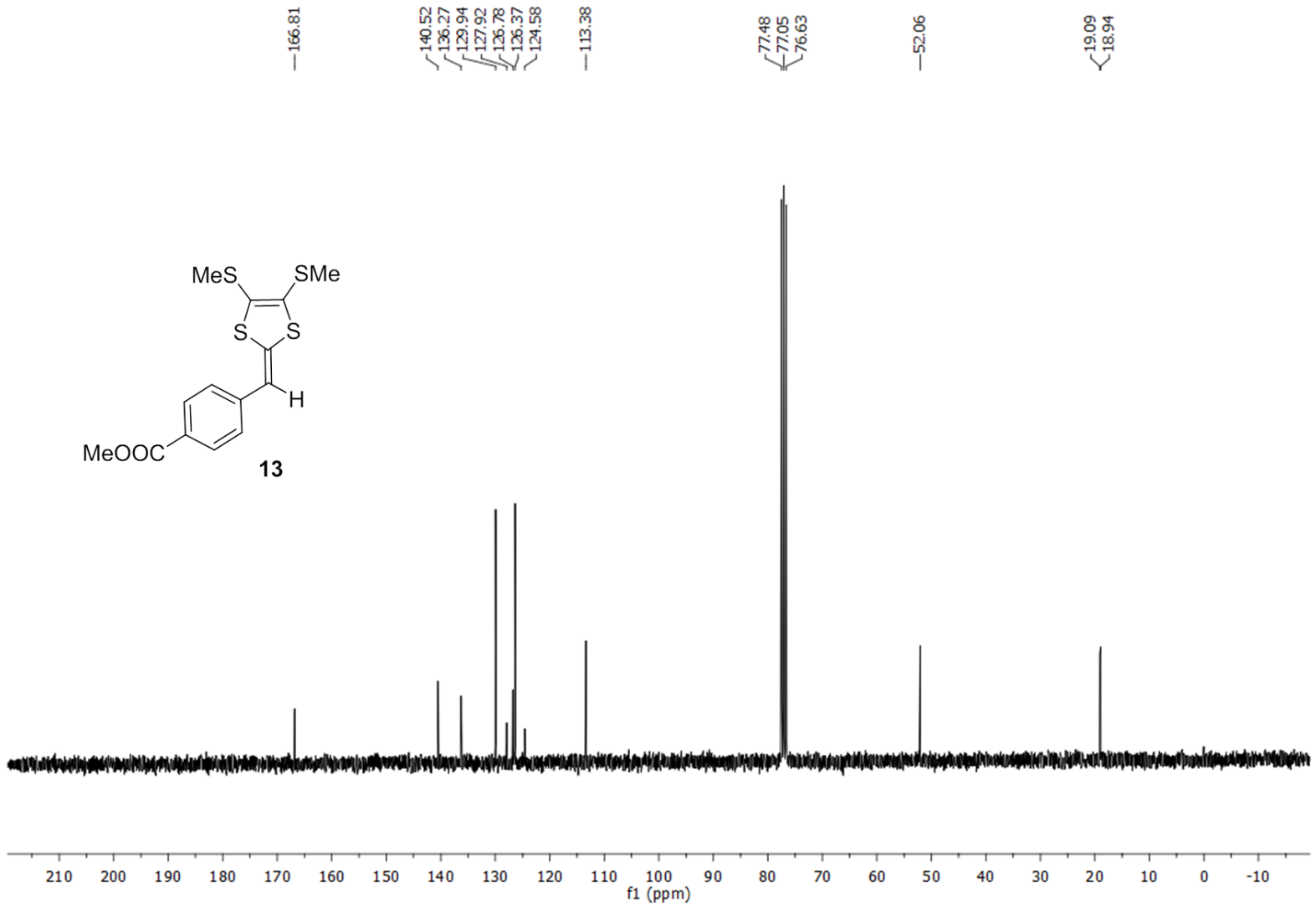
166.81
140.52
136.27
129.94
127.92
126.78
126.37
124.58
113.38
77.48
77.05
76.63
52.06
19.09
18.94
MeS
SMe
S
S
H
MeOOC
13
210 200 190 180 170 160 150 140 130 120 110 100 90 80 70 60 50 40 30 20 10 0 -10
f1 (ppm)

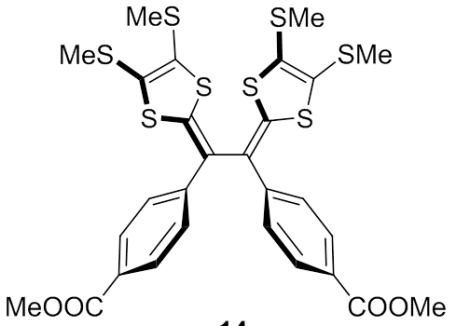
MeS
SMe
MeS
SMe
S
S
S
S
MeOOC
COOMe

14

7.99
7.96
7.47
7.44
7.26
3.89
2.44
2.38
1.54
0.00
4.00
4.02
5.96
5.98
5.99
16
15
14
13
12
11
10
9
8
7
6
5
4
3
2
1
0
-1
-2
-3
-4
f1 (ppm)

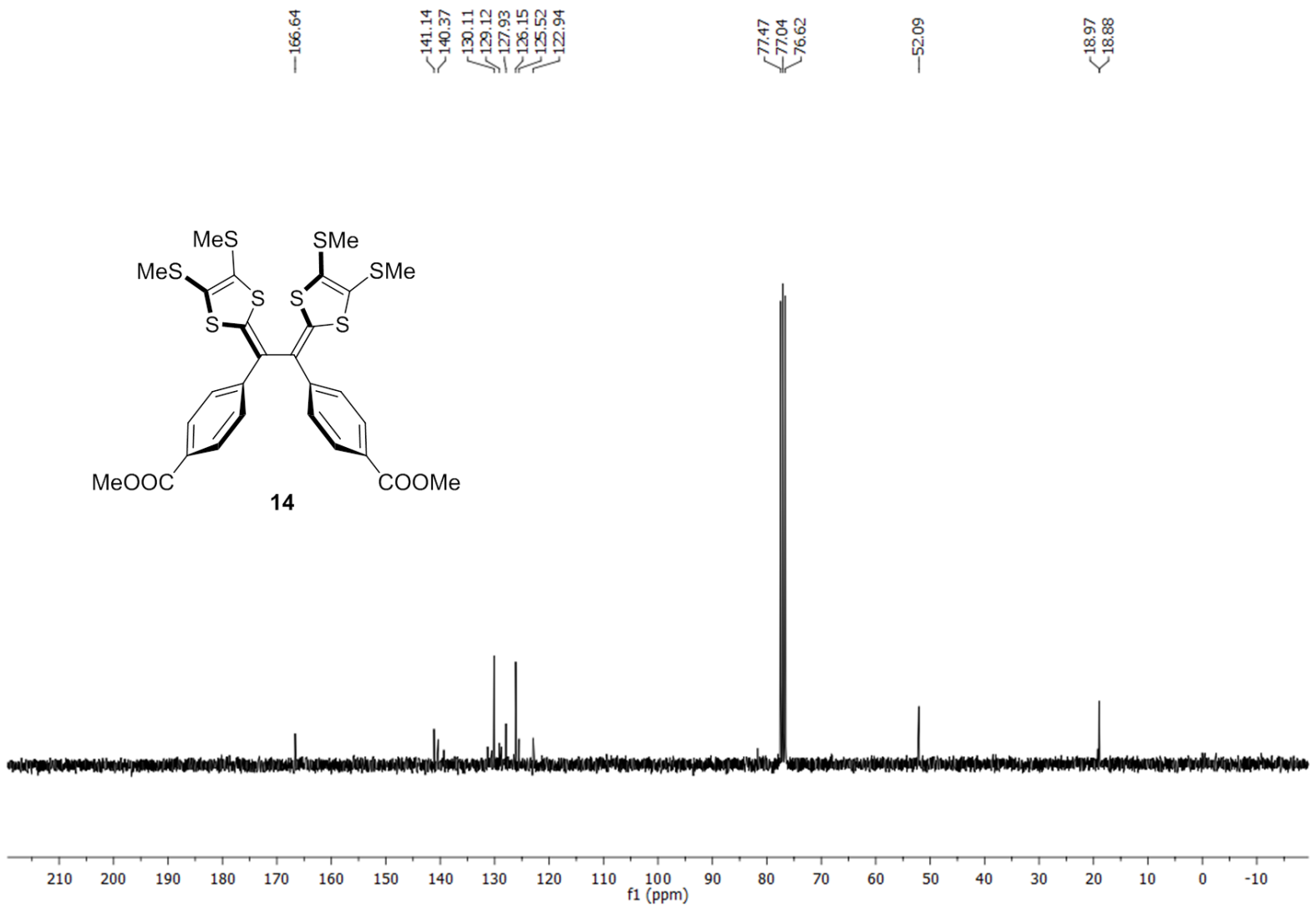
166.64
141.14
140.37
130.11
129.12
127.93
126.15
125.52
122.94
77.47
77.04
76.62
52.09
18.97
18.88
MeS
MeS
SMe
SMe
S
S
S
S
MeOOC
COOMe
14
210
200
190
180
170
160
150
140
130
120
110
100
90
80
70
60
50
40
30
20
10
0
-10
f1 (ppm)

12.86
7.96
7.93
7.33
7.30
6.82
3.34
2.51
2.47
2.45
0.00
0.98
2.03
2.02
1.00
3.02
3.03
f1 (ppm)
SMe
MeS
S
S
H
HOOC
15

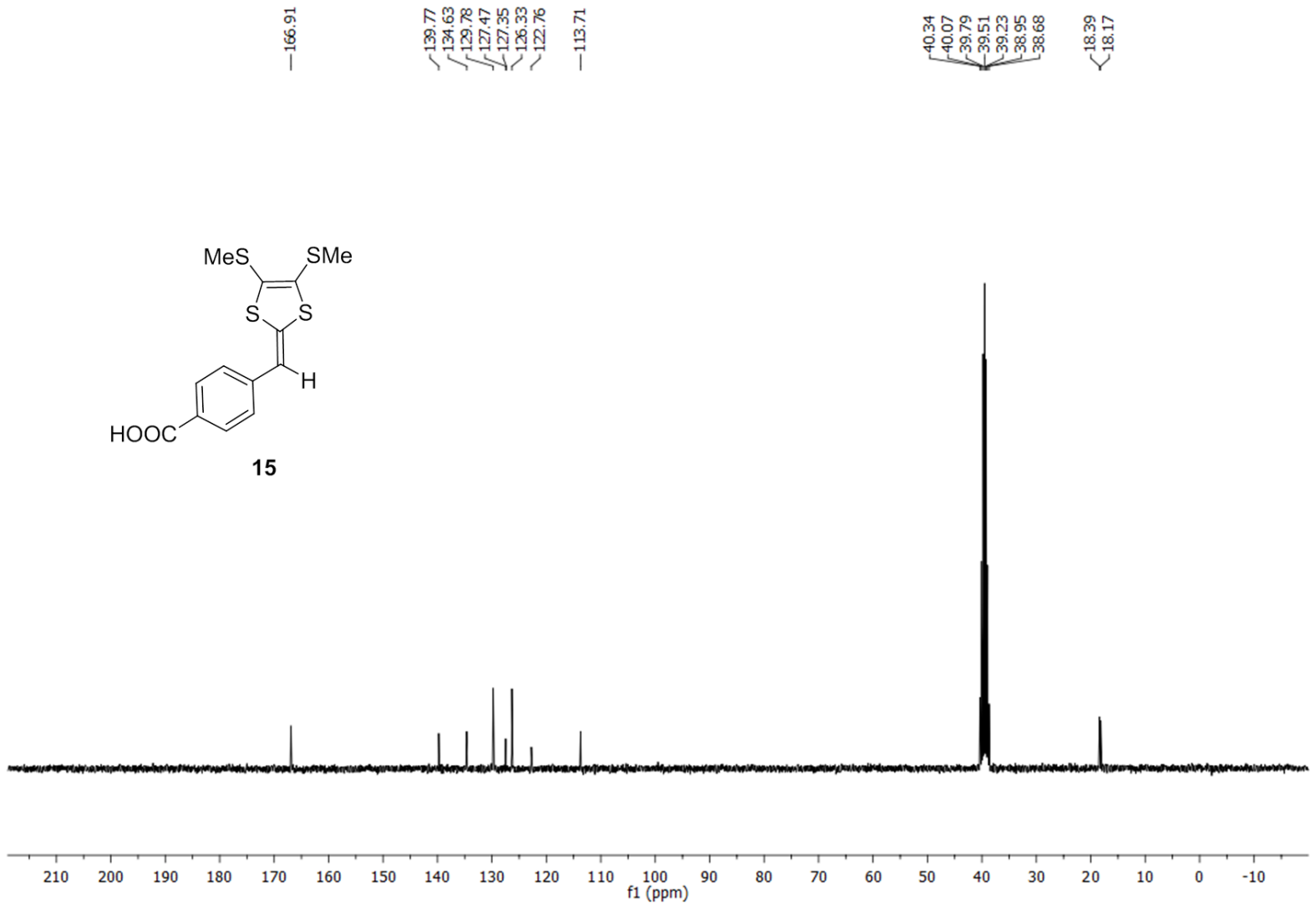
166.91
139.77
134.63
129.78
127.47
127.35
126.33
122.76
113.71
40.34
40.07
39.79
39.51
39.23
38.95
38.68
18.39
18.17
MeS
SMe
S
S
H
HOOC
15
210
200
190
180
170
160
150
140
130
120
110
100
90
80
70
60
50
40
30
20
10
0
-10
f1 (ppm)

7.95
7.93
7.49
7.46
3.36
2.52
2.48
2.40
6.05
6.00
4.04
4.00
f1 (ppm)
SMe
SMe
MeS
MeS
COOH
HOOC
16

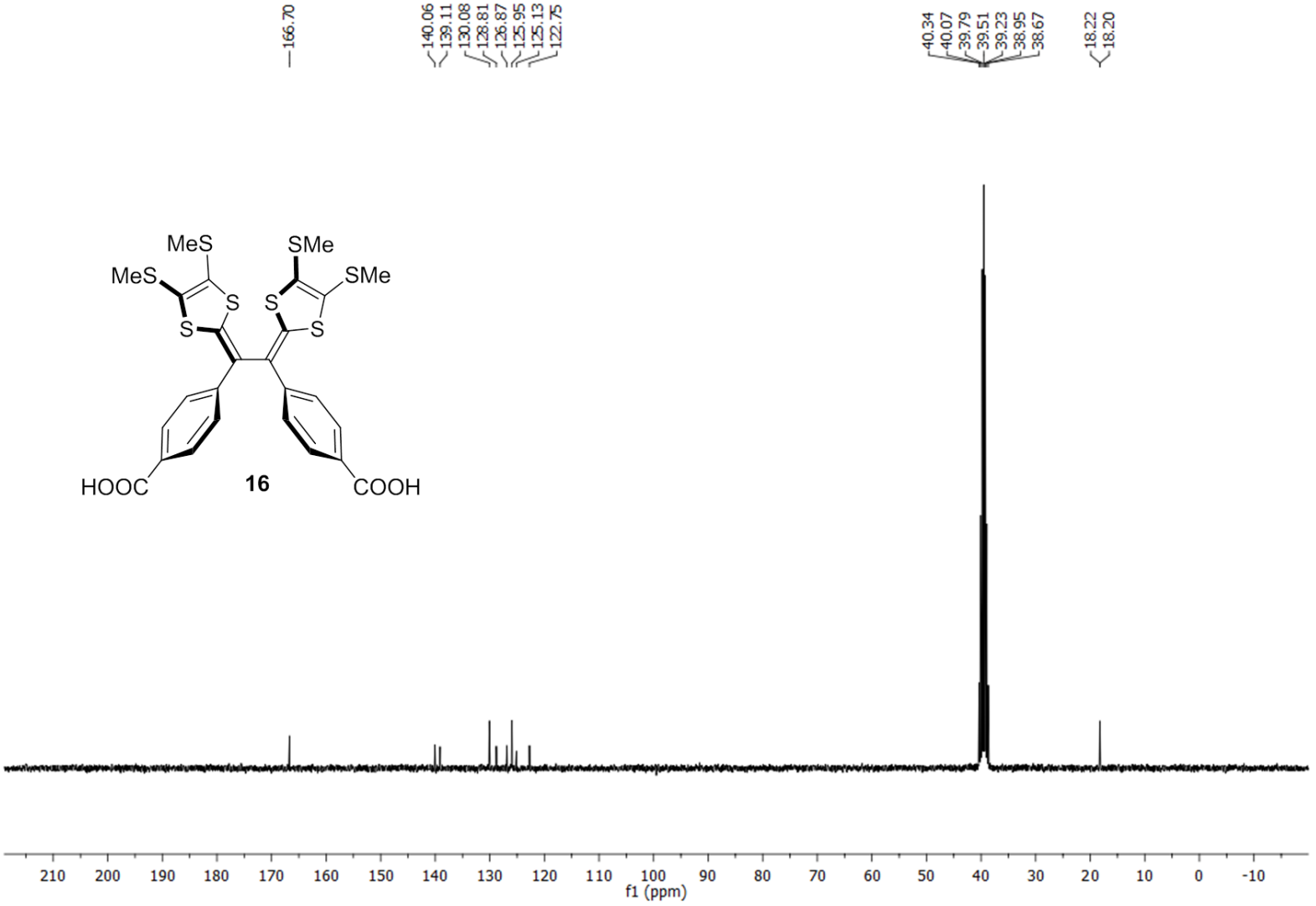
166.70
140.06
139.11
130.08
128.81
126.87
125.95
125.13
122.75
40.34
40.07
39.79
39.51
39.23
38.95
38.67
18.22
18.20
MeS
MeS
SMe
SMe
S
S
S
S
HOOC
COOH
16
210
200
190
180
170
160
150
140
130
120
110
100
90
80
70
60
50
40
30
20
10
0
-10
f1 (ppm)

-0.00
0.25
1.53
2.44
2.43
6.44
7.44
7.42
7.26
7.14
7.11
9.00
5.99
1.00
2.02
2.03
SMe
MeS
S
S
H
TMS
22a
f1 (ppm)

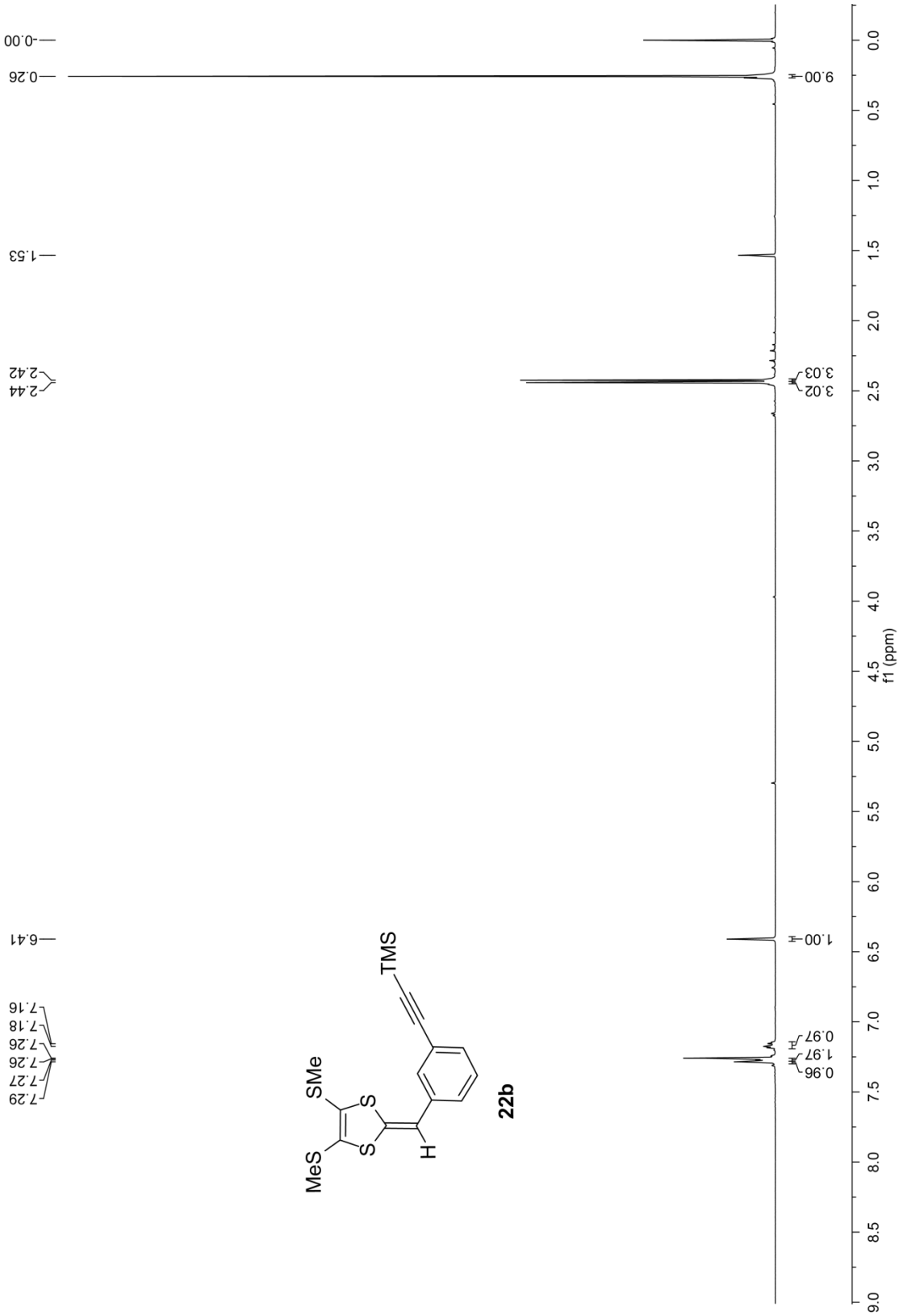
TMS
SMe
MeS
S
S
H
22b
f1 (ppm)

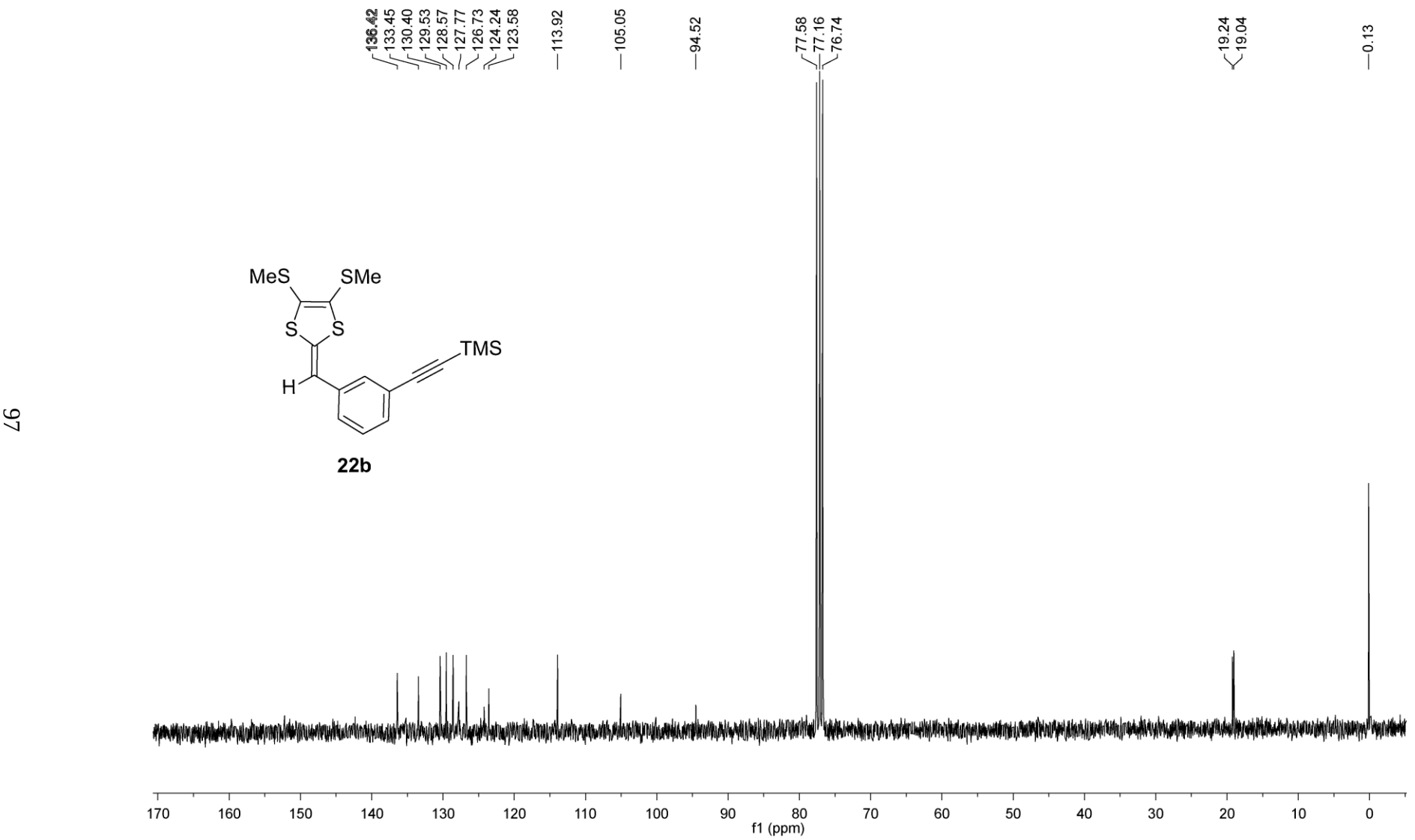
136.42
133.45
130.40
129.53
128.57
127.77
126.73
124.24
123.58
113.92
105.05
94.52
77.58
77.16
76.74
19.24
19.04
0.13
MeS
SMe
S
S
H
TMS
22b
170
160
150
140
130
120
110
100
90
80
70
60
50
40
30
20
10
0
f1 (ppm)

-0.00
0.27
1.53
2.41
2.45
6.98
7.09
7.11
7.26
7.32
7.33
7.44
7.47
9.06
3.03
3.04
1.00
1.05
2.04
1.04
f1 (ppm)
SMe
MeS
S
S
H
TMS
22c

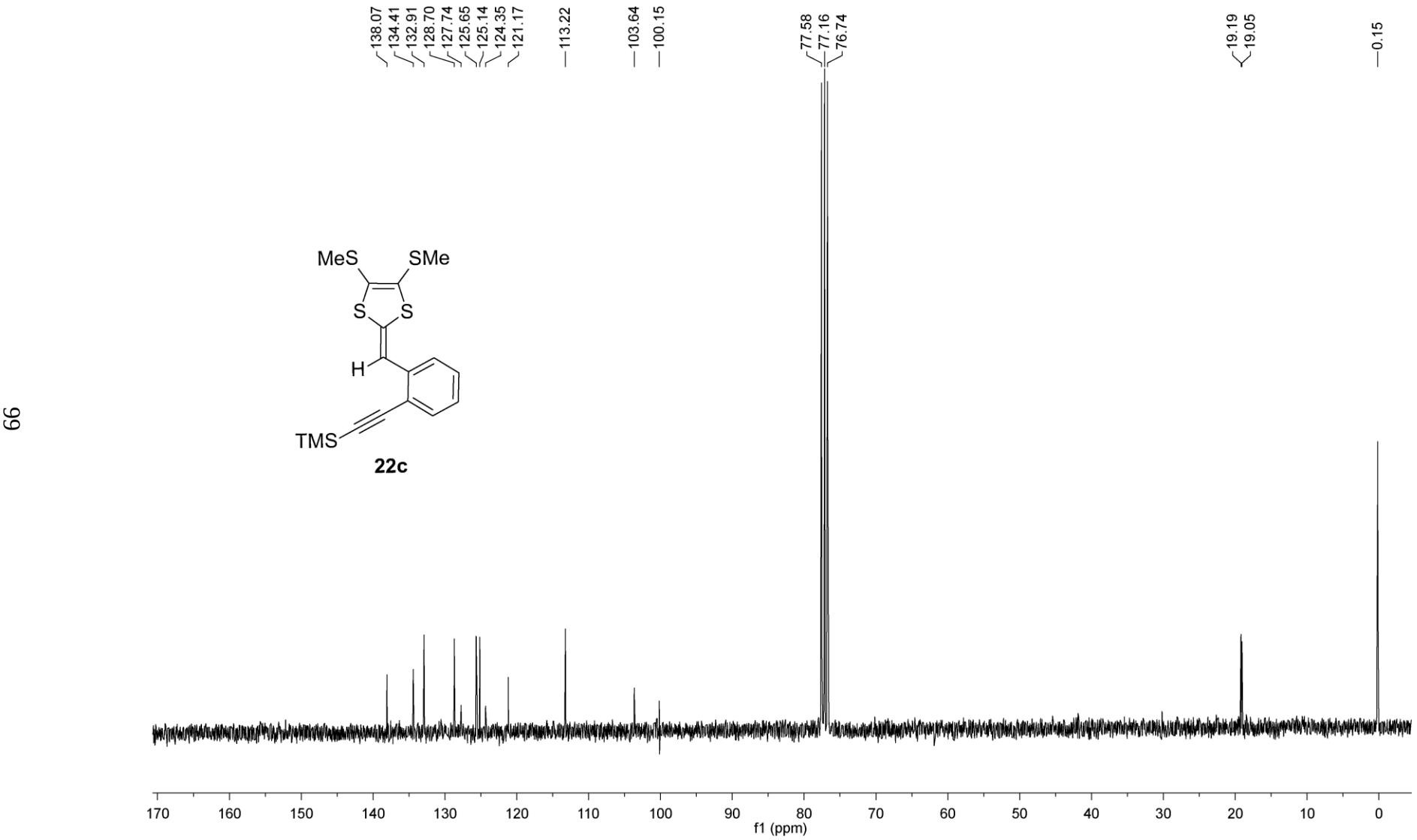
138.07
134.41
132.91
128.70
127.74
125.65
125.14
124.35
121.17
113.22
103.64
100.15
77.58
77.16
76.74
19.19
19.05
0.15
MeS
SMe
S
S
H
TMS
22c
170
160
150
140
130
120
110
100
90
80
70
60
50
40
30
20
10
0
f1 (ppm)

7.39
7.37
7.32
7.29
7.26
2.42
2.38
1.55
0.23
0.00
18.03
6.03
5.99
4.03
4.00
SMe
SMe MeS
MeS
TMS
TMS
S
23a
f1 (ppm)

7.47
7.29
7.27
7.26
7.24
7.22
2.42
2.40
1.54
1.25
0.25
0.07
0.00
-0.19
2.00
4.04
2.02
12.03
18.06
SMe
SMe MeS
MeS
TMS
TMS
S
S
S
S
23b
f1 (ppm)

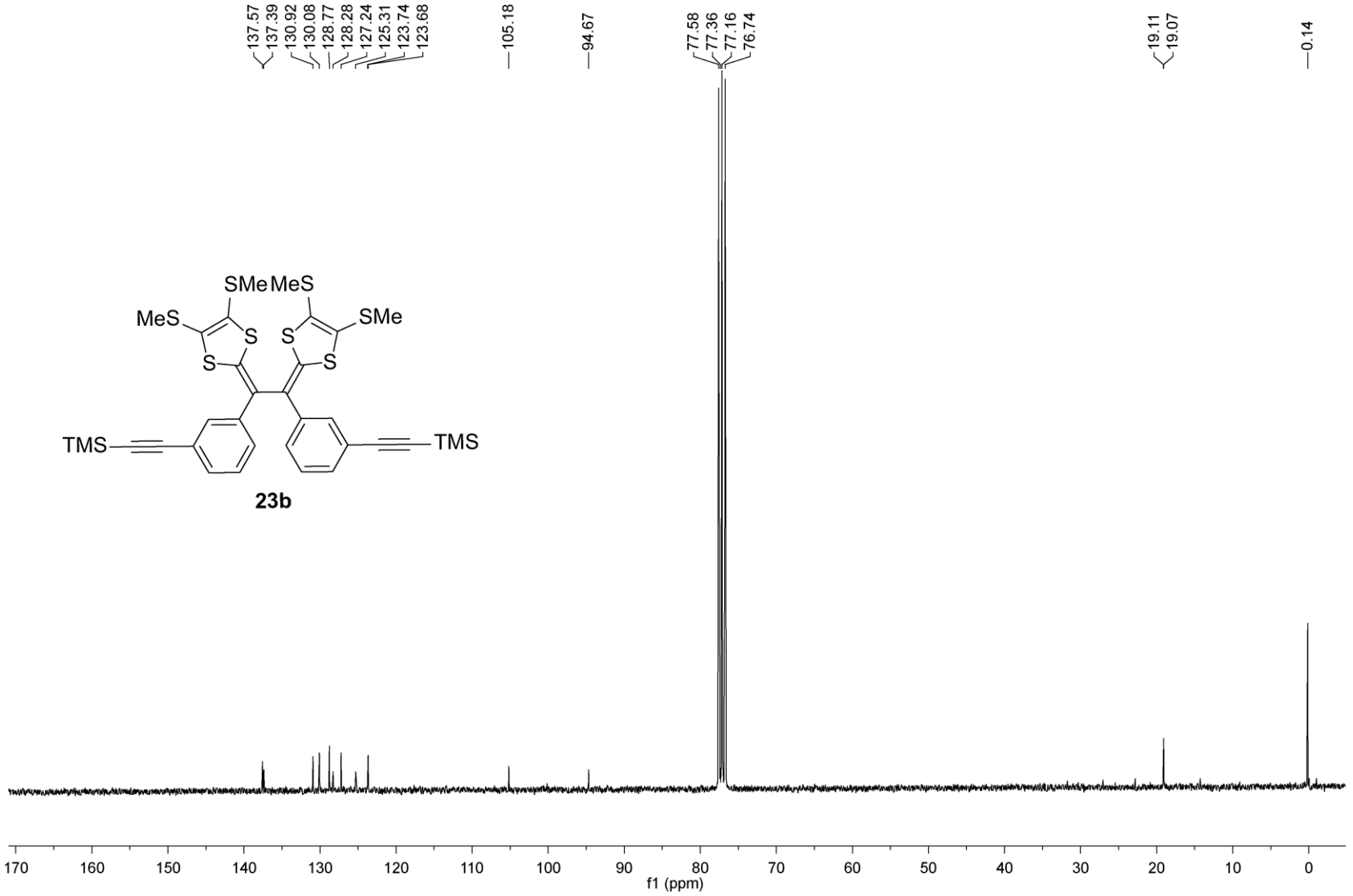
137.57
137.39
130.92
130.08
128.77
128.28
127.24
125.31
123.74
123.68
105.18
94.67
77.58
77.36
77.16
76.74
19.11
19.07
0.14
SMe
MeS
MeS
SMe
S
S
S
S
TMS
TMS
23b
170
160
150
140
130
120
110
100
90
80
70
60
50
40
30
20
10
0
f1 (ppm)

-0.00
0.25
1.54
2.35
2.46
7.09
7.12
7.16
7.26
7.29
7.31
18.04
6.03
6.03
4.06
4.00
f1 (ppm)
SMe
TMS
SMe MeS
MeS
TMS
23c

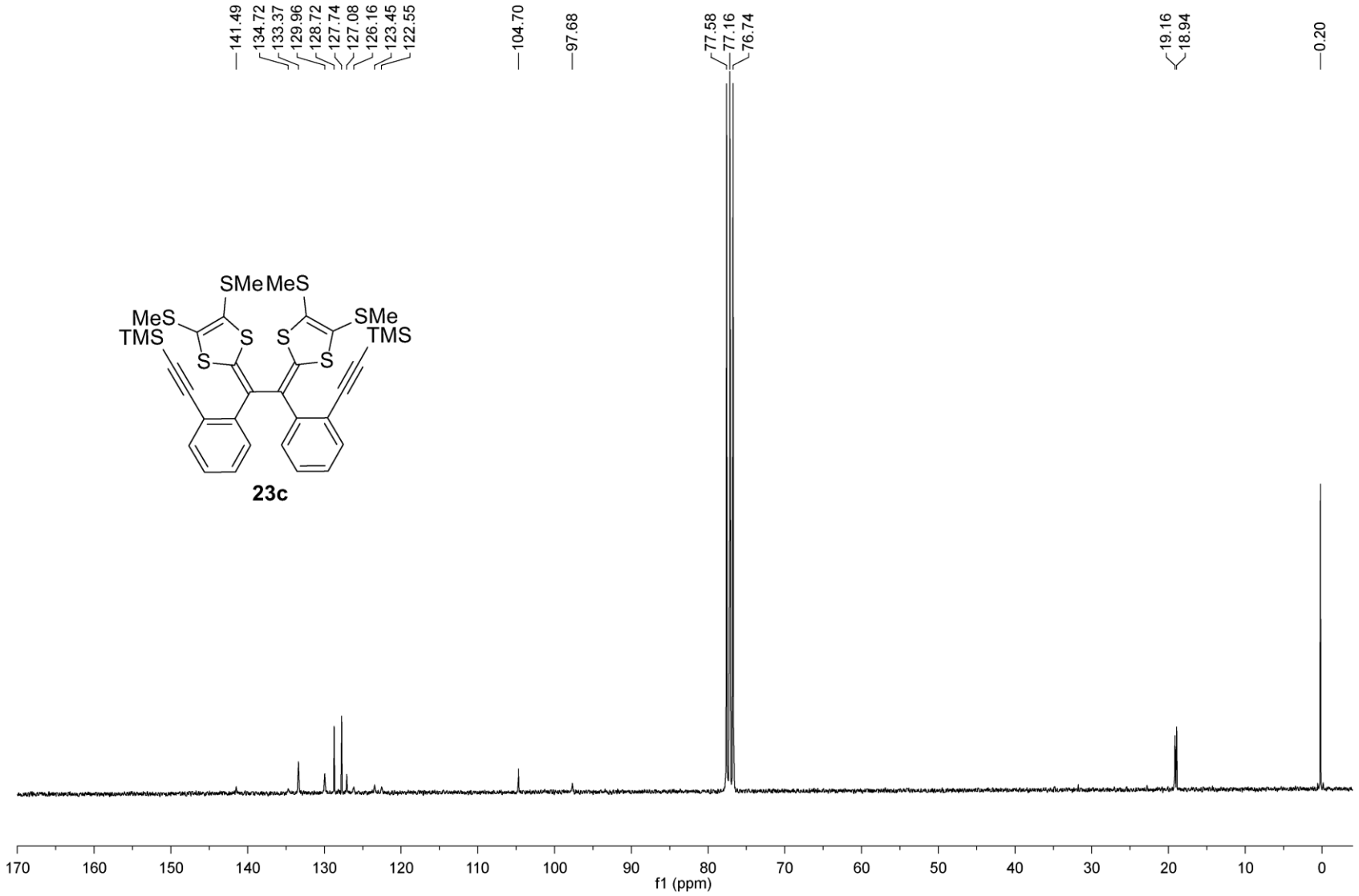
141.49
134.72
133.37
129.96
128.72
127.74
127.08
126.16
123.45
122.55
104.70
97.68
77.58
77.16
76.74
19.16
18.94
0.20
SMe
MeS
MeS
TMS
S
S
S
S
SMe
TMS
170
160
150
140
130
120
110
100
90
80
70
60
50
40
30
20
10
0
f1 (ppm)

23c

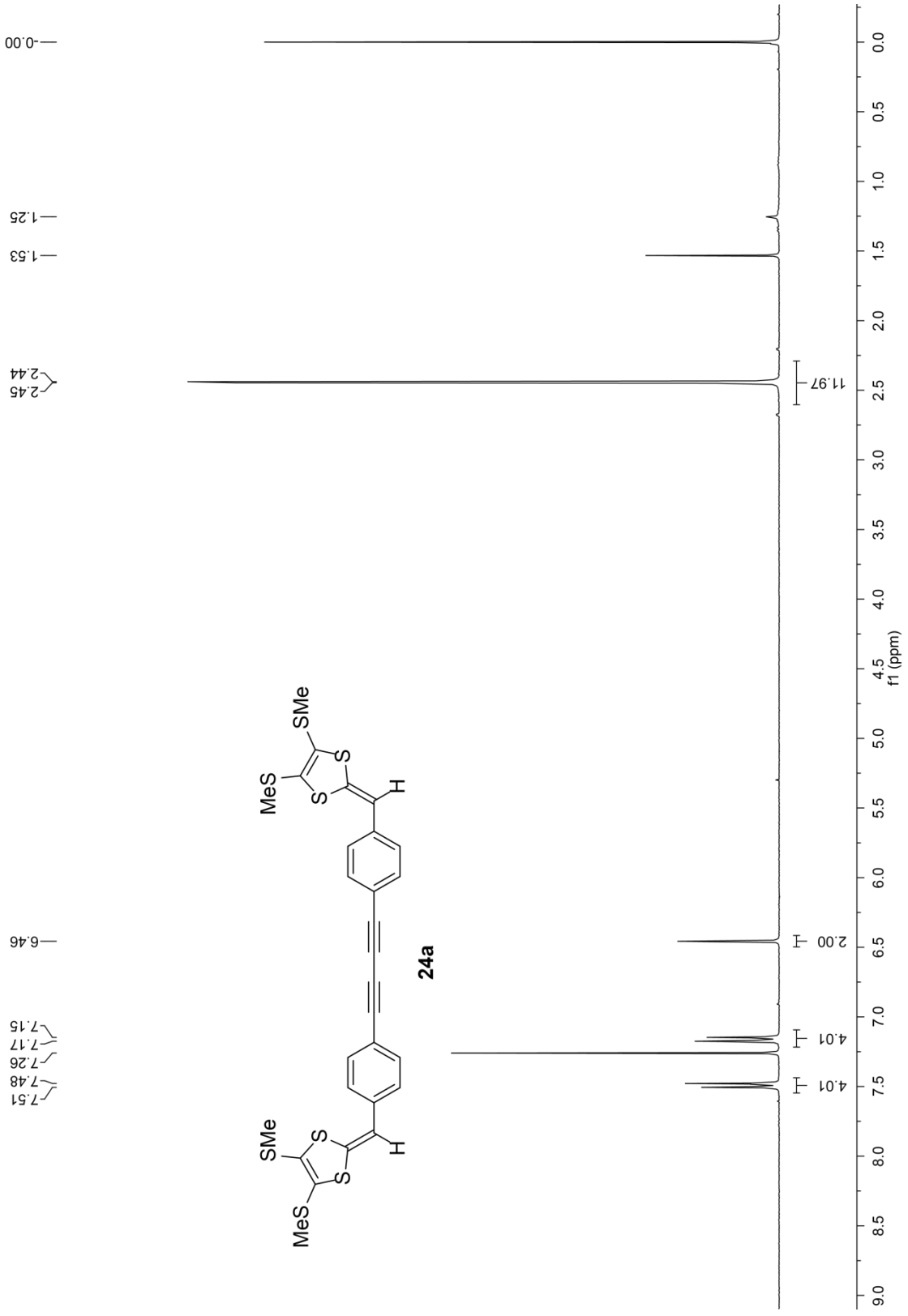
24a
MeS
SMe
H
S
11.97
2.00
4.01
4.01
2.45
2.44
1.53
1.25
0.00
6.46
7.51
7.48
7.26
7.17
7.15
f1 (ppm)

0.00
1.25
1.54
2.44
2.44
6.42
7.20
7.22
7.26
7.31
7.33
7.36
12.04
2.00
1.97
3.97
2.02
f1 (ppm)
SMe
MeS
S
S
H
24b

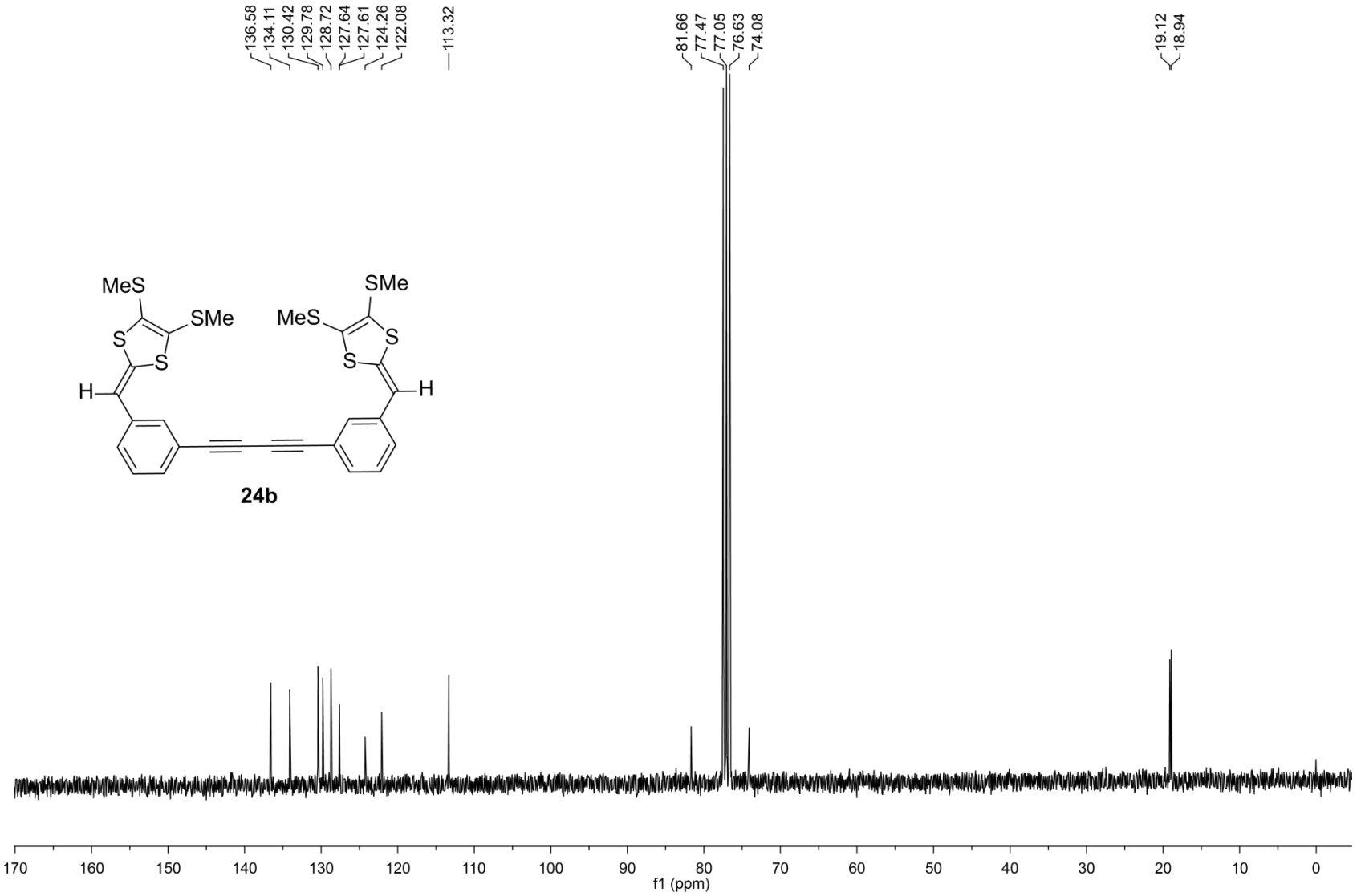
136.58
134.11
130.42
129.78
128.72
127.64
127.61
124.26
122.08
113.32
81.66
77.47
77.05
76.63
74.08
19.12
18.94
MeS
SMe
S
S
H
MeS
SMe
S
S
H
24b
170
160
150
140
130
120
110
100
90
80
70
60
50
40
30
20
10
0
f1 (ppm)

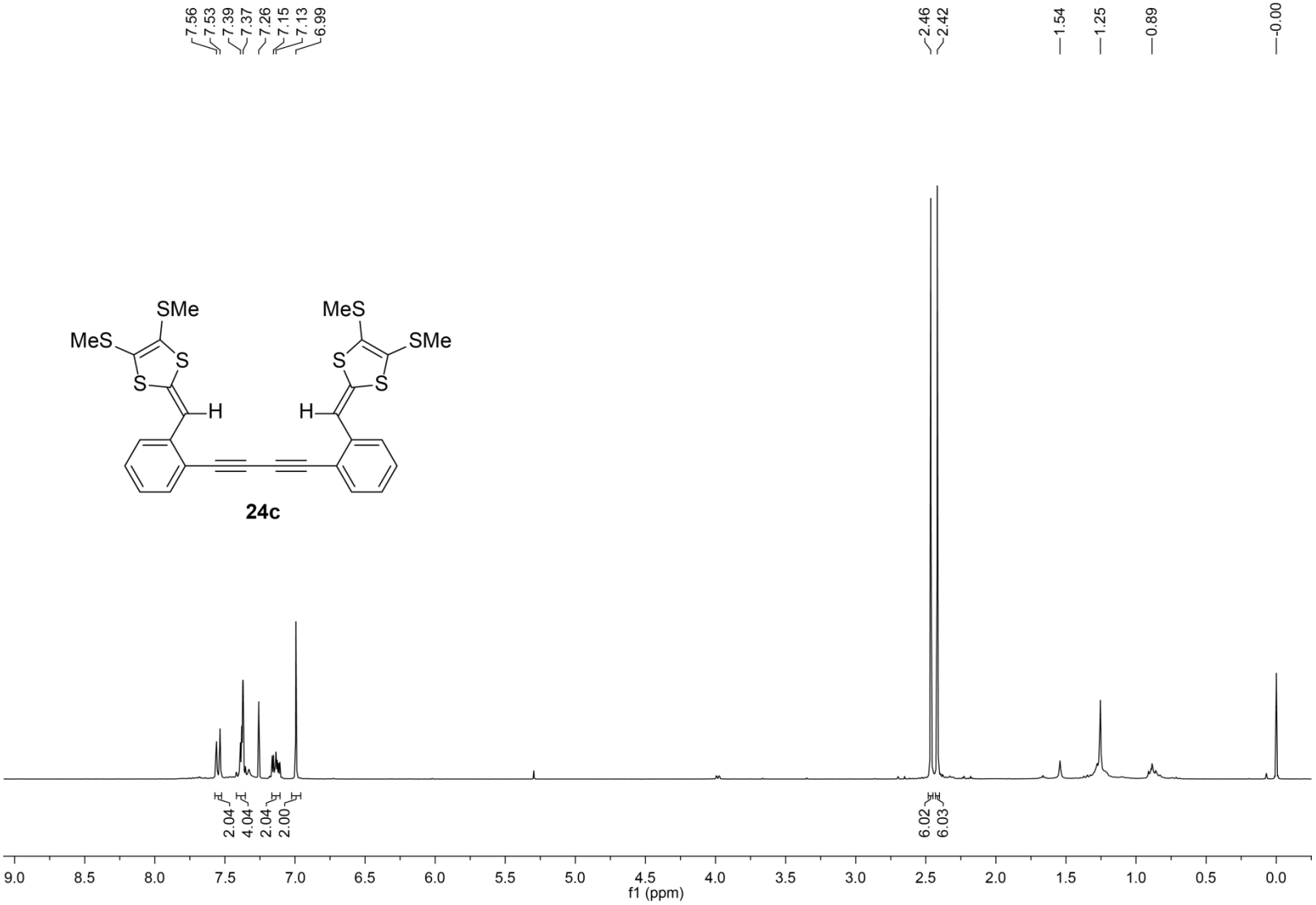
7.56
7.53
7.39
7.37
7.26
7.15
7.13
6.99
2.46
2.42
1.54
1.25
0.89
0.00
SMe
MeS
S
S
H
MeS
SMe
S
S
H
24c
2.04
4.04
2.04
2.00
6.02
6.03
9.0
8.5
8.0
7.5
7.0
6.5
6.0
5.5
5.0
4.5
4.0
3.5
3.0
2.5
2.0
1.5
1.0
0.5
0.0
f1 (ppm)

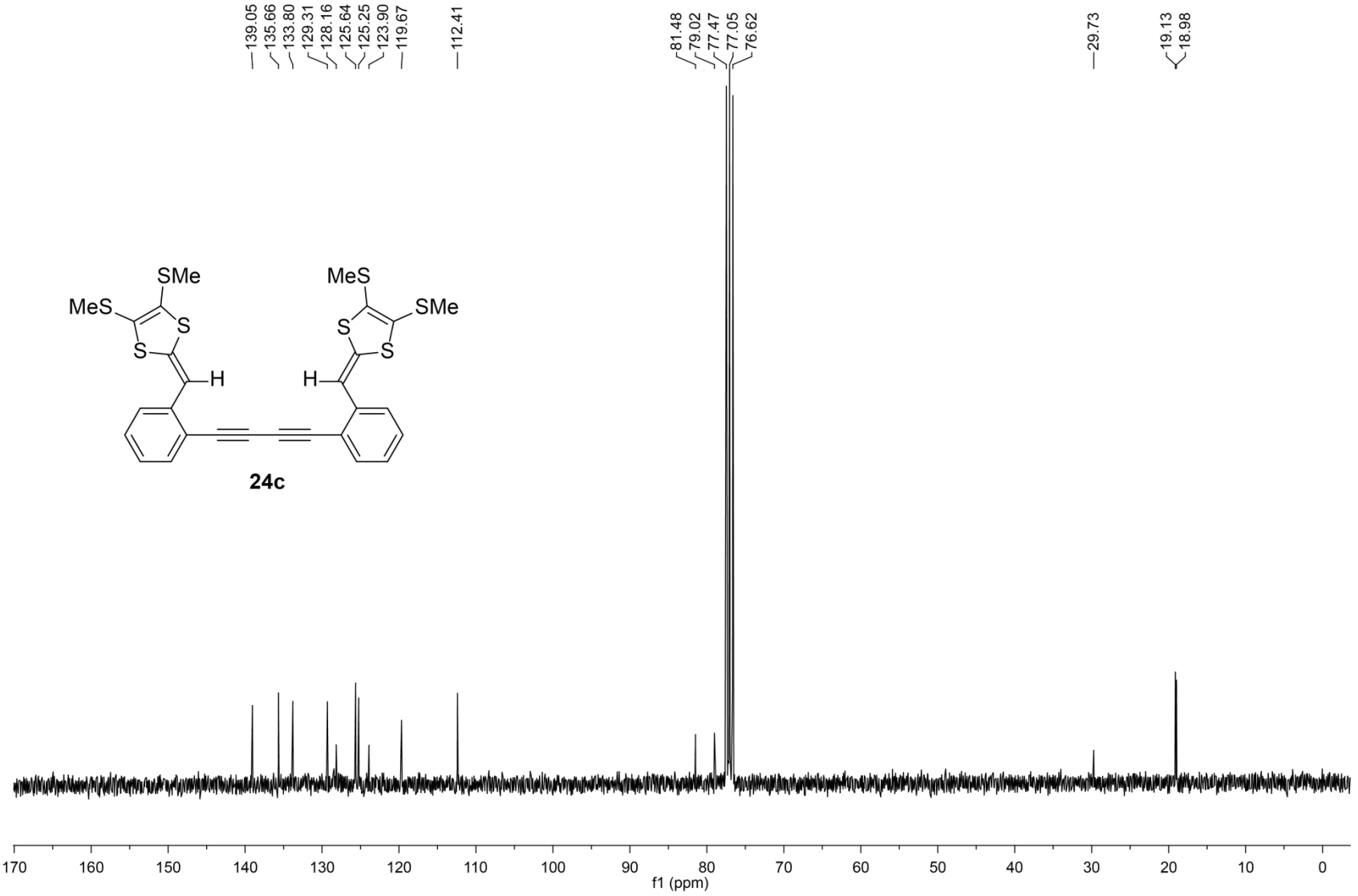
139.05
135.66
133.80
129.31
128.16
125.64
125.25
123.90
119.67
112.41
81.48
79.02
77.47
77.05
76.62
29.73
19.13
18.98
SMe
MeS
S
S
H
MeS
SMe
S
S
H
24c
170
160
150
140
130
120
110
100
90
80
70
60
50
40
30
20
10
0
f1 (ppm)

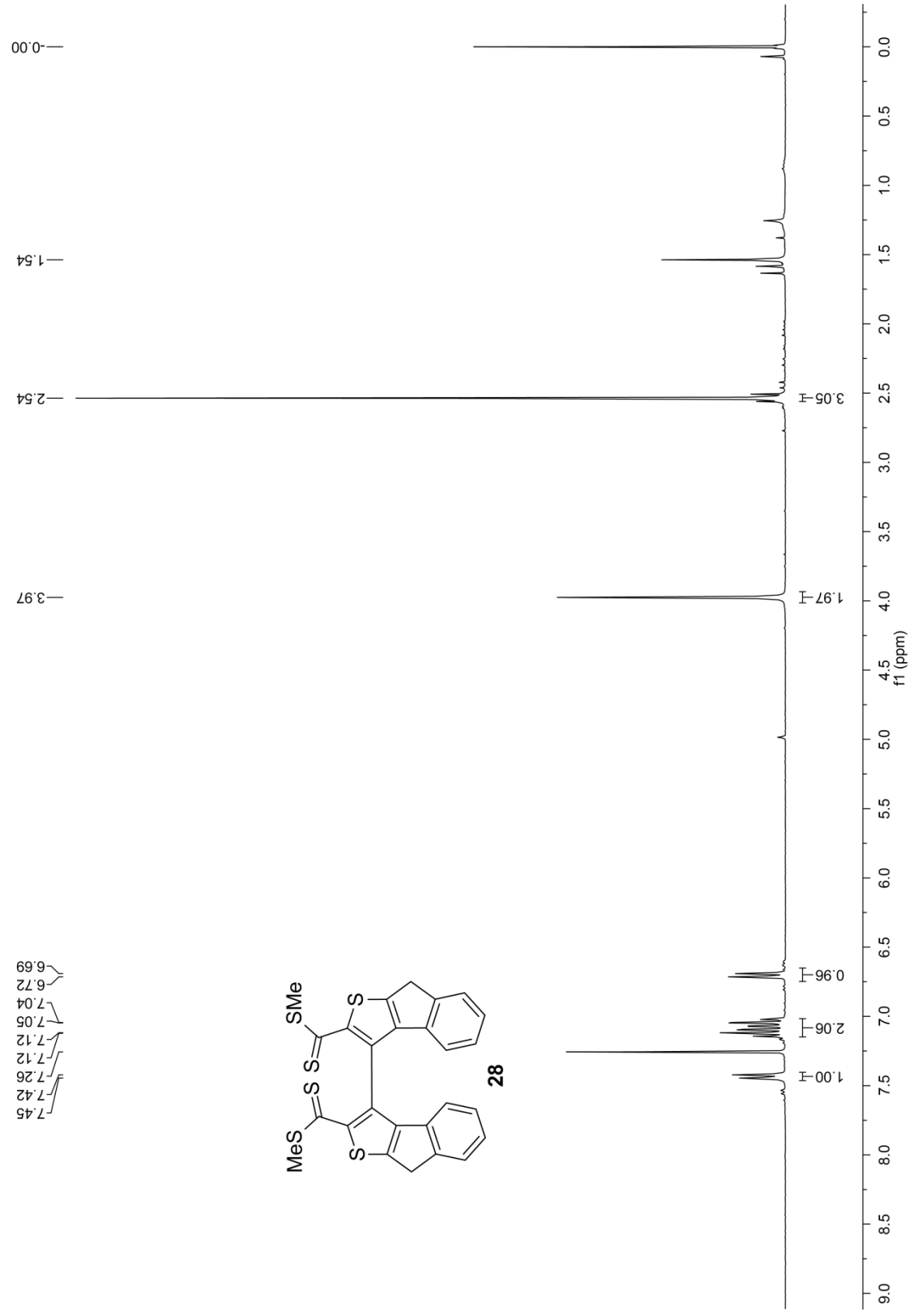
7.45
7.42
7.26
7.12
7.12
7.05
7.04
6.72
6.69
3.97
2.54
1.54
0.00
1.00
2.06
0.96
1.97
3.05
SMe
MeS
S
S
S
S
28
f1 (ppm)

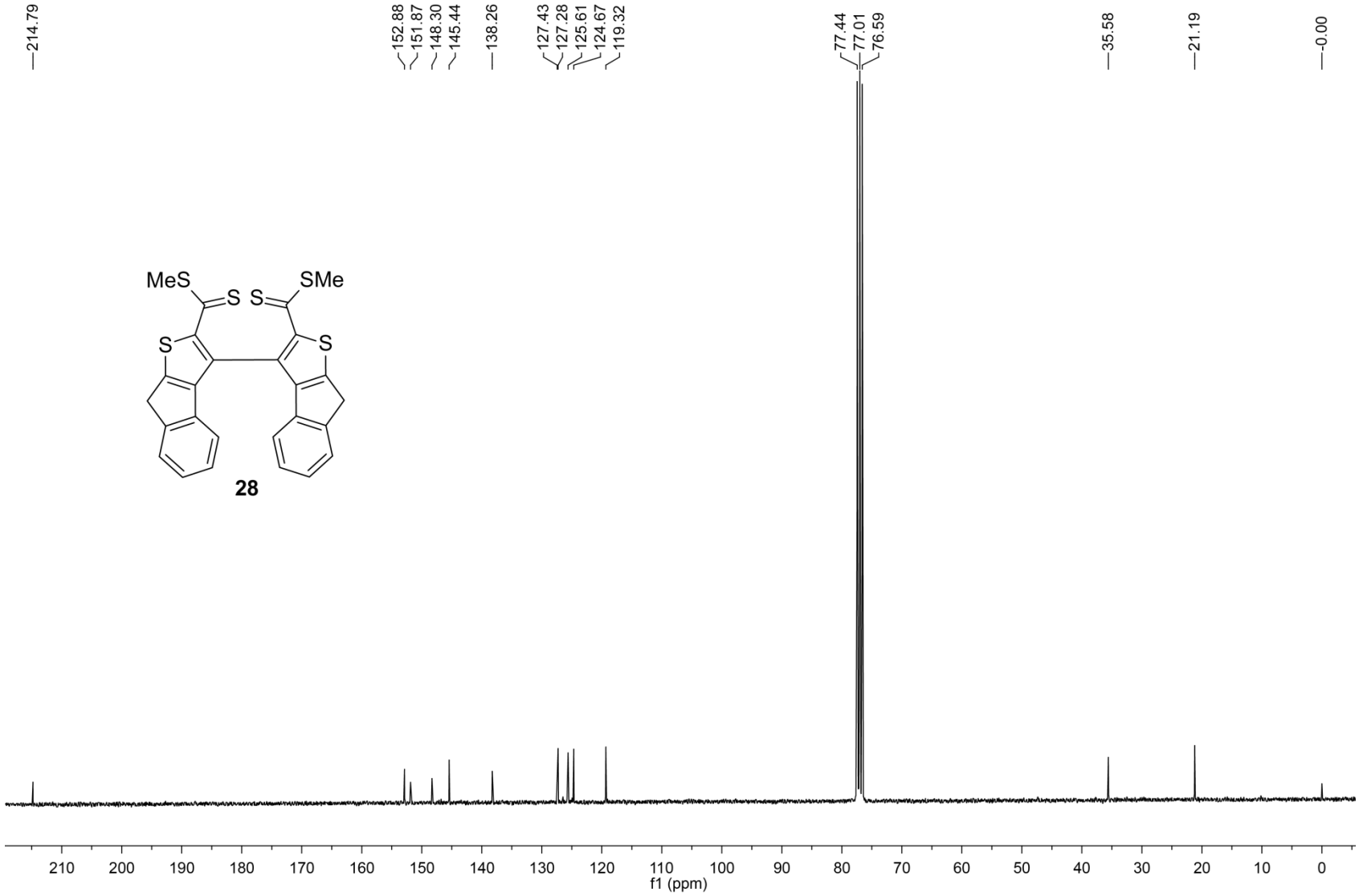
214.79
152.88
151.87
148.30
145.44
138.26
127.43
127.28
125.61
124.67
119.32
77.44
77.01
76.59
35.58
21.19
0.00
MeS
S
S
SMe
S
S
28
210
200
190
180
170
160
150
140
130
120
110
100
90
80
70
60
50
40
30
20
10
0
f1 (ppm)

f1 (ppm)
f2 (ppm)
SMe
MeS
S
28